Charm Meson Molecules and the $X(3872)$

DISSERTATION

Presented in Partial Fulfillment of the Requirements for

the Degree Doctor of Philosophy in the

Graduate School of The Ohio State University

By

Masaoki Kusunoki, B.S.

* * * * *

The Ohio State University

2005

Dissertation Committee:

Professor Eric Braaten, Adviser

Professor Richard J. Furnstahl

Professor Junko Shigemitsu

Professor Brian L. Winer

Approved by

_____

Adviser

Graduate Program in Physics

Abstract

The recently discovered resonance $X(3872)$ is interpreted as a loosely-bound S-wave charm meson molecule whose constituents are a superposition of the charm mesons $D^0\bar{D}^{*0}$ and $D^{*0}\bar{D}^0$. The unnaturally small binding energy of the molecule implies that it has some universal properties that depend only on its binding energy and its width. The existence of such a small energy scale motivates the separation of scales that leads to factorization formulas for production rates and decay rates of the $X(3872)$. Factorization formulas are applied to predict that the line shape of the $X(3872)$ differs significantly from that of a Breit-Wigner resonance and that there should be a peak in the invariant mass distribution for $B \to D^0\bar{D}^{*0}K$ near the $D^0\bar{D}^{*0}$ threshold. An analysis of data by the Babar collaboration on $B \to D^{(*)}\bar{D}^{(*)}K$ is used to predict that the decay $B^0 \to XK^0$ should be suppressed compared to $B^+ \to XK^+$. The differential decay rates of the $X(3872)$ into J/ψ and light hadrons are also calculated up to multiplicative constants. If the $X(3872)$ is indeed an S-wave charm meson molecule, it will provide a beautiful example of the predictive power of universality.

To my family

ACKNOWLEDGMENTS

My greatest thank goes to my advisor Eric Braaten. I am deeply grateful to his advice, encouragement, and the way he has supported me through everything. I have learned more from him than I can acknowledge here. It has been an honor and privilege to work with him.

I would like to thank Hans-W. Hammer, Yu Jia, Tom Mehen, Shmuel Nussinov, and Dongqing Zhang for fruitful collaboration on various research projects. I have truly enjoyed working with them and have learned many things that I could not have gained just from textbooks.

I would also like to thank all of my physics classmates and the past and previous occupants in room 4012 Smith Laboratory. In particular, thanks to Yaojun Du, Emel Gulez, Motomichi Harada, Jongjoo Kim, Youngmin Kim, Kohjiro Kobayashi, Ashish Saxena, Leslie Schradin, and Yuko Shiroyanagi for innumerable reasons that have made my life inside and outside physics enjoyable.

My deepest gratitude goes to my parents Masami and Tomoko Kusunoki, and my brothers Masayoshi and Keizo for their support. Without them this work or my graduate career would not have been possible. Last but not the least, I want to give special thanks to my wife Ruriko for her love, encouragement, and believing in me.

This research was supported in part by the Department of Energy under grant DE-FG02-91-ER4069.

VITA

July 16, 1975	Born - Kamakura city, Japan
1999	B.S. Applied Physics, Waseda University, Tokyo, Japan
1999-present	Graduate Teaching and Research Associate, The Ohio State University

PUBLICATIONS

Research Publications

E. Braaten and M. Kusunoki, "Factorization in the Production and Decay of the X(3872)," Phys. Rev. D **72**, 014012 (2005) [arXiv: hep-ph/0506087].

E. Braaten and M. Kusunoki, "Exclusive Production of the X(3872) in B Meson Decay," Phys. Rev. D **71**, 074005 (2005) [arXiv: hep-ph/0412268].

E. Braaten, M. Kusunoki and S. Nussinov, "Production of the $X(3872)$ in B Meson Decay by the Coalescence of Charm Mesons", Phys. Rev. Lett. **93** 162001 (2004), [arXiv:hep-ph/0404161].

E. Braaten and M. Kusunoki, "Production of the $X(3870)$ at the $\Upsilon(4S)$ by the Coalescence of Charm Mesons", Phys. Rev. D **69**, 114012 (2004) [arXiv: hep-ph/0402177].

E. Braaten and M. Kusunoki, "Low-energy Universality and the New Charmonium Resonance at 3870 MeV", Phys. Rev. D **69**, 074005 (2004) [arXiv:hep-ph/0311147].

E. Braaten, M. Kusunoki, Y. Jia and T. Mehen, "Λ_c^+/Λ_c^- Asymmetry in Hadroproduction from Heavy-Quark Recombination", Phys. Rev. D **70**, 054021 (2004) [arXiv:hep-ph/0304280].

E. Braaten, H.-W. Hammer and M. Kusunoki, "Efimov States in a BEC near a Feshbach Resonance", Phys. Rev. Lett. **90**, 170402 (2003) [arXiv:cond-mat/0206232].

E. Braaten, H.-W. Hammer and M. Kusunoki, "Universal Equation for Efimov States", Phys. Rev. A **67**, 022505 (2003) [arXiv:cond-mat/0201281].

FIELDS OF STUDY

Major Field: Physics

TABLE OF CONTENTS

LIST OF TABLES

LIST OF FIGURES

Figure **Page**

CHAPTER 1

INTRODUCTION

We begin with a brief non-technical introduction to quarks, hadrons, and hadronic molecules. We then describe the discovery of the $X(3872)$ particle in 2003 and summarize what is now known about its properties. Finally we discuss various interpretations of the $X(3872)$ that have been proposed, including the possibility that it is a charm meson molecule.

1.1 From quarks to hadrons

The modern scientific search for the fundamental constituents of matters began with the chemistry and physics of the 19th century which showed that matter is made up of atoms. Some of the important steps were Dalton's theory of the atom in 1803 and Mendeleev's invention of the periodic table of elements in 1869. The discovery of the nucleus of the atom by Rutherford in 1911 led eventually to the realization that the atom is made up of a nucleus and electrons. The discovery of the neutron by Chadwick in 1932 led eventually to the understanding that nuclei are made up of protons and neutrons. The next real progress came in the 1960's with the invention of the quark model, in which protons and neutrons are made up of quarks.

In our current understanding, the elementary particles that are the constituents of matter are classified into quarks and leptons. Each type of quark or lepton has an antiparticle. Six types of quarks are currently known. From the lightest to heaviest, the quarks are named up (u), down (d), strange (s), charm (c), bottom (b), and top (t). The types of quarks are also called *quark flavors*. The antiquarks are labelled $\bar{u}$, $\bar{d}$, $\bar{s}$, $\bar{c}$, $\bar{b}$, and $\bar{t}$. The up quark is often called u quark and its antiparticle is called a u antiquark or a $\bar{u}$ quark and so on. Generic quarks and antiquarks with unspecified flavors are often denoted by q and $\bar{q}$. The 6 quarks are divided into 3 families. Each family is a doublet consisting of an up-type quark (u, c, or t) and a down-type quark (d, s, or b). We denote the three families as (u, d), (c, s), and (t, b). There are also 6 kinds of leptons: electron (e), muon (μ), tau (τ), and three neutrinos (ν_e, ν_μ, and ν_τ). The electric charges of quarks and leptons are usually expressed in units of the proton charge. The electron, muon, and tau have charge -1. The neutrinos have charge 0. Up-type quarks have charge $+2/3$ and down-type quarks have charge $-1/3$. Their antiparticles have the opposite electric charge. Elementary particles can have intrinsic angular momentum. Quantum mechanics restricts the intrinsic angular momentum to discrete possibilities labelled by a quantum number J called the spin, whose possible values are 0, 1/2, 1, 3/2, $\cdots$. The quarks and leptons all have spin 1/2.

Four fundamental forces are known in nature: the gravitational force, the electromagnetic force, the weak force, and the strong force. All the quarks and leptons feel the gravitational force, although its effects on individual elementary particles are negligible. The quarks and the charged leptons interact via the electromagnetic force. The electromagnetic force is mediated by a massless spin-1 particle called the photon

(γ). The coupling of the photon is proportional to the electric charge of the quark or lepton. Quarks and leptons interact via the weak force, which is mediated by three massive spin-1 particles called W^+, W^-, and Z^0. The weak interaction is the only one that can change the quark flavors. Only quarks and antiquarks feel the strong force. A quark carries any one of 3 color charges, which are sometimes called red, blue, and green, while an antiquark carries any one of 3 complimentary color charges. The strong force is mediated by massless spin-1 particles called gluons (g), which couple to the color charge of the quarks. The gluon carries any one of 8 color charges. The strong interaction is generally much more complicated than the electromagnetic interaction, since the color charges of the gluons allow them to interact with each other even in the absence of quarks. The modern language in physics for describing the interactions of elementary particles is quantum field theory, which incorporates both quantum mechanics and special relativity. The theory that describes the strong interactions among quarks and gluons is called Quantum Chromodynamics (QCD). The theory that describes the strong, weak, and electromagnetic interactions among quarks and leptons is called the Standard Model of particle physics.

Isolated quarks and gluons have never been directly observed in experiments, even at the highest energy accelerators. This fact is explained by QCD, which predicts that an isolated quark or gluon has infinite energy. Combinations of quarks, antiquarks, and gluons can have finite energy only if their overall color charge is neutral. A neutral color charge is often referred to as color-singlet. Particles that feel the strong force are called hadrons. Thus QCD predicts that hadrons are color-singlet combinations of quarks, antiquarks, and gluons. The known hadrons are classified into baryons, antibaryons, and mesons. Baryons are made up of three quarks. For example, the

quark contents of the proton (p) and neutron (n) are uud and udd, respectively. Antibaryons are made up of three antiquarks. For example, the quark contents of the antiproton ($\bar{p}$) and antineutron ($\bar{n}$) are $\bar{u}\bar{u}\bar{d}$ and $\bar{u}\bar{d}\bar{d}$, respectively. Mesons are made up of a quark and an antiquark. For example, the quark contents of the pions π^+, π^-, and π^0 are $u\bar{d}$, $\bar{u}d$, and $(u\bar{u} + d\bar{d})/\sqrt{2}$. The quark content of π^0 implies that it spends half the time as $u\bar{u}$ and the other half as $d\bar{d}$. Mesons containing an s or $\bar{s}$ and a lighter quark are called strange mesons or K mesons. Mesons containing a c or $\bar{c}$ and a lighter quark are called charm mesons or D mesons. Mesons containing a b or $\bar{b}$ and a lighter quark are called bottom mesons or B mesons. Almost all the known hadrons have been identified definitively as baryons, antibaryons, or $q\bar{q}$ mesons.

Baryons, antibaryons, and $q\bar{q}$ mesons are not the only kinds of hadrons allowed by QCD. Any color-singlet combination of quarks, antiquarks, and gluons can have finite energy and therefore could conceivably form a hadron. The simplest color-singlet combinations other than $q\bar{q}$ mesons would be glueballs with constituents gg and ggg, hybrid mesons with constituents $q\bar{q}g$, and $qq\bar{q}\bar{q}$ mesons. Whether such a configuration can actually form a single particle that we would identify as a hadron or whether it would immediately decay into several separate hadrons is a detailed question that is in principle answered by QCD. However, we are unable to answer such questions in practice, because QCD is such a complicated theory and because methods for calculating its consequences are still at a relatively primitive stage of development. The most powerful method that is currently available is lattice gauge theory, which involves numerical simulations of QCD on a discrete space-time lattice. This method was invented by Ken Wilson in 1974 [1], but only in recent years have computer technology and theoretical methods advanced to the point where lattice

gauge theory can be used to calculate selected quantities in QCD with few percent accuracy [2]. Lattice gauge theory may eventually be able to address the question of whether there are any hadrons other than baryons, antibaryons, and $q\bar{q}$ mesons.

Another class of hadrons is hadronic molecules whose constituents are mesons and baryons. Ordinary molecules consist of electrically neutral atoms bound together by the electric force between the electrically charged constituents of the atoms. Hadronic molecules consist of color-singlet hadrons bound together by the QCD force between their colored constituents. Baryonic molecules definitely exist. The simplest baryonic molecule is the deuteron, which consists of a proton and a neutron. The heavier nuclei, which are bound states of more protons and neutrons, can also be interpreted as baryonic molecules. Mesonic molecules have been searched for for a long time [3, 4]. There are a few mesons that have not been identified definitively as $q\bar{q}$ mesons. Some researchers have proposed that some of these mesons can be interpreted as $K\bar{K}$ molecules, whose constituents are two strange mesons. However, this interpretation is not universally accepted. To date, no mesonic molecules have been unambiguously identified in experiments.

The existence of charm meson molecules, whose constituents are two charm mesons, was predicted not long after the discovery of the charm quark in 1974. In this thesis, we explore the possibility that a recently discovered particle called the $X(3872)$ is actually a charm meson molecule. Among the lowest mass charm mesons are the D^0 and D^{*0} mesons, which have quark content $c\bar{u}$, and the $\bar{D}^0$ and $\bar{D}^{*0}$ mesons, which have quark content $\bar{c}u$. The superscripts 0 imply that these mesons have 0 electric charge. The D^0 and $\bar{D}^0$ have spin 0 and the D^{*0} and $\bar{D}^{*0}$ have spin 1. The overline on each letter implies that the particle is the antiparticle of the one without the overline.

We will present the case that the $X(3872)$ is a hadronic molecule with hadron content $(D^0\bar{D}^{*0} + D^{*0}\bar{D}^0)/\sqrt{2}$. This implies that the $X(3872)$ spends half its time as a $D^0\bar{D}^{*0}$ molecule and half its time as a $D^{*0}\bar{D}^0$ molecule. If this interpretation of the $X(3872)$ proves to be correct, it is a hadron whose fundamental constituents are $cu\bar{c}\bar{u}$. It will be the first $qq\bar{q}\bar{q}$ meson to have been unambiguously identified.

In addition to charm mesons, we are going to deal with many other types of mesons in this thesis. For the convenience of the reader, their quark contents and their approximate masses in MeV are listed in Table 1.1. For each meson, we give its spin quantum number J and its parity quantum number P, which can be $+$ or $-$. For those mesons that are their own antiparticles, we also give the charge conjugation quantum number C, which can be $+$ or $-$. These quantum numbers are conventionally expressed using the notation J^{PC}.

Throughout this thesis, we use the natural units that are commonly employed in particle physics. In these units, $\hbar = c = 1$, where $\hbar$ is Plank's constant h divided by 2π and c is the speed of light. We quantify energy in units of electron volts or eV for short, where the e stands for the magnitude of the electron charge. An eV is the amount of work necessary to move one electron across a potential of one volt. This is a convenient unit because particle experiments use electric potentials to accelerate electrons and other particles, and smash them together to create new particles. With natural units, mass and momentum have the same unit eV as energy, while length and time have the unit eV^{-1} of inverse energy. We use the abbreviations keV, MeV, and GeV for 10^3 eV, 10^6 eV, and 10^9 eV, respectively.

Meson	Quark Content	Mass (MeV)	J^{PC}
Ordinary mesons			
π^+	$u\overline{d}$	140	0^-
π^-	$\overline{u}d$	140	0^-
π^0	$(\overline{u}u - \overline{d}d)/\sqrt{2}$	135	0^{-+}
ρ^+	$u\overline{d}$	776	1^-
ρ^-	$\overline{u}d$	776	1^-
ρ^0	$(\overline{u}u - \overline{d}d)/\sqrt{2}$	776	1^{--}
ω	$(\overline{u}u + \overline{d}d)/\sqrt{2}$	783	1^{--}
Strange mesons			
K^+	$s\overline{d}$	494	0^-
K^-	$\overline{s}d$	494	0^-
K^0	$s\overline{u}$	498	0^-
$\bar{K}^0$	$\overline{s}u$	498	0^-
K^{*+}	$s\overline{d}$	892	1^-
K^{*-}	$\overline{s}d$	892	1^-
K^{*0}	$s\overline{u}$	896	1^-
$\bar{K}^{*0}$	$\overline{s}u$	896	1^-
Charm mesons			
D^+	$c\overline{d}$	1869	0^-
D^-	$\overline{c}d$	1869	0^-
D^0	$c\overline{u}$	1865	0^-
$\bar{D}^0$	$\overline{c}u$	1895	0^-
D^{*+}	$c\overline{d}$	2010	1^-
D^{*-}	$\overline{c}d$	2010	1^-
D^{*0}	$c\overline{u}$	2007	1^-
$\bar{D}^{*0}$	$\overline{c}u$	2007	1^-
Bottom mesons			
B^+	$b\overline{d}$	5279	0^-
B^-	$\overline{b}d$	5279	0^-
B^0	$b\overline{u}$	5279	0^-
$\bar{B}^0$	$\overline{b}u$	5279	0^-
Charmonium			
J/ψ	$\overline{c}c$	3097	1^{--}
$\psi(2S)$	$\overline{c}c$	3686	1^{--}
χ_{c1}	$\overline{c}c$	3511	1^{++}

Table 1.1: Mesons that appear in this thesis, together with their quark contents, masses, and J^P or J^{PC} quantum numbers. The list includes only three charmonium states. Several other charmonium states are mentioned briefly in Section 1.4.1.

1.2 Discovery of the $X(3872)$

The $X(3872)$ is a narrow resonance discovered by the Belle collaboration in summer 2003 [5]. It was observed through the decay $B^{\pm} \to K^{\pm} J/\psi \pi^+\pi^-$. The invariant mass distribution for $J/\psi \pi^+\pi^-$ has a peak at about 3872 MeV, which implies that the $X(3872)$ is produced via $B^{\pm} \to XK^{\pm}$ and it then decays via $X \to J/\psi \pi^+\pi^-$. The upper limit on its width is very narrow, or equivalently, the lifetime of the X is much longer than expected. Followed the discovery by Belle, the CDF and DØ collaborations observed the X by producing it in proton-antiproton collisions and observing it through the decay $X \to J/\psi \pi^+\pi^-$ [6, 7]. The Babar collaboration has also confirmed the existence of the X through the discovery channel consisting of the decay $B^{\pm} \to XK^{\pm}$ followed by $X \to J/\psi \pi^+\pi^-$ [8].

The discovery mode mentioned above can be expressed schematically in terms of the quark contents of the hadrons: $(\bar{b}u) \to X + (\bar{s}u)$ followed by $X \to (c\bar{c}) + (u\bar{d}) + (\bar{u}d)$. The first sequence of the decay chain involves the decay of the $\bar{b}$ quark into the 3 quark state $\bar{c} + c + \bar{s}$ by the weak interactions. It can also involve QCD interactions, which can not change quark flavors but can create a quark-antiquark pair with the same flavor. The second sequence of the decay chain involves only the QCD interactions. Since both the c and $\bar{c}$ quarks are too heavy to be created in the decay of X, they must have already existed as constituents of the X. The X can also have additional constituents that are created by the QCD interactions such as a gluon or a $u\bar{u}$ pair or a $d\bar{d}$ pair.

For about a year, the only observed decay mode of the X was the discovery mode $J/\psi \pi^+\pi^-$, although experiments had put upper limits on various decay modes. In summer 2004, the Belle collaboration gave a preliminary result for a second decay

mode: $X \to J/\psi\,\pi^+\pi^-\pi^0$ [9]. In May 2005, the same collaboration announced evidence for a third decay mode: $X \to J/\psi\,\gamma$ [10]. In the decay modes $X \to J/\psi\,\pi^+\pi^-$ and $X \to J/\psi\,\pi^+\pi^-\pi^0$, the invariant mass distributions seem to peak near their upper kinematic endpoint of about 770 MeV, which suggests that these decays proceed predominantly through $X \to J/\psi\,\rho^{0*}$ and $X \to J/\psi\,\omega^*$, where the superscript * indicates a virtual particle, followed by the decays of the ρ^{0*} and the ω^* into pions. The branching fractions of the X into $J/\psi\,\pi^+\pi^-$ and $J/\psi\,\pi^+\pi^-\pi^0$ were found to be almost equal.

Soon after the discovery of the $X(3872)$, people noticed a curious fact: its mass is extremely close to the sum of the D^0 mass and the $\bar{D}^{*0}$ mass, which is about 3872 MeV. This fact immediately drove several authors to investigate the possibility that $X(3872)$ is a weakly-bound molecule of the charm mesons $D^0\bar{D}^{*0}$ and $D^{*0}\bar{D}^0$. The energy of a molecule is less than the total mass of its constituents. The difference between these energies is called the binding energy. If the X is indeed a mesonic molecule, the proximity of mass of the X to the $D^0\bar{D}^{*0}$ threshold implies that its binding energy is extremely small compared to any other relevant energy scale.

1.3 Quantum numbers and width of the $X(3872)$

Determining the spin, parity, and charge-conjugation quantum numbers J^{PC} of the $X(3872)$ from experiments can also be used to narrow down the various possible interpretations of the $X(3872)$. In this section, we determine the J^{PC} quantum numbers that are consistent with the narrowness and observed decay modes of the X.

The mass of the $X(3872)$ is about 140 MeV above the $D^0\bar{D}^0$ threshold at 3729.2 ± 1.0 MeV and the D^+D^- threshold at 3738.8 ± 1.0 MeV. The upper limit on the width of the X is 2.3 MeV at 90% confidence level. This is narrow compared to the widths of other charmonium states above the $D\bar{D}$ threshold. For example, the widths of the $\psi(3770)$ and the $\psi(4040)$ are 23.6 ± 2.7 MeV and 52 ± 10 MeV, respectively. Decays into $D\bar{D}$ pairs dominate the widths of $\psi(3770)$ and $\psi(4040)$. Thus the decay mode $X \to D\bar{D}$ must either be forbidden by its quantum numbers or suppressed by some dynamical mechanism. An example of a dynamical mechanism is an angular momentum barrier. If the X consists of two constituents with orbital angular momentum quantum number L, the wavefunction for the constituents to have small separation r is suppressed by a factor of r^L. If the decay requires these constituents to come close together, the rate will be suppressed by this factor.

The D and $\bar{D}$ have spin-parity quantum numbers $J^P = 0^-$. The parity and charge conjugation quantum numbers of a $D\bar{D}$ system with orbital angular momentum quantum number $L = 0, 1, 2, \cdots$ are $P = (-1)^L$ and $C = (-1)^L$. Thus a $D\bar{D}$ system can have spin-parity-charge conjugation quantum numbers in the sequence

$$J^{PC} = 0^{++}, 1^{--}, 2^{++}, \cdots . \tag{1.1}$$

The decay $X \to D\bar{D}$ would be forbidden by the parity conservation of the strong interactions if the quantum numbers of the X were in the sequence

$$J^{PC} = 0^{-\pm}, 1^{+\pm}, 2^{-\pm}, \cdots . \tag{1.2}$$

The decay $X \to D\bar{D}$ would be allowed by parity but forbidden by the charge conjugation symmetry of the strong interactions if the quantum numbers of the X were in

the sequence

$$J^{PC} = 0^{+-}, 1^{-+}, 2^{+-}, \cdots . \tag{1.3}$$

The narrow width of X and the nonobservation of $X \to D\bar{D}$ decay mode can be explained if its quantum numbers are either in the sequence in Eq. (1.2) or in the sequence in Eq. (1.3) or else in the sequence in Eq. (1.1) provided the constituents of X have sufficiently large orbital angular momentum quantum number L.

Since the J/ψ and γ both have $J^{PC} = 1^{--}$, a $J/\psi\,\gamma$ system can have quantum numbers $J^{PC} = 0^{\pm+}, 1^{\pm+}, 2^{\pm+}, \cdots$. The evidence for the radiative decay mode $X \to J/\psi\,\gamma$ experimentally establishes that X has positive charge conjugation [10].

The possible J^{PC} quantum numbers can be further constrained by measurements of angular distributions in the decays of the X [11, 12, 13, 14, 15]. The Belle collaboration has studied the angular distributions for the decays $X \to J/\psi\,\pi^+\pi^-$. They ruled out all J^{P+} assignments with $J \leq 2$ other than 1^{++} and 2^{++} [15]. The most favorable choice is 1^{++}.

1.4 Interpretations of the $X(3872)$

The most predictive interpretations of $X(3872)$ are a charmonium state with constituents $c\bar{c}$ or a hadronic molecule with constituents DD^*. Several other interpretations have also been proposed. We briefly describe all these options in this section.

1.4.1 Charmonium

The fact that the observed decay modes of the X include J/ψ, which has constituents c and $\bar{c}$, motivates its interpretation as a charmonium with constituents c and

$^{2S+1}L_J$	J^{PC}	Notation
$^1S_0$	0^{-+}	$\eta_c(nS)$
$^3S_1$	1^{--}	$J/\psi(1S)$, $\psi(nS)$
$^1P_1$	1^{+-}	$h_c(nP)$
$^3P_{J=\{0,1,2\}}$	$(0,1,2)^{++}$	$\chi_{cJ}(nP)$
$^1D_2$	2^{-+}	$\eta_{c2}(nD)$
$^3D_{J=\{1,2,3\}}$	$(1,2,3)^{--}$	$\psi_J(nD)$

Table 1.2: Standard nomenclature for charmonia. In the notation nL, $n = 1, 2, 3, \cdots$ is the radial excitation quantum number and $L = \mathrm{S}, \mathrm{P}, \mathrm{D}, \cdots$ specifies the orbital angular momentum quantum number $0, 1, 2 \cdots$. The $\psi_1(nD)$ with $J^{PC} = 1^{--}$ is often referred to as $\psi(nD)$ without its subscript.

$\bar{c}$. The charmonium options has been investigated in detail to examine whether any of missing charmonium states can possibly be identified as the X [16, 17, 18, 19, 20].

Charmonium is the bound state of the charm quark c and its antiparticle $\bar{c}$. In general quarkonium levels are specified by the set of quantum numbers n, S, L, and J, where n, S, L, and J are the radial excitation, total spin, orbital angular momentum, and total angular momentum quantum numbers, respectively. The angular momentum quantum numbers are usually specified using the spectroscopic notation $^{2S+1}L_J$. In terms of L and S, the J^{PC} quantum numbers are given by $J = L$ if $S = 0$, $J = |L - 1|$, L, or $L + 1$ if $S = 1$, $P = (-1)^{L+1}$, and $C = (-1)^{L+S}$. Table 1.2 gives the standard nomenclature for charmonium states with $L \leq 2$.

All members of the ground-state S-wave multiplet ($1S$), the ground-state P-wave multiplet ($1P$), and the first excited S-wave multiplet ($2S$) have been observed. Evidence for the $h_c(1P)$, the last member of the $1P$ multiplet, was recently reported by the CLEO [21] and FNAL-E835 collaborations [22]. The $\eta_c(2S)$, the last member of the $2S$ multiplet, has been observed only recently in Refs. [23, 24, 25]. The other

charmonium states that have been observed were seen as resonances in e^+e^- collisions and have quantum numbers $J^{PC} = 1^{--}$. The $\psi(3770)$ is usually interpreted as a ground D-wave state, $1\,^3D_1$. The $\psi(4040)$, $\psi(4160)$, and $\psi(4415)$ are usually interpreted as $3\,^3S_1$, $2\,^3D_1$, and $4\,^3S_1$ charmonium states. Those charmonium states that have been already observed are of course ruled out as candidates for the $X(3872)$.

The possible charmonium candidates for the X include members of the multiplet of the first radial excitation of P-wave charmonium, $h_c(2P)$ and $\chi_{cJ}(2P)$, $J = 0, 1, 2$, and members of the multiplet of ground-state D-wave charmonium, $\eta_{c2}(1D)$ and $\psi_J(1D)$, $J = 1, 2, 3$. The $\psi_1(1D)$ is ruled out, since it has been observed with mass 3770 MeV. The ground-state F-wave charmonia are less likely candidates for X because their masses are expected to be much higher than 3872 MeV. The radially excited S-wave charmonium $\eta_c(3S)$ is ruled out because its width should be greater than the widths of $\eta_c(1S)$ and $\eta_c(2S)$, which are about 20 MeV.

The mass spectrum of the observed charmonium systems are well described by nonrelativistic potential models. It is tempting to compare their predictions to the observed masses of the X. In Table 1.3, we give the predictions of a model by Eichten, Lane, and Quigg (ELQ) and a model by Godfrey and Isgur (GI). The former includes coupled-channel effects among charmonium states and charm meson pairs. The model by Godfrey and Isgur is a relativistic potential model. The masses of 2P charmonium states tend to be above 3872 MeV, and the masses of 1D states tend to be below 3872 MeV. In both models, the state whose predicted mass is closest to 3872 MeV is the $\psi_3(1D)$. A few predictions by quenched lattice QCD simulations are currently available for 1D and 2P states, but they have with large errors of roughly $\pm$100 MeV [26, 27].

State	$n\,^{2S+1}L_J$	J^{PC}	Mass (MeV)	
			ELQ model [18]	GI model [28]
$h_c(2P)$	2^1P_1	1^{+-}	3968.0	3956.0
$\chi_{c0}(2P)$	2^3P_0	0^{++}	3931.9	3916.0
$\chi_{c1}(2P)$	2^3P_1	1^{++}	4007.5	3953.0
$\chi_{c2}(2P)$	2^3P_2	2^{++}	3966.5	3979.0
$\eta_{c2}(1D)$	1^1D_2	2^{-+}	3838.0	3837.0
$\psi_1(1D)$	1^3D_1	1^{--}	(3769.9)	3819.0
$\psi_2(1D)$	1^3D_2	2^{--}	3830.6	3838.0
$\psi_3(1D)$	1^3D_3	3^{--}	3868.3	3849.0

Table 1.3: Potential model predictions for masses of 1D and 2P states. In the ELQ potential model, the value of the 1^3D_1 state is an input.

The experimental observation of $X \to J/\psi\,\gamma$ unambiguously eliminates all $C = -$ charmonium candidates. The narrowness of the X can be explained by the parity symmetry of the strong interactions, which constrains the J^{PC} quantum numbers to the list in Eq. (1.2), or by the charge conjugation symmetry of the strong interactions, which constrains J^{PC} to the list in Eq. (1.3). There are no $2P$ or $1D$ charmonium states with $C = +$ and J^{PC} in the list in Eq. (1.3). The $2P$ and $1D$ charmonium candidates with $C = +$ and J^{PC} in the list in Eq. (1.2) are the $\chi_{c1}(2P)$ with $J^{PC} = 1^{++}$ and the $\eta_{c2}(1D)$ with $J^{PC} = 2^{-+}$. The $\eta_{c2}(1D)$ is ruled out by measurements of angular distributions in the decay $X \to J/\psi\,\pi^+\pi^-$ [15]. Thus the only charmonium candidate that remains is $\chi_{c1}(2P)$.

Further evidence against charmonium interpretations of the $X(3872)$ comes from the approximate isospin symmetry of the strong interactions. Any charmonium state has isospin 0. Measurements of the $\pi^+\pi^-$ invariant mass distribution for the discovery mode $X \to J/\psi\,\pi^+\pi^-$ by the Belle and the CDF collaborations imply that the $\pi^+\pi^-$

comes from a virtual ρ resonance, which has isospin 1. Since the J/ψ has isospin 0, the $J/\psi\,\rho^*$ system has isospin 1. If the X is a charmonium state with isospin 0, the discovery mode must proceed through an isospin-violating process. The only observed isospin-violating charmonium decay is $\psi(2S) \to \eta_c\,\pi^0$ with partial decay width ~ 0.3 keV and branching fraction $\sim 0.1\%$. If the X is a charmonium, we expect isospin-violating modes to have small branching fractions compared to isospin-conserving decay modes. However, the branching fraction of the discovery mode is approximately equal to that of $X \to J/\psi\,\pi^+\pi^-\pi^0$. This is an isospin-conserving decay mode because the $\pi^+\pi^-\pi^0$ are dominated by a virtual ω resonance, which has isospin 0. The large violation of isospin symmetry disfavors all $C = +$ charmonium states with the exception of $\chi_{c1}(2P)$. This state is special, because it can have resonant S-wave interactions with $D^0\bar{D}^{*0}$ that transform it into a charm meson molecule.

1.4.2 Charm meson molecules

The option of a charm meson molecule is motivated by the proximity of the X to the threshold for the charm mesons D^0 and $\bar{D}^{*0}$ [29, 30, 31, 32, 33]. The measured mass of the X coincides with the $D^0\bar{D}^{*0}$ threshold energy to within experimental errors. Since the X has charge conjugation $C = +$, it could be a hadronic molecule with constituents $(D^0\bar{D}^{*0} + D^{*0}\bar{D}^0)/\sqrt{2}$. We will refer to such a state as a DD^* molecule.

The possibility that a charm meson and an anticharm meson might form molecular states was considered shortly after the discovery of charm in 1974 [34, 35, 36, 37]. The first quantitative study of the possibility of molecular states of charm mesons was carried out by Törnqvist in 1993 using a one-pion-exchange potential model.

Constituents	J^{PC}	Mass (MeV)
$D\bar{D}^*$	0^{-+}	≈ 3870
$D\bar{D}^*$	1^{++}	≈ 3870
$D^*\bar{D}^*$	0^{++}	≈ 4015
$D^*\bar{D}^*$	0^{-+}	≈ 4015
$D^*\bar{D}^*$	1^{+-}	≈ 4015
$D^*\bar{D}^*$	2^{++}	≈ 4015

Table 1.4: Possible weakly-bound states of charm mesons due to the one-pion-exchange potential [38].

He found that there could be weakly-bound states in various isospin-0 channels [38]. Note that the one-pion-exchange potential must be regulated at short distances by introducing an ultraviolet cutoff. Thus the binding energies in this model can only be predicted approximately, because they depend upon the choice of the cutoff. There are no $D\bar{D}$ bound states because of the absence of a one-pion-exchange interaction between D and $\bar{D}$. The channels that are possibly bound by a one-pion-exchange potential are given in Table 1.4. In the case of $D\bar{D}^*$ molecules, the possible channels have isospin 0 and charge conjugation +, which corresponds to the particle content

$$|D\bar{D}^*\rangle_{I=0,C=+} = \frac{1}{2}\left(|D^0\bar{D}^{*0}\rangle + |D^{*0}\bar{D}^0\rangle + |D^+D^{*-}\rangle + |D^{*+}D^-\rangle\right). \tag{1.4}$$

Since the binding energy is small compared to the 8.4 MeV splitting between the $D^0\bar{D}^{*0}$ threshold and the D^+D^{*-} threshold, there are large isospin breaking effects [29, 39]. After the discovery of the $X(3872)$, Swanson considered a potential model that includes both one-pion-exchange and quark-exchange potentials, and found that the $C = +$ superposition of $D^0\bar{D}^{*0}$ and $D^{*0}\bar{D}^0$ could form a weakly-bound state in

the S-wave 1^{++} channel [33]. Its particle content is

$$|X\rangle = \frac{1}{\sqrt{2}}\left(|D^0\bar{D}^{*0}\rangle + |D^{*0}\bar{D}^0\rangle\right). \tag{1.5}$$

Another mechanism for generating a DD^* molecule is the accidental fine-tuning of the mass of the $\chi_{c1}(2P)$ or $h_c(2P)$ to the $D^0\bar{D}^{*0}/D^{*0}\bar{D}^0$ threshold which creates a DD^* molecule with quantum number 1^{++} or 1^{+-}, respectively [32].

The identification of the observed modes as $X \to J/\psi\,\rho^*$ and $X \to J/\psi\,\omega^*$ is compatible with the interpretation of $X(3872)$ as an S-wave $D^0\bar{D}^{*0}$ molecule with quantum numbers 1^{++}. The X is within 1 MeV of the $D^0\bar{D}^{*0}$ threshold and about 8 MeV below the D^+D^{*-} threshold. If it was a DD^* molecule, it would naturally be a superposition of states with isospins 0 and 1 with almost equal probabilities.

The assumption that the $X(3872)$ is a loosely-bound S-wave DD^* molecule is very predictive [40]. This assumption has been used by Voloshin to predict the rates and momentum distributions for the decays of X into $D^0\bar{D}^0\pi^0$ and $D^0\bar{D}^0\gamma$ [41]. It has also been used to calculate the rate for the exclusive decay of $\Upsilon(4S)$ into the X and two light hadrons [42], to estimate the decay rate for the discovery mode $B^+ \to XK^+$ [43], to predict the suppression of the decay rate for $B^0 \to XK^0$ [44], and to predict the line shape of the X [45]. We shall discuss the possibility of DD^* molecule in detail in the subsequent chapters.

1.4.3 Other options

Several other options for the $X(3872)$ have been proposed. One of them is also motivated by the proximity of its mass to the $D^0\bar{D}^{*0}$ threshold. Bugg has suggested that the X could be just an enhancement at the $D^0\bar{D}^{*0}$ threshold associated with a strong coupling to $D^0\bar{D}^{*0}$ or $D^{*0}\bar{D}^0$ [46, 47]. He referred to this possibility as a "cusp

state" because the line shape of the X has a cusp at the $D^0\bar{D}^{*0}$ threshold. Such cusp occurs if the binding energy of the $D^0\bar{D}^{*0}/D^{*0}\bar{D}^0$ system is small but negative, as we shall see explicitly in Chapter 5.

Other proposed interpretations of the $X(3872)$ include the following.

- A "hybrid charmonium" state with constituents $c\bar{c}g$ has been considered as an option for X in Ref. [48, 49]. These states can have exotic J^{PC} quantum numbers as shown in Eq. (1.3). A quenched lattice simulation in Ref. [50], for example, suggests that lowest hybrid charmonium states with exotic quantum numbers are 0^{+-}, 1^{-+}, and 2^{+-} with masses about 4.2 GeV. If the X is a hybrid charmonium, the discovery mode $X \to J/\psi\,\pi^+\pi^-$ comes predominantly from the decay $(c\bar{c}g) \to J/\psi\,gg$ followed by $gg \to \pi^+\pi^-$. The $\pi^+\pi^-$ system must therefore be an isoscalar, which implies that it has charge conjugation $+$. This is inconsistent with the fact that X has charge conjugation $+$, which requires the $\pi^+\pi^-$ to have charge conjugation $-$.

- A glueball with constituents ggg has been considered as an option for X in Ref. [51]. The proposed J^{PC} quantum numbers are 1^{--}. Such a vector glueball can mix with nearby vector charmonium states with $J^{PC} = 1^{--}$ and decay into the $J/\psi\,\pi^+\pi^-$ through the charmonium states. In the absence of such mixing, a lattice simulation predicts a 3-gluon glueball with $J^{PC} = 1^{--}$ and mass $3850 \pm 50 \pm 190$ MeV [52]. However, its mass also depends on unknown mixing parameters with charmonium states. The proposed $J^{PC} = 1^{--}$ glueball state is ruled out by the observation of $X \to J/\psi\,\gamma$ which implies $C = +$.

- A tetraquark with constituents $c\bar{c}q\bar{q}$ [53] or a diquark-antidiquark bound state with constituents $cu + \bar{c}\bar{u}$ [54] have been considered as options for X. The authors of Ref. [53] argue that their predictions of masses for $I = 0$ and 1 components with constituents $c\bar{c}q\bar{q}$ are far below 3872 MeV and rule out the $J^P = 1^+$ tetraquark interpretation. The authors of Ref. [54] argue that the $X(3872)$ would be an admixture of bound states of $cu + \bar{c}\bar{u}$ and $cd + \bar{c}\bar{d}$ with $J^{PC} = 1^{++}$. They predict charged parters of the X: $cu + \bar{c}\bar{d}$ and $cd + \bar{c}\bar{u}$. The Babar collaboration has searched for them in vain and put upper limits on the productions of charged partners [55].

1.5 Thesis structure

In this thesis, we pursue the possibility that the $X(3872)$ is a loosely-bound S-wave DD^* molecule. We begin with a review of current experimental results in Chapter 2. In Chapter 3, we describe some of universal properties of the $X(3872)$. In Chapter 4, we discuss various scattering models with its possible fine-tuning mechanisms for large scattering lengths. In Chapter 5, we derive factorization formulas for the production and decay of the $X(3872)$ using an effective field theory with a large scattering length for the DD^* system. We predict the invariant mass distribution for $B \to D^0\bar{D}^{*0}K$ decays near the $D^0\bar{D}^{*0}$ threshold and the line shape of the X in B decays. In Chapter 6, we apply the factorization formulas developed in Chapter 5 to the exclusive production of the X in $B \to XK$. We estimate the short-distance amplitude in $B \to XK$ decays using data by the Babar collaboration on $B \to D^{(*)}\bar{D}^{(*)}K$ and we predict that the decay rate for $B^0 \to XK^0$ should be suppressed compared to $B^+ \to XK^+$. In Chapter 7, we study the decays of X into J/ψ and light hadrons. We

calculate the differential decay rates using the factorization formulas and an effective lagrangian for light pseudoscalar and vector mesons. We conclude with a discussion of our results in Chapter 8.

CHAPTER 2

EXPERIMENTAL RESULTS

The $X(3872)$ has been observed through exclusive production in $B^{\pm}$ decays and through inclusive production in proton-antiproton ($p\bar{p}$) collisions. So far its observed decay modes are $X \to J/\psi\,\pi^+\pi^-$, $X \to J/\psi\,\pi^+\pi^-\pi^0$, and $J/\psi\,\gamma$. Upper limits have been set on various other decay modes. These experimental results on $X(3872)$ are summarized in this chapter.

2.1 Observed decay modes

In summer 2003, the Belle collaboration announced the discovery of a new hadronic resonance with energy near 3872 MeV. Since the nature of this resonance was not known, it was given the temporary name $X(3872)$. The discovery was made using 152 million $B\bar{B}$ event sample collected at the KEKB asymmetric e^+e^- collider operating with center-of-mass energy 10.58 GeV corresponding to the $\Upsilon(4S)$ resonance. They observed a narrow peak in the $J/\psi\,\pi^+\pi^-$ invariant mass distribution from $B^{\pm}$ decay into $K^{\pm}J/\psi\,\pi^+\pi^-$ [5]. The J/ψ was identified by detecting the dilepton that arises from the process $J/\psi \to \ell^+\ell^-$, where ℓ represents the electron e or the muon μ. The peak in the $J/\psi\,\pi^+\pi^-$ invariant mass distributions indicates that the $X(3872)$ is produced by the decay $B^{\pm} \to XK^{\pm}$ and that it subsequently decays by $X \to J/\psi\,\pi^+\pi^-$.

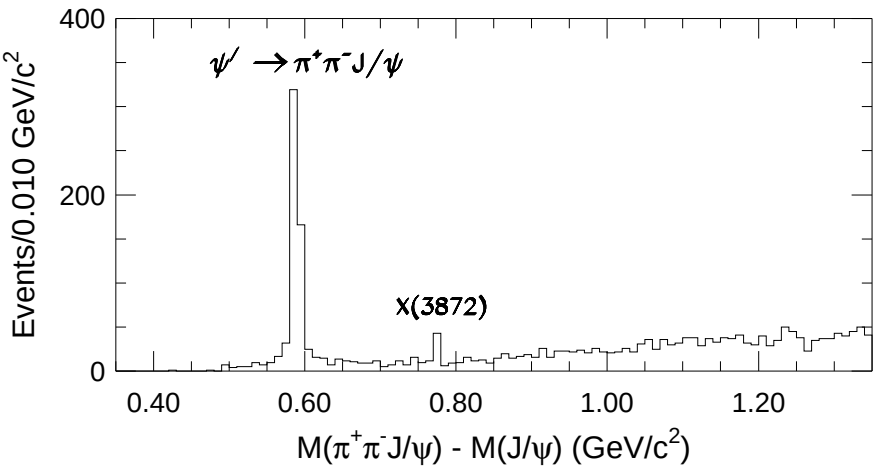

Figure 2.1: $M(J/\psi\,\pi^+\pi^-) - M(J/\psi)$ for $B^\pm \to K^\pm J/\psi\,\pi^+\pi^-$ seen in the Belle experiment. The large peak at 0.59 GeV corresponds to $B^\pm \to K^\pm\psi(2S)$ followed by $\psi(2S) \to J/\psi\pi^+\pi^-$. The small peak at 0.776 GeV is the signal for $X(3872) \to J/\psi\,\pi^+\pi^-$. Figure is taken from Ref. [16].

Fig. 2.1 shows the discovery mode. This discovery mode $B^\pm \to XK^\pm$ has been confirmed by the Babar collaboration at the PEP-II asymmetric e^+e^- collider [8]. The CDF and DØ collaborations have also observed the production of the $X(3872)$ in proton-antiproton ($p\bar{p}$) collisions at the Tevatron [6, 7].

The measurements of the mass of the $X(3872)$ by these experiments are shown in Table. 2.1. The combined averaged mass is [16]

$$m_X = 3871.9 \pm 0.5 \ \text{MeV}. \tag{2.1}$$

Note that the mass of the X is quite close to the $D^0\bar{D}^{*0}$ threshold, 3871.3 ± 1.0 MeV. The Belle collaboration has placed an upper limit on the full width of the $X(3872)$ [5]:

$$\Gamma < 2.3 \ \text{MeV} \quad (90\%\text{C.L.}). \tag{2.2}$$

	Mass (MeV)
Belle [5]	$3872.0 \pm 0.6 \pm 0.5$
Babar [8]	3873.4 ± 1.4
CDF [6]	$3871.3 \pm 0.7 \pm 0.4$
DØ[7]	$3871.8 \pm 3.1 \pm 3.0$

Table 2.1: Measured mass of the $X(3872)$. In each measurement, the first error is statistical error and the second is systematic error. Babar's result includes both statistical and systematic errors.

The decay into J/ψ suggests that the X could be a missing charmonium state, but its width is much narrower than other charmonium states above the $D\bar{D}$ threshold.

The product of the branching fractions associated with the discovery channel has been measured by the Belle and Babar collaborations: [5, 8, 16]

$$\mathrm{Br}[B^+ \to XK^+]\,\mathrm{Br}[X \to J/\psi\,\pi^+\pi^-] = (1.3 \pm 0.3) \times 10^{-5}. \tag{2.3}$$

The peak at $M(J/\psi\,\pi^+\pi^-) - M(J/\psi) = 0.59$ GeV in Fig. 2.1 corresponds to the decay $B^+ \to \psi(2S)K^+$ followed by $\psi(2S) \to J/\psi\,\pi^+\pi^-$. For comparison, the corresponding product of the branching fractions for the production of $\psi(2S)$ is [56]

$$\mathrm{Br}[B^+ \to \psi(2S)K^+]\,\mathrm{Br}[\psi(2S) \to J/\psi\,\pi^+\pi^-] = (2.2 \pm 0.1) \times 10^{-4}. \tag{2.4}$$

Comparing Eq. (2.3) by Eq. (2.4), we see that the product of the branching fractions for X is smaller than that for $\psi(2S)$ by about a factor of 20. In the decay $X \to J/\psi\,\pi^+\pi^-$, the invariant mass distribution of the two pions seems to peak near the upper endpoint as shown in Fig. 2.2 [57]. This suggests that they come from the decay of a virtual ρ^0 resonance.

The Belle collaboration recently observed the $X(3872)$ in a second decay mode: $X \to J/\psi\,\pi^+\pi^-\pi^0$ [57, 58]. The invariant mass distribution of the three pions is

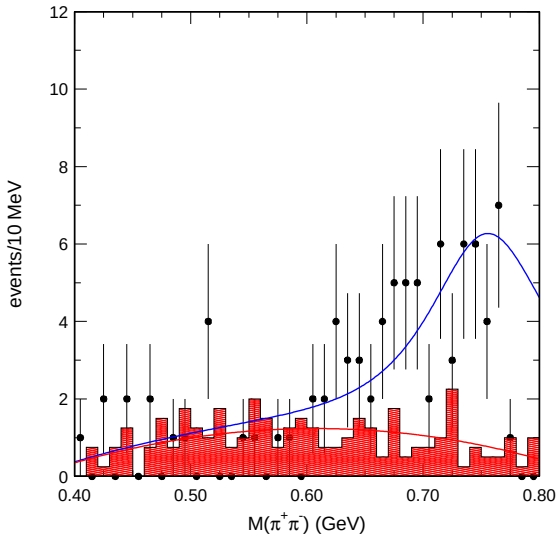

Figure 2.2: The dipion invariant mass $M(\pi^+\pi^-)$ distribution for events in the $X(3872)$ signal peak. The shaded histogram is the sideband-determined background; the curve is the result of a fit with a $\rho \to \pi^+\pi^-$ line shape. Figure is taken from Ref. [58].

dominated by a virtual ω resonance. The branching ratio relative to the discovery decay channel is [10]

$$\frac{\mathrm{Br}[X \to J/\psi\,\pi^+\pi^-\pi^0]}{\mathrm{Br}[X \to J/\psi\,\pi^+\pi^-]} = 1.0 \pm 0.4_{\mathrm{stat}} \pm 0.3_{\mathrm{syst}}. \tag{2.5}$$

The J/ψ is an isosinglet, while the ρ and ω have isospin 1 and 0, respectively. If the $X(3872)$ had definite isospin quantum number and if the observed decay modes have been correctly interpreted as $X \to J/\psi\,\rho^*$ and $X \to J/\psi\,\omega^*$, the roughly equal branching fractions in Eq. (2.5) would imply large isospin violations. Since conventional charmonium states have isospin 0, the measurement in Eq. (2.5) casts doubt on any interpretation of X as a missing charmonium state.

The Belle collaboration has recently reported evidence for another decay mode: $X \to J/\psi\,\gamma$ [15]. The product of the branching fractions for the production and decay processes is

$$\mathrm{Br}[B^+ \to X K^+]\,\mathrm{Br}[X \to J/\psi\,\gamma] = (1.8 \pm 0.6_{\mathrm{stat}} \pm 0.1_{\mathrm{syst}}) \times 10^{-5}. \tag{2.6}$$

The corresponding branching ratio relative to the discovery decay channel is

$$\frac{\mathrm{Br}[X \to J/\psi\,\gamma]}{\mathrm{Br}[X \to J/\psi\,\pi^+\pi^-]} = 0.14 \pm 0.05. \tag{2.7}$$

The decay $X \to J/\psi\,\gamma$ establishes that the charge conjugation quantum number of the X must be even ($C = +$). This unambiguously eliminates all the $C = -$ interpretations for the X. The result also implies that the pions in $X \to J/\psi\,\pi^+\pi^-$ and $X \to J/\psi\,\pi^+\pi^-\pi^0$ are in $C = +$ states, which provides further support for their coming from decays of virtual ρ and ω mesons, respectively.

2.2 Upper limits on other decay modes

Upper limits have been placed on the branching fractions for other decay modes of the X, including $D^0\bar{D}^0$, D^+D^-, $D^0\bar{D}^0\pi^0$ [59], $\chi_{c1}\gamma$, $\chi_{c2}\gamma$, $J/\psi\,\pi^0\pi^0$ [57], and $J/\psi\,\eta$ [60]. Upper limits have also been placed on the partial widths for the decay of $X(3872)$ into e^+e^- [61, 62] and into $\gamma\gamma$ [62]. Measurements of these upper limits are summarized in this section.

Nonobservation of the decay of X into open charm is important to narrow down the possible interpretations of the X. The Belle collaboration has put upper limits on the product of the branching fractions of $B^+ \to X K^+$ and $X \to D\bar{D}$, where D is

either D^+ or D^0 [59]:

$$\mathrm{Br}[B^+ \to XK^+]\mathrm{Br}[X \to D^0\bar{D}^0] < 6 \times 10^{-5} \quad (90\%\ \mathrm{C.L.}), \tag{2.8}$$

$$\mathrm{Br}[B^+ \to XK^+]\mathrm{Br}[X \to D^+D^-] < 4 \times 10^{-5} \quad (90\%\ \mathrm{C.L.}). \tag{2.9}$$

It has also put an upper limit on the product of the branching fractions of $B^+ \to XK^+$ and $X \to D^0\bar{D}^0\pi^0$ [59]:

$$\mathrm{Br}[B^+ \to XK^+]\mathrm{Br}[X \to D^0\bar{D}^0\pi^0] < 6 \times 10^{-5} \quad (90\%\ \mathrm{C.L.}). \tag{2.10}$$

If the mass of the X is above the $D^0\bar{D}^{*0}$ threshold, the decay of X into $D^0\bar{D}^0\pi^0$ could proceed through the decay $X \to D^0\bar{D}^{*0}$ followed by the decay $\bar{D}^{*0} \to \bar{D}^0\pi^0$ or by the decay $X \to D^{*0}\bar{D}^0$ followed by the decay $D^{*0} \to D^0\pi^0$. In this case, the constraint in Eq. (2.10) also provides a constraint on the branching fractions for decays into $D^0\bar{D}^{*0}$ and $D^{*0}\bar{D}^0$.

The only observed radiative decay mode of the X is $X \to J/\psi\,\gamma$. The Belle collaboration has put upper limits on the radiative decay rates of the X into another charmonium states:

$$\frac{\mathrm{Br}[X \to \gamma\chi_{c1}]}{\mathrm{Br}[X \to J/\psi\,\pi^+\pi^-]} < 0.89 \quad (90\%\ \mathrm{C.L.}), \tag{2.11}$$

$$\frac{\mathrm{Br}[X \to \gamma\chi_{c2}]}{\mathrm{Br}[X \to J/\psi\,\pi^+\pi^-]} < 1.1 \quad (90\%\ \mathrm{C.L.}). \tag{2.12}$$

The Belle collaboration has given an upper limit on the decay rate of X into $J/\psi\,\pi^0\pi^0$ in the following form:

$$\frac{\mathrm{Br}[X \to J/\psi\,\pi^0\pi^0]}{\mathrm{Br}[X \to J/\psi\,\pi^+\pi^-]} < 1.3\,\frac{\mathrm{Br}[\psi(2S) \to J/\psi\,\pi^0\pi^0]}{\mathrm{Br}[\psi(2S) \to J/\psi\,\pi^+\pi^-]} \quad (90\%\ \mathrm{C.L.}). \tag{2.13}$$

If we use the Particle Data Group (PDG) central values for the $\psi(2S)$ branching fractions [56], the right side of Eq. (2.13) becomes 0.77. Nonobservation of $X \to$

$J/\psi\,\pi^0\pi^0$ would be consistent with the pions in the decay $X \to J/\psi\,\pi^+\pi^-$ coming from a virtual ρ resonance. However the current upper limit of Eq. (2.13) is not strong enough to constrain this possibility.

The Babar collaboration has put an upper limit on the product of branching fractions of $B^+ \to XK^+$ and $X \to J/\psi\,\eta$ [60]:

$$\mathrm{Br}[B^+ \to XK^+]\mathrm{Br}[X \to J/\psi\,\eta] < 7.7 \times 10^{-6} \quad (90\%\ \mathrm{C.L.}). \tag{2.14}$$

The BES collaboration has searched for $\psi(2S)$ produced only in association with an energetic photon resulting from initial state radiation (ISR) in e^+e^- annihilation at center-of-mass energy of 4.03 GeV at the Beijing Electron Positron Collider (BEPS) [63]. ISR resonance production occurs when the invariant mass of the initial e^+e^- system is lowered to a resonance by emitting a hard photon from the initial electron or positron. The process is therefore $e^+e^- \to \gamma\,e^+e^-$ followed by $e^+e^- \to X$. Yuan, Mo, and Wang used the same ISR data sample to set an upper limit on the partial decay width of the X into e^+e^-:

$$\Gamma[X \to e^+e^-]\mathrm{Br}[X \to J/\psi\ \pi^+\pi^-] < 10\ \mathrm{eV} \quad (90\%\ \mathrm{C.L.}). \tag{2.15}$$

This constraint is relevant if the X has quantum numbers $J^{PC} = 1^{--}$.

The CLEO collaboration has also searched for the X from initial state radiation (ISR) resonance production and from resonance production by untagged $\gamma\gamma$ fusion using the CLEO III detector. Using its ISR data sample, CLEO set an upper limit on the partial decay width of X into e^+e^-:

$$\Gamma[X \to e^+e^-]\mathrm{Br}[X \to J/\psi\ \pi^+\pi^-] < 8.0\ \mathrm{eV} \quad (90\%\ \mathrm{C.L.}). \tag{2.16}$$

This limit is consistent with the limit by Yuan, Mo, and Wang in Eq. (2.15). Resonance production by $\gamma\gamma$ fusion occurs when the incident electron and positron both

emit a photon and the two photons annihilate into a resonance. The process is therefore $e^+e^- \to e^+e^-\gamma\gamma$ followed by $\gamma\gamma \to X$. Untagged $\gamma\gamma$ fusion means that the scattered electron and positron are not detected. Using its untagged $\gamma\gamma$ fusion sample, CLEO set an upper limit on the partial decay width of the X into $\gamma\gamma$:

$$(2J+1)\Gamma[X \to \gamma\gamma]\mathrm{Br}[X \to J/\psi\,\pi^+\pi^-] < 12.9\ \mathrm{eV}\ \ (90\%\ \mathrm{C.L.}), \tag{2.17}$$

where J is the spin quantum number of the X. This constraint is relevant if the X has quantum numbers $J^{PC} = 0^{++}, 2^{++}, 3^{++}, \cdots$. If the X has quantum numbers 1^{++}, the decay $X \to \gamma\gamma$ is forbidden by Yang's theorem.

The Babar collaboration has searched for a charged partner $X^\pm$ of the X through the decays $B^\pm \to X^\pm K^0_S$ and $B^0/\bar{B}^0 \to X^\pm K^\mp$ followed by the decay $X^\pm \to J/\psi\,\pi^\pm\pi^0$ [55]. The possibility of such a charged partner of the X was excluded by Babar's upper limit on the product of branching fractions:

$$\mathrm{Br}[B^\pm \to X^\pm K^0_S]\,\mathrm{Br}[X^\pm \to J/\psi\,\pi^\pm\pi^0] < 1.1 \times 10^{-6}\ \ (90\%\ \mathrm{C.L.}), \tag{2.18}$$

$$\mathrm{Br}[B^0/\bar{B}^0 \to X^\pm K^\mp]\,\mathrm{Br}[X^\pm \to J/\psi\,\pi^\pm\pi^0] < 5.2 \times 10^{-6}\ \ (90\%\ \mathrm{C.L.}). \tag{2.19}$$

It is convenient to express the upper limits on the decay modes of X in terms of the branching ratio $R[X \to h]$ defined by

$$R[X \to h] \equiv \frac{\mathrm{Br}[X \to h]}{\mathrm{Br}[X \to J/\psi\,\pi^+\pi^-]}. \tag{2.20}$$

Upper limits on the products of the branching fractions for $B^+ \to XK^+$ and $X \to h$ can be expressed in terms of $R[X \to h]$ by dividing them by Eq. (2.3). Using the 90% C.L. limits for the products of the branching fractions and the central value in Eq. (2.3), we obtain the upper limits in Table 2.2.

Decay mode	Upper limit on $R[X \to h]$
$X \to D^0\bar{D}^0$	5
$X \to D^+D^-$	3
$X \to D^0\bar{D}^0\pi^0$	5
$X \to \gamma\chi_{c1}$	0.89
$X \to \gamma\chi_{c2}$	1.1
$X \to J/\psi\pi^0\pi^0$	0.77
$X \to J/\psi\eta$	0.59

Table 2.2: Upper limits on the ratio of the branching fractions for various decay mode of the X into final states h discussed in text.

2.3 Inclusive production at the Tevatron

The existence of the state X was confirmed by the CDF [6] and DØ [7] collaborations through its inclusive production in proton-antiproton ($p\bar{p}$) collisions at the Tevatron at center-of-momentum energy 1.96 TeV. The CDF and DØ collaborations collected 730±90 and 522±100 candidates for the X, respectively. The measurements of the mass by CDF and DØ are shown in Table 2.1.

The $J/\psi\,\pi^+\pi^-$ invariant mass distribution from CDF is shown in Fig. 2.3. The large peak at 3.686 GeV corresponds to the $\psi(2S)$ and the smaller peak at 3.872 GeV corresponds to the state X. As can be seen in Fig. 2.3, requiring the dipion invariant mass to be greater than 0.5 GeV shows a clear signal for the X, while requiring the dipion invariant mass to be less than 0.5 GeV shows no signal. This indicates that the dipion in $X \to J/\psi\,\pi^+\pi^-$ is dominated by large $\pi^+\pi^-$ masses greater than 0.5 GeV, which supports the observation by the Belle collaboration shown in Fig. 2.2.

The DØ collaboration compared the production of the $X(3872)$ with the production of the $\psi(2S)$ by separating the events according to various production and decay

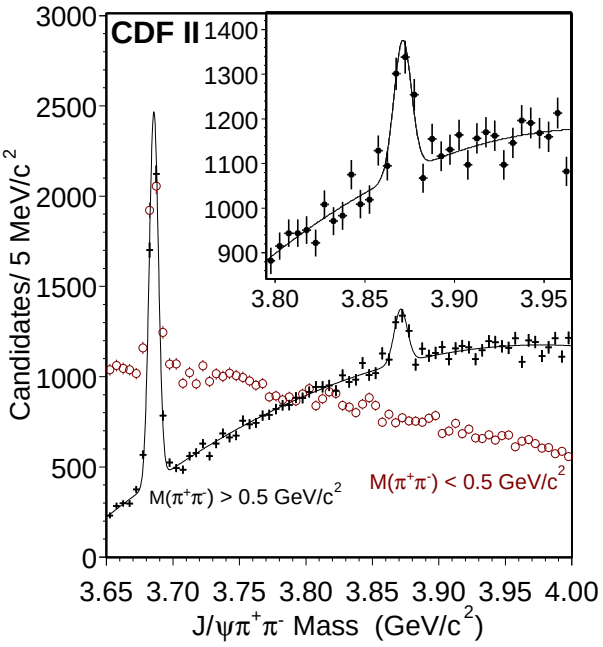

Figure 2.3: The mass distributions of $J/\psi\,\pi^+\pi^-$ candidates with $M(\pi^+\pi^-) > 0.5$ GeV (points) and $M(\pi^+\pi^-) < 0.5$ GeV (open circles). The curve is a fit with two Gaussians and a quadratic background. The inset shows an enlargement of the high dipion-mass data and fit [6].

variables, such as the transverse momentum of the $J/\psi\,\pi^+\pi^-$ system and the rapidity of the $J/\psi\,\pi^+\pi^-$ system [7]. They found no significant differences between the X and the $\psi(2S)$ production and decay and decay variables.

Recently, the CDF collaboration determined the fractions of the X's that arise from B hadron decays and from prompt production at the Tevatron by looking at the decay mode $X \to J/\psi\,\pi^+\pi^-$ [64]. Since B hadrons decay by the weak interactions, they have a relatively large lifetimes. When they are produced in $p\bar{p}$ collisions, they typically travel a measurable distance before decaying. In contrast, the X decays so quickly that the distance it travels before decaying can not be measured. The decay

products of an X produced by B hadron decay therefore typically emerge from a secondary vertex that is well-separated from the primary vertex defined by the $p\bar{p}$ collision point. An X whose decay products emerge from the primary vertex is called prompt. A prompt X is most likely produced by QCD interactions in the $p\bar{p}$ collisions. For the $X(3872)$ with the dipion invariant mass greater than 0.5 GeV, CDF found that $16.1 \pm 4.9_{\rm stat} \pm 2.0_{\rm syst}\%$ of produced X from $p\bar{p}$ collisions are from B hadron decays. This fraction is significantly smaller than that for the $\psi(2S)$, $28.3 \pm 1.0_{\rm stat} \pm 0.7_{\rm syst}\%$ of which come from B hadron decays. Thus, CDF's result indicates that large fraction of X produced at the Tevatron comes from prompt production mechanisms rather than from the decay of hadrons containing a b quark.

CHAPTER 3

UNIVERSALITY FOR LARGE SCATTERING LENGTH

We interpret the observed narrow resonance $X(3872)$ as a loosely-bound S-wave molecule of charm mesons $D^0\bar{D}^{*0}$ and $D^{*0}\bar{D}^0$. The small binding energy implies a large $D^0\bar{D}^{*0}$ and $D^{*0}\bar{D}^0$ scattering length. The molecule therefore has some universal properties that are determined by the unnaturally large scattering length.

3.1 Universal properties of the DD^* molecule

The combined averaged mass of the $X(3872)$ in Eq. (2.1) is extremely close to the threshold for the charm mesons D^0 and $\bar{D}^{*0}$:

$$m_X - (m_{D^0} + m_{D^{*0}}) = +0.6 \pm 1.1 \text{ MeV}. \tag{3.1}$$

We will assume that the closeness of m_X to the $D^0\bar{D}^{*0}$ threshold is no accident and that $X(3872)$ is indeed a hadronic molecule whose constituents are a superposition of the charm mesons $D^0\bar{D}^{*0}$ and $\bar{D}^0D^{*0}$. Among all the hadrons that can be interpreted as 2-body bound states of other hadrons, what makes this molecule unique is its extremely small binding energy. If the low-energy interaction between two hadrons is mediated by pion exchange, the natural scale for the binding energy of a molecule composed of the two hadrons is $m_\pi^2/(2\mu)$, where μ is their reduced mass. In the case

of D^0 and $\bar{D}^{*0}$, the reduced mass is

$$\mu = \frac{m_{D^0}\, m_{D^{*0}}}{m_{D^0} + m_{D^{*0}}} = 966.5 \pm 0.3 \text{ MeV}. \tag{3.2}$$

The natural energy scale is therefore $m_\pi^2/(2\mu) \approx 10$ MeV. The 2-body bound state of hadrons with the next smallest binding energy is the deuteron. Its binding energy is measured to be 2.24 MeV, which is small compared to the natural energy scale of 20 MeV for a pn molecule.

We will further assume that $X(3872)$ is an S-wave bound state of $D^0\bar{D}^{*0}$ or $\bar{D}^0 D^{*0}$, because this has particularly interesting implications. We call it the DD^* molecule. Since the constituents have J^P quantum numbers 0^- and 1^-, the J^{PC} quantum numbers of the molecule must be 1^{++} or 1^{+-}. The $C = -$ option is ruled out by the observation of the decay $X \to J/\psi\,\gamma$. The energy difference between the mass of X and the $D^0\bar{D}^{*0}$ threshold, which is given in Eq. (3.1) is much smaller than the natural energy scale. The interaction between D^0 and $\bar{D}^{*0}$ at energies less than $m_\pi^2/\mu \approx 10$ MeV is dominated by the S-wave channel and can be described by the S-wave $D^0\bar{D}^{*0}$ scattering length. A shallow S-wave bound state implies an S-wave scattering length that is large compared to the natural length scale $1/m_\pi$. We assume that there is a large scattering length a in the channel $(DD^*)^0_+$ with even charge conjugation defined by

$$|(DD^*)^0_+\rangle = \frac{1}{\sqrt{2}}\left(|D^0\bar{D}^{*0}\rangle + |D^{*0}\bar{D}^0\rangle\right). \tag{3.3}$$

If the scattering length in the $C = -$ channel is negligible in comparison, the scattering lengths for elastic $D^0\bar{D}^{*0}$ scattering and elastic $D^{*0}\bar{D}^0$ scattering are both $a/2$. We identify the X as a bound state in the $(DD^*)^0_+$ channel.

Nonrelativistic few-body systems with short-range interactions and a large scattering length a have universal properties that depend on the scattering length but are otherwise insensitive to the details at distances small compared to a [40]. In any specific system, there is a natural momentum scale Λ that sets the scale of most low-energy scattering parameters. The scattering length is large if it satisfies $|a| \gg \Lambda^{-1}$.

Universality predicts that the T-matrix element for 2-body elastic scattering with relative momentum $p \ll \Lambda$ is

$$\mathcal{T}(p) = \frac{2\pi/\mu}{-1/a - ip}, \tag{3.4}$$

where μ is the reduced mass of the two particles. If a is real and positive, universality predicts that there is a weakly-bound state with binding energy

$$E_X = \frac{1}{2\mu a^2}. \tag{3.5}$$

For example, if the binding energy of $X(3872)$ were 0.5 MeV or 0.1 MeV, the scattering length would be 6.3 fm or 14.2 fm, respectively. These are both much larger than the natural length scale $1/m_\pi = 1.5$ fm.

Universality has other implications for the interpretation of $X(3872)$ as a DD^* molecule. The wavefunction of the X for DD^* separations $r \gg 1/\Lambda$ is universal. The normalized wavefunction for $r \gg 1/\Lambda$ is

$$\psi(r) = (2\pi a)^{-1/2} \frac{\exp(-r/a)}{r}. \tag{3.6}$$

Its Fourier transform is the universal momentum-space wavefunction of this bound state:

$$\tilde{\psi}(p) = \frac{(8\pi/a)^{1/2}}{p^2 + 1/a^2}. \tag{3.7}$$

The universal amplitude for transitions from the bound state to a scattering state consisting of two particles with relative momentum $p \ll \Lambda$ is

$$\mathcal{A}_X = \frac{\sqrt{2\pi}}{\mu}\, a^{-1/2}. \tag{3.8}$$

These results are all encoded in the universal expression for the truncated connected transition amplitude:

$$\mathcal{A}(E) = \frac{2\pi/\mu}{-1/a + \sqrt{-2\mu E}}. \tag{3.9}$$

3.2 Complex scattering length

If the 2-body system has inelastic scattering channels, the large scattering length a will have a negative imaginary part. It is convenient to express the complex scattering length in the form

$$\frac{1}{a} = \gamma_{\rm re} + i\gamma_{\rm im}, \tag{3.10}$$

where $\gamma_{\rm re}$ and $\gamma_{\rm im}$ are real and $\gamma_{\rm im} \geq 0$. In the case $\gamma_{\rm re} > 0$ where there is a weakly-bound state, it can decay into the inelastic channel. The expression for the binding energy on the right side of Eq. (3.5) is complex-valued. Its real part $E_{X,\rm pole}$ and its imaginary part $\Gamma_X/2$ are given by

$$E_{X,\rm pole} = (\gamma_{\rm re}^2 - \gamma_{\rm im}^2)/(2\mu), \tag{3.11a}$$

$$\Gamma_X = 2\gamma_{\rm re}\gamma_{\rm im}/\mu. \tag{3.11b}$$

These quantities specify that there is a pole in the S-matrix at the energy $E = -E_{X,\rm pole} - i\Gamma_X/2$. As we shall see in Section 5.4, Γ_X can be interpreted as the full width at half-maximum of a resonance in the inelastic channel provided $\gamma_{\rm im} < \gamma_{\rm re}$.

The peak of the resonance is below the threshold for the two particles by

$$E_X = \gamma_{\rm re}^2/(2\mu). \tag{3.12}$$

We therefore interpret E_X as the binding energy rather than $E_{X,\rm pole}$.

The decays of the X imply that the scattering length a is complex-valued. It can be parameterized in terms of the real and imaginary parts of $1/a$ as in Eq. (3.10). Our interpretation of X as a bound state requires $\gamma_{\rm re} > 0$. The energy difference in Eq. (3.1) puts an upper bound on $\gamma_{\rm re}$:

$$\gamma_{\rm re} < 40 \text{ MeV} \qquad (90\% \text{ C.L.}). \tag{3.13}$$

The upper bound on the width in Eq. (2.2) puts an upper bound on the product of $\gamma_{\rm re}$ and $\gamma_{\rm im}$:

$$\gamma_{\rm re}\gamma_{\rm im} < (33 \text{ MeV})^2 \qquad (90\% \text{ C.L.}). \tag{3.14}$$

There is also a lower bound on the width of the X from its decays into $D^0\bar{D}^0\pi^0$ and $D^0\bar{D}^0\gamma$, which both proceed through the decay of a constituent D^*. These decays involve interesting interference effects, but the decay rates have smooth limits as the binding energy is tuned to 0 [41]. In this limit, the constructive interference increases the decay rate by a factor of 2: the partial width of X reduces to $2\,\Gamma[D^{*0}]$. The width of D^{*0} has not been measured, but it can be deduced from other information about the decays of D^{*0} and D^{*+}. Using the total width of the D^{*+}, its branching fraction into $D^+\pi^0$, and isospin symmetry, we can deduce the partial width of D^{*0} into $D^0\pi^0$: $\Gamma[D^{*0} \to D^0\pi^0] = 42 \pm 10$ keV. The total width of the D^{*0} can then be obtained by dividing by its branching fraction into $D^0\pi^0$: $\Gamma[D^{*0}] = 68 \pm 16$ keV. The sum of the partial widths of X into $D^0\bar{D}^0\pi^0$ and $D^0\bar{D}^0\gamma$ is therefore 136 ± 32 keV. The resulting

lower bound on the product of $\gamma_{\rm re}$ and $\gamma_{\rm im}$ is

$$\gamma_{\rm re}\gamma_{\rm im} > (7 \text{ MeV})^2 \qquad (90\% \text{ C.L.}). \tag{3.15}$$

By combining this with the upper bound on $\gamma_{\rm re}$ in Eq. (3.13), we can infer that $\gamma_{\rm im} > 1$ MeV.

3.3 Hadronic states with nearby thresholds

The scattering states $D^{\pm}D^{*\mp}$, $J/\psi\,\rho$, and $J/\psi\,\omega$ have thresholds that are relatively close to the $D^0\bar{D}^{*0}$ threshold. These states can undergo S-wave scattering to $D^0\bar{D}^{*0}$ and $D^{*0}\bar{D}^0$. If their thresholds differ from the $D^0\bar{D}^{*0}$ threshold by much less than the natural energy scale of 10 MeV set by pion exchange, the mechanism for the S-wave resonance in the $D^0\bar{D}^{*0}/D^{*0}\bar{D}^0$ system could also generate resonant S-wave interactions in those other channels as well. In this case, it would be necessary to treat all the resonating channels as a coupled-channel system, with a large elastic scattering length for each channel and a large "transition" scattering length for each pair of channels. The energy gaps between the $D^0\bar{D}^{*0}$ threshold and each of these other thresholds are

$$m_{D^\pm} + m_{D^{*\mp}} - (m_{D^0} + m_{D^{*0}}) = +8.1 \pm 0.1 \text{ MeV}, \tag{3.16a}$$

$$m_{J/\psi} + m_{\rho} - (m_{D^0} + m_{D^{*0}}) = +1.4 \pm 1.1 \text{ MeV}, \tag{3.16b}$$

$$m_{J/\psi} + m_{\omega} - (m_{D^0} + m_{D^{*0}}) = +8.2 \pm 1.0 \text{ MeV}. \tag{3.16c}$$

The small uncertainty in Eq. (3.16a) comes from using mass differences between charm mesons to calculate the energy gap. The uncertainties in Eqs. (3.16b) and (3.16c) are dominated by the uncertainty in $2m_{D^0}$. The energy gaps in the $D^{\pm}D^{*\mp}$ and $J/\psi\,\omega$ channels are comparable to the natural energy scale of about 10 MeV

associated with pion exchange. The energy gap in Eq. (3.16b) for the $J/\psi\,\rho$ channel is much smaller. However whether any of these channels can have resonant interactions with $D^0\bar{D}^{*0}$ or $D^{*0}\bar{D}^0$ is determined not only by the real parts of the energy gaps, which are given in Eqs. (3.16), but also by the imaginary parts, which can be obtained by replacing each mass m by $m - i\Gamma/2$, where Γ is the width of the particle. If there are large differences between the widths of the various particles, it is necessary only to take into account the largest width among the particles in each channel. The real energy gap in Eqs. (3.16) becomes the complex energy gap Δ by adding $-i\Gamma/2$. The largest width in each of the three channels is

$$\Gamma[D^{*\pm}] = 0.096 \pm 0.022 \text{ MeV}, \tag{3.17a}$$

$$\Gamma[\rho] = 150.3 \pm 1.6 \text{ MeV}, \tag{3.17b}$$

$$\Gamma[\omega] = 8.49 \pm 0.08 \text{ MeV}. \tag{3.17c}$$

For the $D^{\pm}D^{*\mp}$ and $J/\psi\,\omega$ channels, the magnitude $|\Delta|$ of the complex energy gap is comparable to the natural energy scale 10 MeV associated with pion exchange between D and D^*. The large width of the ρ makes $|\Delta|$ for the $J/\psi\,\rho$ channel much larger than the natural energy scale.

Because the complex energy gap Δ for the other hadronic channels with nearby thresholds are comparable to or larger than the natural energy scale, these channels need not be taken into account explicitly in calculations of quantities that have nontrivial universal limits as $a \to \pm\infty$. Their dominant effects enter through the complex-valued scattering length a. A coupled-channel model that includes other hadronic states with nearby thresholds could still be useful for estimating nonuniversal quantities or for calculating nonuniversal corrections to the universal predictions.

3.4 Discussion

The state of the X can be written schematically as

$$|X\rangle = \frac{Z^{1/2}}{\sqrt{2}} \left(|D^0 \bar{D}^{*0}\rangle + |D^{*0} \bar{D}^0\rangle \right) + \sum_H Z_H^{1/2} |H\rangle, \tag{3.18}$$

where Z is the probability for the X to be in the $D^0 \bar{D}^{*0}/D^{*0} \bar{D}^0$ state and Z_H is the probability for the X to be in another hadronic state H. Universality applied to the X shows that Z approaches to 1 and Z_H scales as $1/|a|$ as $|a| \to \infty$ [32]. The hadronic states H in (3.18) could include charmonium states, scattering states of charm mesons such as $D^{\pm} D^{*\mp}$, and scattering states of a charmonium and a light hadron such as $J/\psi\,\rho$ or $J/\psi\,\omega$. An expansion of $|X\rangle$ in terms of hadronic states can be valid only in a limited region. An ultraviolet cutoff on the energy difference with respect to the $D^0 \bar{D}^{*0}$ threshold must therefore be specified, and the probabilities Z_H depend on that cutoff. As the cutoff is decreased below the threshold for a given hadronic state $|H\rangle$, that component of the wavefunction is eliminated. If the cutoff is sufficiently close to the $D^0 \bar{D}^{*0}$ threshold, the only states that remain are $|D^0 \bar{D}^{*0}\rangle$ and $|D^{*0} \bar{D}^0\rangle$. The sum of their probabilities is $Z < 1$, but $Z \to 1$ as $\mathrm{Re}(1/a) \to 0$.

A scattering length that is large compared to the natural length scale necessarily requires a fine-tuning. In the case of the DD^* molecule, the fine-tuning parameters can be identified with the up and down quark masses m_u and m_d. The masses of D^0 and $\bar{D}^{*0}$ are sensitive to m_u, because these hadrons contain an up quark as a constituent. The $D^0 \bar{D}^{*0}$ potential is sensitive to m_u and m_d through the pion mass. There are two distinct mechanisms for generating a large $(DD^*)^0_+$ scattering length. The first mechanism is a fine-tuning of parameters that have a large effect on the

$(DD^*)^0_+$ channel without significantly affecting other channels. This could be a fine-tuning of the range and depth of the $(DD^*)^0_+$ potential so that there is a bound state very close to threshold and thus a large scattering length. Equivalently, it could be a fine-tuning of the masses of the D^0 and $\bar{D}^{*0}$ to obtain a bound state very close to threshold in the $(DD^*)^0_+$ potential. This mechanism requires the quantum numbers of X to be $J^{PC} = 1^{++}$, because this is the only S-wave channel for which the potential due to pion exchange is sufficiently attractive to produce a bound state [29]. In the limit $a \to \infty$, the probabilities for components of the wavefunction other than $(DD^*)^0_+$ scale as $1/a$ and approach to 0 as a increases. This mechanism will be illustrated in Section 4.2. using an explicit field theory model.

Another mechanism for a large $D^0\bar{D}^{*0}$ scattering length is an accidental fine-tuning of the excited P-wave charmonium state $\chi_{c1}(2P)$, whose quantum numbers are $J^{PC} = 1^{++}$, to the $D^0\bar{D}^{*0}$ threshold. This mechanism is analogous to the Feshbach resonances [65] that can be used to control the scattering lengths for atoms by adjusting the magnetic field [66, 67, 68]. Feshbach resonances are currently being used to tune the scattering lengths for atoms to arbitrarily large values in order to study Bose-Einstein condensates of bosonic atoms and degenerate gases of fermionic atoms in the strongly-interacting regime. In the case of the $D^0\bar{D}^{*0}$ molecule, the fine-tuning parameter can be identified as m_u, which can shift the D^0 and $\bar{D}^{*0}$ masses, thus changing the energy gap ν between the $\chi_{c1}(2P)$ and the $D^0\bar{D}^{*0}$ threshold. If the mass of the $\chi_{c1}(2P)$ is very close to the $D^0\bar{D}^{*0}$ threshold, it could fortuitously tune the energy gap ν for $\chi_{c1}(2P)$ to be smaller than the natural low-energy scale $m_\pi^2/(2\mu) \approx 10$ MeV associated with pion exchange. In this case, a resonant interaction between the $\chi_{c1}(2P)$ and $D^0\bar{D}^{*0}$ states generates a large $(DD^*)^0_+$ scattering length a that increases as $1/\nu$. If $a > 0$,

there is a shallow bound state whose binding energy approaches Eq. (3.5) as $\nu \to 0$. In the expression (3.18) for the quantum state, the hadrons should be interpreted as those in the absence of the fine-tuning that generates the resonant interaction. In the limit $a \to \infty$, the probability Z_χ for $\chi_{c1}(2P)$ scales as $1/a$, as do the probabilities Z_H for all other channels besides the $(DD^*)^0_+$ channel. This mechanism will be illustrated using an explicit field theory model in Section 4.2.

The coupling between $(DD^*)^0_+$ and nearby hadronic states such as $J/\psi\,\rho$ and $J/\psi\,\omega$ could also give rise to a large scattering length in the $(DD^*)^0_+$ channel. The large scattering length could be produced by an accidental fine-tuning of the scattering parameters associated with the coupled channels. If $a > 0$, there is a shallow bound state whose binding energy approaches Eq. (3.5) as $a \to \infty$. The probabilities for the coupled channel components of the bound state go to 0 as $1/a$ as $a \to \infty$. This mechanism will be illustrated in Section 4.3 using an explicit field theory model. Independent of the mechanism for the large scattering length, the shallow bound state has the same universal properties. In Chapter 5, these universal properties will be applied to the $X(3872)$.

Universality gives highly nontrivial predictions for 3-body systems, such as $D^0 D^0 \bar{D}^{*0}$. Unfortunately, as shown in Appendix A, the spectacular possibility of shallow $D^0 D^0 \bar{D}^{*0}$ molecules called Efimov states can be excluded.

CHAPTER 4

SCATTERING MODELS

If we consider only momenta small compared to the natural momentum scale m_π, hadrons such as D^0 and $\bar{D}^{*0}$ can be treated as point particles with pointlike interactions and can therefore be described by a local nonrelativistic quantum field theory. In the following sections, we discuss three fine-tuning mechanisms that can generate a large scattering length for the $(D\bar{D}^*)^0_+$ channel. These fine-tuning mechanisms are represented by the zero-range model, the resonance model, and the two-channel model, respectively. All of them give the universal amplitude in Eq. (3.9) in the limit of a large scattering length.

4.1 Zero-range model

The universal amplitude in Eq. (3.9) can be obtained from a local effective field theory for two particles that interact through an S-wave contact interaction only. The nonrelativistic field theory has fields ψ_a and ψ_b for the two particles with masses m_a and m_b. The hamiltonian density is the sum of mass terms, kinetic terms, and

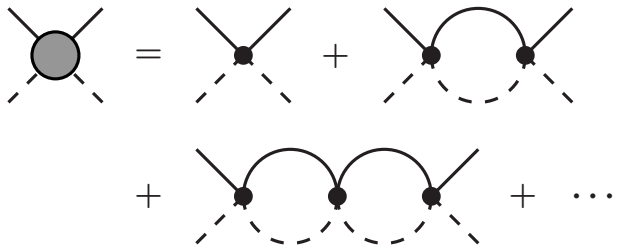

Figure 4.1: The geometric series of Feynman diagrams whose sum is the universal amplitude $\mathcal{A}(E)$.

interaction terms:

$$\mathcal{H}_{\rm mass} = m_a\,\psi_a^\dagger\,\psi_a + m_b\,\psi_b^\dagger\,\psi_b, \tag{4.1a}$$

$$\mathcal{H}_{\rm kin} = -\frac{1}{2m_a}\,\psi_a^\dagger\,\nabla^2\,\psi_a - \frac{1}{2m_b}\,\psi_b^\dagger\,\nabla^2\,\psi_b, \tag{4.1b}$$

$$\mathcal{H}_{\rm int} = \lambda_0\,(\psi_a\,\psi_b)^\dagger\,(\psi_a\,\psi_b)\,. \tag{4.1c}$$

This model has ultraviolet divergence that can be regularized by an ultraviolet cutoff $|\boldsymbol{p}| < \Lambda$ on the momentum in loop integral. The Feynman rule associated with the interaction is $-i\lambda_0(\Lambda)$. It is convenient to express the coupling constant for the contact interaction in the form

$$\lambda_0(\Lambda) = \frac{2\pi}{\mu}\,a_0(\Lambda), \tag{4.2}$$

where the parameter $a_0(\Lambda)$ is a bare scattering length that depends on the ultraviolet momentum cutoff Λ.

The connected truncated transition amplitude $\mathcal{A}(E)$ in the center-of-momentum frame depends only on the total energy E of the two particles. It can be obtained by summing the geometric series of Feynman diagrams in Fig. 4.1:

$$\mathcal{A}(E) = -\frac{(2\pi/\mu)a_0(\Lambda)}{1 + (2\pi/\mu)a_0(\Lambda)L(\Lambda, E)}, \tag{4.3}$$

where $L(\Lambda, E)$ is the amplitude for the propagation of the particles between successive contact interactions:

$$L(\Lambda, E) = \frac{\mu}{\pi^2}\left(\Lambda - \frac{\pi}{2}\sqrt{-2\mu E}\right). \tag{4.4}$$

Renormalization is accomplished by eliminating $a_0(\Lambda)$ in favor of the physical scattering length:

$$a = \frac{a_0(\Lambda)}{1 + (2/\pi)\Lambda a_0(\Lambda)}. \tag{4.5}$$

With this substitution, the expression for $\mathcal{A}(E)$ in Eq. (4.3) reduces without approximation to the universal result in Eq. (3.9). Note that the scattering length a can be tuned to $\pm\infty$ by tuning the bare scattering length to a critical value of order Λ^{-1}:

$$a_0(\Lambda) \longrightarrow -\frac{\pi}{2}\Lambda^{-1}. \tag{4.6}$$

To describe the $D^0\bar{D}^{*0}/D^{*0}\bar{D}^0$ system, we need to take into account the facts that the D^{*0} and $\bar{D}^{*0}$ are spin-1 particles and that the large scattering length is in the $C = +$ channel. The spin-0 particles D^0 and $\bar{D}^0$ can be described by single component scalar fields D and $\bar{D}$, but the spin-1 particles D^{*0} and $\bar{D}^{*0}$ require 3-component vector fields $\mathbf{D}$ and $\bar{\mathbf{D}}$. The large scattering length can be introduced through a contact interaction for the combination of fields $(D\,\bar{\mathbf{D}} + \bar{D}\,\mathbf{D})/\sqrt{2}$ that is even under charge conjugation. The hamiltonian density is the sum of mass terms, kinetic terms, and interaction terms:

$$\mathcal{H}_{\rm mass} = m_{D^0}\left(D^\dagger D + \bar{D}^\dagger \bar{D}\right) + m_{D^{*0}}\left(\mathbf{D}^\dagger \cdot \mathbf{D} + \bar{\mathbf{D}}^\dagger \cdot \bar{\mathbf{D}}\right) \tag{4.7a}$$

$$\mathcal{H}_{\rm kin} = -\frac{1}{2m_{D^0}}\left(D^\dagger \nabla^2 D + \bar{D}^\dagger \nabla^2\, \bar{D}\right) - \frac{1}{2m_{D^{*0}}}\left(\mathbf{D}^\dagger \cdot \nabla^2 \mathbf{D} + \bar{\mathbf{D}}^\dagger \cdot \nabla^2\, \bar{\mathbf{D}}\right) \tag{4.7b}$$

$$\mathcal{H}_{\rm int} = \frac{\lambda_0}{2}\left(D\,\bar{\mathbf{D}} + \bar{D}\,\mathbf{D}\right)^\dagger \cdot \left(D\,\bar{\mathbf{D}} + \bar{D}\,\mathbf{D}\right). \tag{4.7c}$$

Renormalization can be accomplished by eliminating the bare coupling constant $\lambda_0(\Lambda)$ in favor of the scattering length a for the $C = +$ channel using Eqs. (4.2) and (4.5). The resulting connected truncated transition amplitudes are proportional to the universal amplitude $\mathcal{A}(E)$ in Eq. (3.9), and diagonal in the spin projection quantum number m of the vector meson. For example, the transition amplitude for $D^0\bar{D}^{*0} \to D^0\bar{D}^{*0}$ is

$$\mathcal{A}[D^0\bar{D}^{*0} \to D^0\bar{D}^{*0}] = \frac{1}{2}\,\delta_{mm'}\,\mathcal{A}(E). \tag{4.8}$$

The factor of $1/2$ comes from projecting the initial and final state onto the channel $C = +$ with the large scattering length.

4.2 Resonance model

The universal amplitude in Eq. (3.9) can also be obtained from a local effective field theory for two particles that interact through an S-wave contact interaction and through a coupling to a nearby particle. The nonrelativistic field theory has fields ψ_a, ψ_b, and χ. The hamiltonian density is the sum of mass terms, kinetic terms, and interaction terms:

$$\mathcal{H}_{\rm mass} = m_a\,\psi_a^\dagger\,\psi_a + m_b\,\psi_b^\dagger\,\psi_b + (m_a + m_b + \nu_0)\,\chi^\dagger\chi, \tag{4.9a}$$

$$\mathcal{H}_{\rm kin} = -\frac{1}{2m_a}\,\psi_a^\dagger\,\nabla^2\,\psi_a - \frac{1}{2m_b}\,\psi_b^\dagger\,\nabla^2\,\psi_b - \frac{1}{2(m_b+m_b)}\,\chi^\dagger\,\nabla^2\,\chi, \tag{4.9b}$$

$$\mathcal{H}_{\rm int} = \lambda_0\,(\psi_a\,\psi_b)^\dagger\,(\psi_a\,\psi_b) + g_0\left(\chi^\dagger\psi_a\psi_b + \psi_a^\dagger\psi_b^\dagger\chi\right). \tag{4.9c}$$

Generalization of the hamiltonian density in Eqs. (4.9) to the $D^0\bar{D}^{*0}/D^{*0}\bar{D}^0$ system that couples to $\chi_{c1}(2P)$ is straightforward. The nonrelativistic field theory has

local fields D, $\bar{D}$, $\mathbf{D}$, $\bar{\mathbf{D}}$, and $\boldsymbol{\chi}$ for the D^0, $\bar{D}^0$, D^{*0}, $\bar{D}^{*0}$, and $\chi_{c1}(2P)$. The hamiltonian density is the sum of mass terms, kinetic terms, and interaction terms:

$$\begin{aligned}
\mathcal{H}_{\rm mass} &= m_{D^0}\left(D^\dagger D + \bar{D}^\dagger \bar{D}\right) + m_{D^{*0}}\left(\mathbf{D}^\dagger\cdot\mathbf{D} + \bar{\mathbf{D}}^\dagger\cdot\bar{\mathbf{D}}\right) \\
&\quad + (m_{D^0} + m_{D^{*0}} + \nu_0)\boldsymbol{\chi}^\dagger\cdot\boldsymbol{\chi} \qquad (4.10a) \\
\mathcal{H}_{\rm kin} &= -\frac{1}{2m_{D^0}}\left(D^\dagger\nabla^2 D + \bar{D}^\dagger\nabla^2\bar{D}\right) - \frac{1}{2m_{D^{*0}}}\left(\mathbf{D}^\dagger\cdot\nabla^2\mathbf{D} + \bar{\mathbf{D}}^\dagger\cdot\nabla^2\bar{\mathbf{D}}\right) \\
&\quad - \frac{1}{2(m_{D^0}+m_{D^{*0}})}\boldsymbol{\chi}^\dagger\cdot\nabla^2\boldsymbol{\chi}, \qquad (4.10b) \\
\mathcal{H}_{\rm int} &= \frac{\lambda_0}{2}\left(D\bar{\mathbf{D}} + \bar{D}\mathbf{D}\right)^\dagger\cdot\left(D\bar{\mathbf{D}} + \bar{D}\mathbf{D}\right) \\
&\quad + g_0\left[\boldsymbol{\chi}^\dagger\cdot(D\bar{\mathbf{D}} + \bar{D}\mathbf{D}) + (D\bar{\mathbf{D}} + \bar{D}\mathbf{D})^\dagger\cdot\boldsymbol{\chi}\right], \qquad (4.10c)
\end{aligned}$$

where λ_0, g_0, and ν_0 are bare parameters that require renormalization. A similar field theory has been used to describe the behavior of cold atoms near a Feshbach resonance [69]. If we impose an ultraviolet cutoff Λ on loop momenta and drop terms that decrease as inverse powers of Λ, the cutoff dependence can be removed by eliminating λ_0, g_0, and ν_0 in favor of renormalized parameters λ, g, and ν defined by

$$\begin{aligned}
\lambda &= Z_\lambda^{-1}\lambda_0, \qquad (4.11a) \\
g &= Z_\lambda^{-1} g_0, \qquad (4.11b) \\
\nu &= \nu_0 + [Z_\lambda^{-1} - 1]g_0^2/\lambda_0, \qquad (4.11c)
\end{aligned}$$

where the renormalization constant Z_λ is

$$Z_\lambda = 1 + \frac{2}{\pi^2}\mu\lambda_0\Lambda \qquad (4.12)$$

and $\mu = m_{D^0}m_{D^{*0}}/(m_{D^0} + m_{D^{*0}})$ is the reduced mass. Note that the combinations $g_0/\lambda_0 = g/\lambda$ and $\nu_0 - g_0^2/\lambda_0 = \nu - g^2/\lambda$ are renormalization invariants.

The natural scale for the ultraviolet momentum cutoff is $\Lambda \sim m_\pi$. The natural magnitude for the bare coupling constant λ_0 can be deduced by dimensional analysis:

$|\lambda_0| \sim 1/(\mu m_\pi)$. This can be made evident by writing the renormalization condition Eq. (4.11a) in the form

$$\frac{1}{\lambda} = \frac{1}{\lambda_0} + \frac{2}{\pi^2}\mu\Lambda. \tag{4.13}$$

If the renormalized coupling constant λ is fixed and Λ is sufficiently large, λ_0 must scale like $(\mu\Lambda)^{-1}$ to compensate for the effect of the ultraviolet cutoff. The natural magnitude for g_0 is $\zeta m_\pi^{1/2}/\mu$, where the factor of $m_\pi^{1/2}/\mu$ comes from dimensional analysis and ζ is a numerical suppression factor associated with the violation of Zweig's rule by the process $\chi_{c1}(2P) \to D^0\bar{D}^{*0}$, which requires the creation of a light quark-antiquark pair. The renormalization condition Eq. (4.11b) implies that the numerical suppression factor ζ is stable under renormalization and does not require fine-tuning. There is no natural magnitude for the bare parameter ν_0: it is completely adjustable. In the absence of fine-tuning, the renormalization constant Z_λ in Eq. (4.12) is comparable to 1. The renormalization conditions Eqs. (4.11a), (4.11b), and (4.11c) then imply that the natural magnitudes of the renormalized coupling constants are $|\lambda| \sim (\mu m_\pi)^{-1}$, $|g| \sim \zeta m_\pi^{1/2}/\mu$, and $|\nu| \sim \max(|\nu_0|, \zeta^2 m_\pi^2/\mu)$.

The 2-body scattering amplitude in this model can be calculated analytically. The scattering length is

$$a = \frac{\mu}{\pi}\left(\lambda - \frac{g^2}{\nu}\right). \tag{4.14}$$

The natural magnitude for $|a|$ is $1/m_\pi$. The scattering length can be made unnaturally large either by making λ sufficiently large, which corresponds to tuning the potential between D^0 and $\bar{D}^{*0}$, or by making ν sufficiently small, which corresponds to tuning

the energy gap between the $\chi_{c1}(2P)$ and the $D^0\bar{D}^{*0}$ threshold. In either case, low-energy universality implies that as a increases, the binding energy of the molecule approaches Eq. (3.5) and the $D^0\bar{D}^{*0}$ or $\bar{D}^0D^{*0}$ wavefunction approaches Eq. (3.6).

The first mechanism for generating a large scattering length is to make λ unnaturally large: $|\lambda| \gg |\lambda_0|$. This can be accomplished by tuning λ_0 towards the critical value $-\pi^2/(2\mu\Lambda)$, so that there is a near cancellation between the two terms on the right side of Eq. (4.13). This fine-tuning makes the renormalization constant Z_λ much less than 1. The renormalization condition Eq. (4.11b) implies that this fine-tuning also increases the strength of the effective coupling constant between $\boldsymbol{\chi}$ and $D\bar{\mathbf{D}}$: $|g| \gg |g_0|$. This is also evident from the fact that $g/\lambda = g_0/\lambda_0$ is a renormalization invariant. There is a limit to how large the scattering length can be made using this mechanism. When Z_λ becomes smaller than $g_0^2/|\lambda_0\nu_0|$, the g_0^2/λ_0 term in Eq. (4.11c) begins to dominate over the ν_0 term. In this case, both terms in the scattering length Eq. (4.14) become large and they tend to cancel each other. Thus, with this mechanism, the maximum magnitude of the scattering length is of order $(\lambda_0/g_0)^2\mu|\nu_0|$ which is of order $\zeta^{-2}\mu|\nu_0|/m_\pi^3$.

The second mechanism for generating a large scattering length is to make ν sufficiently small. This can be accomplished by tuning ν_0 towards the critical value $-[Z_\lambda^{-1} - 1]g_0^2/\lambda_0$ for which there is a near cancellation between the two terms on the right side of Eq. (4.11c). The scattering length can be made arbitrarily large using this mechanism.

The calculation of the binding energy E_X of X and of the probability Z_χ for the $\chi_{c1}(2P)$ component of the wavefunction can both be reduced to the solution of a cubic polynomial. The binding momentum κ defined by $E_X = \kappa^2/(2\mu)$ satisfies the cubic

equation

$$\kappa^2 + 2\mu\nu = \frac{\mu}{\pi}\lambda\kappa\left[\kappa^2 + 2\mu\left(\nu - g^2/\lambda\right)\right]. \tag{4.15}$$

In either of the two limits $\lambda \to \infty$ or $\nu \to 0$, one of the three roots of this polynomial has the limiting behavior $\kappa \to 1/a$. If $a > 0$, the probability Z_χ for the $\chi_{c1}(2P)$ component of the wavefunction is

$$Z_\chi = \frac{1}{2\pi}\left(\frac{g^2/\lambda^2}{[\kappa^2 + 2\mu(\nu - g^2/\lambda)]^2} + \frac{1}{4\pi\kappa}\right)^{-1} \frac{\kappa - \pi/(\mu\lambda)}{\kappa^2 + 2\mu(\nu - g^2/\lambda)}. \tag{4.16}$$

After expressing the observables E_X and Z_χ as functions of a and the renormalization invariants g/λ and $\nu - g^2/\lambda$, they can be expanded in powers of $1/a$:

$$E_X \approx \frac{1}{2\mu a^2}\left(1 - \frac{\pi(g/\lambda)^2}{\mu^2(\nu - g^2/\lambda)^2 a} + \ldots\right), \tag{4.17a}$$

$$Z_\chi \approx \frac{\pi(g/\lambda)^2}{\mu^2(\nu - g^2/\lambda)^2 a} + \ldots. \tag{4.17b}$$

For any fine-tuning that produces a large scattering length, the bare coupling constants approach definite limiting values and therefore the renormalization invariants g/λ and $\nu - g^2/\lambda$ approach definite limiting values. Thus the probability Z_χ decreases like $1/a$.

The radiative and hadronic transitions and the annihilation decays of $X(3872)$ produce particles with momenta larger than m_π. They therefore cannot be described explicitly within an effective theory in which hadrons are treated as point particles with pointlike interactions. The inclusive effects of these decays can however be taken into account implicitly through local terms in the hamiltonian density. The inclusive effects of transitions of $D^0\bar{D}^{*0}$ or $\bar{D}^0 D^{*0}$ to charmonium states and of their annihilation into light hadrons can be taken into account through an imaginary part of the bare coupling constant λ_0. The inclusive effects of transitions of $\chi_{c1}(2P)$

to other charmonium states and of its decays into light hadrons can be taken into account through an imaginary part of the bare parameter ν_0: $\mathrm{Im}\nu_0 = -\frac{1}{2}\Gamma_{\chi_{c1}(2P)}$. The imaginary part of g_0 can take into account interference effects associated with transitions of $D^0\bar{D}^{*0}$ and $\chi_{c1}(2P)$ to the same final states. If the parameters λ_0, g_0, and ν_0 have small imaginary parts, the scattering length Eq. (4.14) is complex-valued with a small imaginary part. If a fine-tuning makes the real part of a large, the binding energy of X is given by the real part of the expression Eq. (3.5). Its imaginary part should be interpreted as $\frac{1}{2}\Delta\Gamma_X$, where $\Delta\Gamma_X$ is the contribution to the width from the decays whose effects are taken into account through $\mathrm{Im}\lambda_0$, $\mathrm{Im}g_0$, and $\mathrm{Im}\nu_0$. At first order in the imaginary parts of λ_0, g_0, and ν_0, the contribution to the width is

$$\Delta\Gamma_X = \frac{2}{\pi|a|^3}\left[(1-2a\Lambda/\pi)^2(-\mathrm{Im}\lambda_0) + 2\frac{g}{\nu}(1-2a\Lambda/\pi)\mathrm{Im}g_0 + \frac{g^2}{\nu^2}(-\mathrm{Im}\nu_0)\right]. \quad (4.18)$$

If we express g/ν in terms of a and the renormalization invariants, we see that it increases linearly with a: $g/\nu = a(g/\lambda)/(\nu - g^2/\lambda)$. Thus all three terms in Eq. (4.18) scale as $1/a$ in the limit $a \to \infty$.

4.3 Two-channel model

Cohen, Gelman, and van Kolck have constructed a renormalizable effective field theory that describes two scattering channels with S-wave contact interactions [70]. We will refer to this model as the *two-channel scattering model*. An essentially equivalent model has been used to describe the effects of $\Delta\Delta$ states on the two-nucleon system [71]. The parameters of this model can be tuned to produce a large scattering length in the lower energy channel. It can therefore be used as a simple model

for the effects on the $D^0\bar{D}^{*0}/D^{*0}\bar{D}^0$ system of other hadronic channels with nearby thresholds, such as $J/\psi\,\rho$, $J/\psi\,\omega$, and $D^{\pm}D^{*\mp}$.

4.3.1 Two-body amplitudes

The two-channel model of Ref. [70] describes two scattering channels with S-wave contact interactions only. We label the particles in the first channel $1a$ and $1b$ and those in the second channel $2a$ and $2b$. We denote the reduced masses in the two channels by μ_1 and μ_2. The nonrelativistic field theory has fields ψ_{1a}, $\psi_1 b$, ψ_{2a}, and ψ_{2b}. The hamiltonian density is the sum of mass terms, kinetic terms, and interaction terms:

$$\mathcal{H}_{\rm mass} = \sum_i m_{ia}\,\psi_{ia}^\dagger\,\psi_{ia} + m_{ib}\,\psi_{ib}^\dagger\,\psi_{ib}, \tag{4.19a}$$

$$\mathcal{H}_{\rm kin} = -\sum_i \left(\frac{1}{2m_{ia}}\,\psi_{ia}^\dagger\,\nabla^2\,\psi_{ia} + \frac{1}{2m_{ib}}\,\psi_{ib}^\dagger\,\nabla^2\,\psi_{ib}\right), \tag{4.19b}$$

$$\mathcal{H}_{\rm int} = \sum_{i,j} \lambda_{0,ij}(\Lambda)\,(\psi_{ja}\,\psi_{jb})^\dagger\,(\psi_{ia}\,\psi_{ib}), \tag{4.19c}$$

where the sums are over the two channels 1 and 2. The three bare interaction parameters $\lambda_{0,11}(\Lambda)$, $\lambda_{0,12}(\Lambda) = \lambda_{0,21}(\Lambda)$, and $\lambda_{0,22}(\Lambda)$ can be eliminated in favor of three renormalized interaction parameters a_{11}, a_{12}, and a_{22} with dimensions of length. The renormalized scattering parameters in Ref. [70] were defined in such a way that a_{11} and a_{22} reduce in the limit $a_{12} \to \pm\infty$ to the scattering lengths for the two channels. It is also convenient to define the energy gap Δ between the two scattering channels, which is determined by the masses of the particles:

$$\Delta \;=\; m_{2a} + m_{2b} - (m_{1a} + m_{1b}). \tag{4.20}$$

The truncated connected transition amplitude $\mathcal{A}(E)$ for this coupled-channel system is a 2×2 matrix that depends only on the energy E in the center-of-mass frame. If

that energy is measured relative to the threshold $m_{1a} + m_{1b}$ for the first scattering channel, the inverse of the matrix $\mathcal{A}(E)$ is[1]

$$\mathcal{A}(E)^{-1} = \frac{1}{2\pi} \begin{pmatrix} \mu_1 \big[-1/a_{11} + \sqrt{-2\mu_1 E}\,\big] & \sqrt{\mu_1\mu_2}/a_{12} \\ \sqrt{\mu_1\mu_2}/a_{12} & \mu_2 \big[-1/a_{22} + \sqrt{2\mu_2(\Delta - E)}\,\big] \end{pmatrix}. \quad (4.21)$$

The square roots are defined for negative real arguments by the prescription $E \to E + i\epsilon$ with $\epsilon \to 0^+$. The amplitudes defined by Eq. (4.21) are for transitions between states with the standard nonrelativistic normalizations. The transitions between states with the standard relativistic normalizations are obtained by multiplying by a factor $\sqrt{2m_i}$ for every particle in the initial and final state. We will need explicit expression for the 11 and 12 entries of this matrix:

$$\mathcal{A}_{11}(E) = \frac{2\pi}{\mu_1} \left(-\frac{1}{a_{11}} + \sqrt{-2\mu_1 E} - \frac{1}{a_{12}^2} \Big[-1/a_{22} + \sqrt{2\mu_2(\Delta - E)}\,\Big]^{-1} \right)^{-1}, \quad (4.22a)$$

$$\mathcal{A}_{12}(E) = \frac{2\pi}{\sqrt{\mu_1\mu_2}} \left(\frac{1}{a_{12}} - a_{12} \left[-\frac{1}{a_{11}} + \sqrt{-2\mu_1 E} \right] \left[-\frac{1}{a_{22}} + \sqrt{2\mu_2(\Delta - E)} \right] \right)^{-1}. \quad (4.22b)$$

The T-matrix element for the elastic scattering of particles in the first channel with relative momentum p is obtained by evaluating $\mathcal{A}_{11}(E)$ in Eq. (4.22a) at the energy $E = p^2/(2\mu_1)$:

$$\mathcal{T}_{11}(p) = \frac{2\pi}{\mu_1} \left(-\frac{1}{a_{11}} - ip - \frac{1}{a_{12}^2} \Big[-1/a_{22} + \sqrt{2\mu_2\Delta - (\mu_2/\mu_1)p^2}\,\Big]^{-1} \right)^{-1}. \quad (4.23)$$

The effective range expansion for $T_{11}(p)$ can be expressed in the form

$$\frac{1}{T_{11}(p)} \;=\; \frac{\mu_1}{2\pi} \left(-\frac{1}{a} - ip + \tfrac{1}{2}\, r_s\, p^2 + \cdots \right). \quad (4.24)$$

[1]The expression for the matrix T_s^{-1} in Eq. (2.18) of Ref. [70] should be equal to $\mathcal{A}(E)^{-1}$ evaluated at $E = p^2/(2\mu_1)$. There is an error in the 22 component of T_s^{-1}: the square root $\sqrt{p^2 - 2\mu_2\Delta}$ should be $\sqrt{(\mu_2/\mu_1)p^2 - 2\mu_2\Delta}$.

Comparing with Eq. (4.23), we can read off the inverse scattering length $1/a$ and the effective range r_s for the first channel:

$$\frac{1}{a} = \frac{1}{a_{11}} + \frac{1}{a_{12}^2}\Big[\sqrt{2\mu_2\Delta} - 1/a_{22}\Big]^{-1}, \tag{4.25a}$$

$$r_s = -\frac{\mu_2/\mu_1}{a_{12}^2\sqrt{2\mu_2\Delta}}\Big[\sqrt{2\mu_2\Delta} - 1/a_{22}\Big]^{-2}. \tag{4.25b}$$

Note that the effective range is negative definite.

If there is a bound state with energy $-\kappa^2/(2\mu_1)$ below the scattering threshold for the first channel, the matrix $\mathcal{A}(E)$ given by Eq. (4.21) has a pole at $E = -\kappa^2/(2\mu_1)$. The binding momentum κ satisfies

$$\kappa = \frac{1}{a_{11}} + \frac{1}{a_{12}^2}\Big[-1/a_{22} + \sqrt{2\mu_2\Delta + (\mu_2/\mu_1)\kappa^2}\Big]^{-1}. \tag{4.26}$$

The behavior of the matrix $\mathcal{A}(E)$ as the energy E approaches the pole associated with the bound state is

$$\mathcal{A}(E) \longrightarrow -\frac{1}{E + \kappa^2/(2\mu_1)} \begin{pmatrix} \mathcal{A}_{X1} \\ \mathcal{A}_{X2} \end{pmatrix} \otimes \begin{pmatrix} \mathcal{A}_{X1} & \mathcal{A}_{X2} \end{pmatrix}. \tag{4.27}$$

The components $\mathcal{A}_{X1}$ and $\mathcal{A}_{X2}$ of the column vector are the amplitudes for transitions from the bound state to particles in the first and second channels, respectively. The column vector is an eigenvector of the matrix $\mathcal{A}(E)^{-1}$ in Eq. (4.21) with eigenvalue zero, so its components must satisfy

$$\mu_1[-1/a_{11} + \kappa]\,\mathcal{A}_{X1} + [\sqrt{\mu_1\mu_2}/a_{12}]\,\mathcal{A}_{X2} = 0. \tag{4.28}$$

Because the only interactions in the two-channel model are contact interactions, the dependence of the wavefunction on the relative momentum of the constituents comes only from propagators. The wavefunction can be expressed in the form

$$\psi(p) = N \begin{pmatrix} 2\mu_1\mathcal{A}_{X1}[p^2 + \kappa^2]^{-1} \\ 2\mu_2\mathcal{A}_{X2}[p^2 + 2\mu_2\Delta + (\mu_2/\mu_1)\kappa^2]^{-1} \end{pmatrix}, \tag{4.29}$$

where N is a normalization constant. The normalization condition

$$\int \frac{d^3p}{(2\pi)^3} \left(|\psi_1(p)|^2 + |\psi_2(p)|^2\right) = 1 \tag{4.30}$$

can be expressed as $Z_1 + Z_2 = 1$, where Z_1 and Z_2 are the probabilities for the bound state to consist of the particles in the first and second channels, respectively. The probability Z_1 for the first channel is given by

$$Z_1^{-1} = 1 + \frac{(\mu_2/\mu_1)a_{12}^2(-1/a_{11} + \kappa)^2\kappa}{\sqrt{2\mu_2\Delta + (\mu_2/\mu_1)\kappa^2}}. \tag{4.31}$$

The renormalizability of the two-channel model [70] implies that the renormalized scattering parameters are independent of the ultraviolet cutoff Λ and it guarantees that Λ can be made arbitrarily large without compromising the consistency of the model. In any specific application, there will be a physical ultraviolet cutoff that sets an upper limit on the momenta for which the scattering model is valid. This physical ultraviolet cutoff Λ sets the natural scale for other scattering parameters, such as P-wave parameters or S-wave parameters that correspond to momentum-dependent interactions.

4.3.2 Large scattering length

The two-channel model of Ref. [70] can be used as a phenomenological model for a system with a large scattering length a in the first channel. The large scattering length requires a fine-tuning of the parameters a_{11}, a_{22}, a_{12}, and Δ. There are various ways to tune the parameters so that $a \to \pm\infty$. For example, if $a_{11} < a_{12}^2/a_{22}$, the energy gap Δ can be tuned to the critical value where the right side of Eq. (4.25a) vanishes. Alternatively, the scattering parameter a_{11} can be tuned to the critical value $-a_{12}^2[\sqrt{2\mu_2\Delta} - 1/a_{22}]$. The coefficients in the low-energy expansion of $\mathcal{T}_{11}(p)^{-1}$

are proportional to various powers of $1/a_{11}$, $1/a_{12}$, and $\sqrt{2\mu_2\Delta}$. We assume that these momentum scales are comparable in magnitude. We refer to that common momentum scale as the natural low-energy scale and we denote it by Λ.

For $|a| \gg \Lambda^{-1}$ and $|E| \ll \Lambda^2/(2\mu_1)$, the amplitude $\mathcal{A}_{11}(E)$ in Eq. (4.22a) approaches the universal amplitude $\mathcal{A}(E)$ in Eq. (3.9) with $\mu = \mu_1$. It follows that for $p \ll \Lambda$ the T-matrix element $\mathcal{T}_{11}(p)$ in Eq. (4.23) approaches the universal T-matrix element $\mathcal{T}(p)$ in Eq. (3.4). For $a \gg \Lambda^{-1}$, the solution to Eq. (4.26) for the binding momentum κ approaches $1/a$, so $\kappa^2/(2\mu)$ approaches the universal binding energy E_X in Eq. (3.5). The probability for the bound state to consist of particles in the first channel Z_1, which is given by Eq. (4.31), approaches to 1 and Z_2 scales as $1/a$ as $1/a \to 0$. Finally the amplitude $\mathcal{A}_{X1}$ for transitions from the bound state to particles in the first channel, which is defined in Eq. (4.27), approaches the universal amplitude $\mathcal{A}_X$ in Eq. (3.8).

4.3.3 Unstable particle in the second channel

Now let us suppose one of the scattering particles in the second channel has a nonzero width. We take that particle to be $2b$. We assume that its width Γ_{2b} arises from its decay into particles with relativistic momenta that are much greater than the ultraviolet cutoff $\Lambda_{\rm UV}$ that defines the domain of validity of the two-channel model. The momenta of the decay products are therefore also much greater than $\sqrt{2\mu_2\Delta}$. We assume that Γ_{2b} is small compared to the mass m_{2b}, but not necessarily small compared to the energy gap Δ between the two channels. This makes it necessary to take into account the contribution to the self-energy of particle $2b$ from the coupling to its decay products.

If the self-energy of particle $2b$ was taken into account, it would modify the term $\sqrt{2\mu_2(\Delta - E)}$ in the inverse of the matrix of transition amplitudes given in Eq. (4.21). That term arises from the amplitude for the propagation of particles in the second channel between contact interactions, which is given by the integral

$$\int \frac{d^3p}{(2\pi)^3} \frac{-1}{E - \Delta - p^2/(2\mu_2) + i\epsilon} = \frac{\mu_2}{\pi^2} \left(\Lambda_{\rm UV} - \frac{\pi}{2} \sqrt{2\mu_2(\Delta - E - i\epsilon)} \right). \qquad (4.32)$$

The cutoff constrains the momentum to the region in which the nonrelativistic approximation for the energy of the particle $2b$ is valid. In this region, the self-energy Π can be expressed as a function of $E' = E - \Delta - p^2/(2\mu_2)$. It can be taken into account by replacing Δ in the integral in Eq. (4.32) by $\Delta + \Pi(E')$. The assumption that the decay products of particle $2b$ have relativistic momenta comparable to m_{2b} implies that their contributions to $\Pi(E')$ have significant dependence on E' only for variations in E' that are comparable to m_{2b}. For energies satisfying $|E| \ll \Lambda_{\rm UV}^2/(2\mu_2)$ and loop momenta $p < \Lambda_{\rm UV}$, the dependence on E' can be neglected and the argument of $\Pi(E')$ can be set to a constant, such as $-\Delta$. The prescription for taking into account the self-energy then reduces to replacing Δ in the integral in Eq. (4.32) by $\Delta + \Pi(-\Delta)$. The real part of $\Pi(-\Delta)$ can be absorbed into Δ so that it becomes the physical threshold. The imaginary part of $\Pi(-\Delta)$ is related to the width of particle $2b$: ${\rm Im}\Pi(-\Delta) = -\Gamma_{2b}/2$. Thus the leading effect of the self-energy can be taken into account by replacing Δ in Eq. (4.21) by the complex-valued energy gap

$$\Delta \;=\; m_{2a} + m_{2b} - (m_{1a} + m_{1b}) - i\Gamma_{2b}/2. \qquad (4.33)$$

For example, the imaginary part of the inverse scattering length given by Eq. (4.25a) is

$${\rm Im}\frac{1}{a} = -\frac{{\rm Im}\sqrt{2\mu_2\Delta}}{a_{12}^2 \left| \sqrt{2\mu_2\Delta} - 1/a_{22} \right|^2}. \qquad (4.34)$$

If Δ is complex, the solution to Eq. (4.26) for the binding momentum κ is complex. It determines the pole mass $m_{X,\rm pole}$ and the width Γ_X of the weakly-bound state according to

$$m_{1a} + m_{1b} - \kappa^2/(2\mu_1) = m_{X,\rm pole} - i\Gamma_X/2. \tag{4.35}$$

The imaginary part reflects the fact that the bound state can decay into particle 2a and decay products of particle 2b. The quantities $m_{X,\rm pole}$ and Γ_X in Eq. (4.35) give the location of a pole in the S-matrix. They need not have the standard interpretations as the location of the peak and the full width at half maximum of a Breit-Wigner resonance.

4.3.4 Factorization

There are universal features associated with transitions from the first channel to the second channel. If $|a| \gg \Lambda^{-1}$ and $|E| \ll \Lambda^2/\mu_1$, the leading term in the transition amplitude $\mathcal{A}_{12}(E)$ in Eq. (4.22b) reduces to

$$\mathcal{A}_{12}(E) = -\frac{\sqrt{\mu_1/\mu_2}}{a_{12}}\Big[\sqrt{2\mu_2\Delta} - 1/a_{22}\Big]^{-1}\mathcal{A}(E), \tag{4.36}$$

where $\mathcal{A}(E)$ is the universal amplitude in Eq. (3.9) with μ replaced by μ_1. For $a \gg \Lambda^{-1}$, the leading term in the amplitude $\mathcal{A}_{X2}$ for transitions of the weakly-bound state X to particles in the second channel, which is defined in Eq. (4.27), reduces to

$$\mathcal{A}_{X2} = -\frac{\sqrt{\mu_1/\mu_2}}{a_{12}}\Big[\sqrt{2\mu_2\Delta} - 1/a_{22}\Big]^{-1}\mathcal{A}_X, \tag{4.37}$$

where $\mathcal{A}_X$ is the universal amplitude in Eq. (3.8). Note that the ratio $\mathcal{A}_{12}(E)/\mathcal{A}_{X2}$ of the amplitudes in Eqs. (4.36) and (4.37) is a universal function of a and E only.

The expressions for $\mathcal{A}_{12}(E)$ and $\mathcal{A}_{X2}$ in Eqs. (4.36) and (4.37) are examples of *factorization formulas*. They express the leading terms in the amplitudes as products

of the same short-distance factor and different long-distance factors $\mathcal{A}(E)$ and $\mathcal{A}_X$. The long-distance factors involve the large scattering length a. The limit $|a| \to \infty$ has been taken in the short-distance factors. The conditions $|E| \ll \Lambda^2/(2\mu)$ or $E = -E_X$ require the particles in the second channel to be off the energy shell by approximately Δ. In the short time $1/\Delta$ allowed by the uncertainty principle, those particles can propagate only over short distances of order $(2\mu_2\Delta)^{-1/2}$. This is small compared to the distance scales $(2\mu|E|)^{-1/2}$ or $|a|$ associated with the particles in the first channel. Thus as far as they are concerned, the particles in the second channel act only as a point source for particles in the first channel. The amplitudes for particles from such a point source to evolve into particles of energy E and into the weakly-bound state are $L(\Lambda, E)\mathcal{A}(E)$ and $L(\Lambda, -E_X)\mathcal{A}_X$, respectively. By using the conditions $|E|, E_X \ll \Lambda^2/(2\mu)$, these amplitudes reduce to $(\mu\Lambda/\pi^2)\mathcal{A}(E)$ and $(\mu\Lambda/\pi^2)\mathcal{A}_X$, respectively. In these expressions, the short-distance factors are identical and the long-distance factors are the same as those in Eqs. (4.36) and (4.37).

Using Eq. (4.31), the probability $Z_2 = 1 - Z_1$ for the bound state to consist of particles in the second channel reduces to

$$Z_2 = \frac{(\mu_2/\mu_1)}{a_{12}^2\sqrt{2\mu_2\Delta}}\Big[\sqrt{2\mu_2\Delta} - 1/a_{22}\Big]^{-2}\frac{1}{a}. \tag{4.38}$$

Note that the probability Z_2 differs from $|\mathcal{A}_{X2}|^2$ only by kinematic factors:

$$|\mathcal{A}_{X2}|^2 = \sqrt{8\pi^2\Delta/\mu_2^3}\, Z_2. \tag{4.39}$$

This relation also follows directly from the wavefunction in Eq. (4.29) if we use the fact that the normalization factor N approaches 1 as $a \to \infty$. Thus the relation between the probability and the transition amplitude in Eq. (4.39) is not specific to the 2-channel model. It applies more generally to any 2-particle component of

the bound state whose wavefunction can be approximated by $(p^2 + 2\mu_2\Delta)^{-1}$, where Δ is the energy gap. It requires only that Δ is small enough that the interaction in that channel can be approximated by an S-wave contact interaction at momenta comparable to $\sqrt{2\mu_2\Delta}$.

CHAPTER 5

FACTORIZATION IN THE PRODUCTION AND DECAY OF THE $X(3872)$

The production and decay of the $X(3872)$ are analyzed under the assumption that the X is a weakly-bound molecule of the charm mesons $D^0\bar{D}^{*0}$ and $D^{*0}\bar{D}^0$. The decays imply that the large $D^0\bar{D}^{*0}$ scattering length has an imaginary part. An effective field theory for particles with a large complex scattering length is used to derive factorization formulas for production rates and decay rates of X. The factorization formulas relate the rates for production of X to those for production of $D^0\bar{D}^{*0}$ and $D^{*0}\bar{D}^0$ near threshold. They also imply that the line shape of X differs significantly from that of a Breit-Wigner resonance.

5.1 Short-distance decays of X

The decay modes of the $X(3872)$ can be classified into *long-distance decays* and *short-distance decays*. The long-distance decay modes are $D^0\bar{D}^0\pi^0$ and $D^0\bar{D}^0\gamma$, which proceed through the decay of a constituent D^{*0} or $\bar{D}^{*0}$. These decays are dominated by a component of the wavefunction of the X in which the separation of the D and D^* is of order $|a|$. These long-distance decays involve interesting interference effects

between the $D^0\bar{D}^{*0}$ and $D^{*0}\bar{D}^0$ components of the wavefunction [41]. The short-distance decays involve a component of the wavefunction in which the separation of the D and D^* is of order $1/m_\pi$ or smaller. Examples are the observed decay modes $J/\psi\,\pi^+\pi^-$, $J/\psi\,\pi^+\pi^-\pi^0$, and $J/\psi\,\gamma$.

Short-distance decays of the X into a hadronic final state H involve well-separated momentum scales. The DD^* wavefunction of the X involves the momentum scale $1/|a|$ set by the large scattering length. The transition of the DD^* to H involves momentum scales m_π or larger. We will refer to momentum scales of order $1/|a|$ and smaller as *long-distance* scales and momentum scales of order m_π and larger as *short-distance* scales. We denote the arbitrary boundary between these two momentum regions by Λ.

The separation of scales $|a| \gg 1/m_\pi$ in the decay process $X \to H$ can be exploited through a factorization formula for the T-matrix element:

$$\mathcal{T}[X \to H] = \sqrt{2m_X}\,\mathcal{A}_X \times \mathcal{A}_{\rm short}[(DD^*)^0_+ \to H]. \tag{5.1}$$

In the long-distance factor, $\mathcal{A}_X$ is the universal amplitude given in Eq. (3.8) and the factor of $\sqrt{2m_X}$ takes into account the difference between the standard nonrelativistic and relativistic normalizations of states. If the complex scattering length is parameterized as in Eq. (3.10), this factor is

$$\mathcal{A}_X = \frac{\sqrt{2\pi}}{\mu}\,(\gamma_{\rm re} + i\gamma_{\rm im})^{1/2}\,. \tag{5.2}$$

The short-distance factor $\mathcal{A}_{\rm short}$ in Eq. (5.1) is insensitive to a, and one can therefore take the limit $|a| \to \infty$ in this factor. The factorization formula in Eq. (5.1) can serve as a definition of the short-distance factor. The content of the factorization statement then resides in the fact that, up to corrections suppressed by powers of

$1/(am_\pi)$, the same short-distance factor appears in the factorization formula for the T-matrix element for the scattering process $D^0\bar{D}^{*0} \to H$ at energies E near the $D^0\bar{D}^{*0}$ threshold:

$$\mathcal{T}[D^0\bar{D}^{*0} \to H] = \frac{1}{\sqrt{2}}\sqrt{4m_{D^0}m_{D^{*0}}}\,\mathcal{A}(E) \times \mathcal{A}_{\rm short}[(DD^*)^0_+ \to H]. \tag{5.3}$$

In the long-distance factor, the $1/\sqrt{2}$ is the amplitude for $D^0\bar{D}^{*0}$ to be in the channel $(DD^*)^0_+$ with the large scattering length, the factor of $\sqrt{4m_{D^0}m_{D^{*0}}}$ takes into account the difference between the standard nonrelativistic and relativistic normalizations of states, and $\mathcal{A}(E)$ is the universal amplitude given in Eq. (3.9). If the complex scattering length is parameterized as in Eq. (3.10), this factor is

$$\mathcal{A}(E) = \frac{2\pi/\mu}{-\gamma_{\rm re} - i(\gamma_{\rm im} + \sqrt{2\mu E})}. \tag{5.4}$$

The factorization formulas in Eqs. (5.3) and (5.1) are analogous to those in Eqs. (4.36) and (4.37) for the two-channel model with a large scattering length in the first channel.

The factorization formulas in Eqs. (5.1) and (5.3) can be motivated diagrammatically by separating virtual particles into *soft* particles and *hard* particles according to whether they are off their energy shells by less than or by more than $\Lambda^2/(2\mu)$, where Λ is the arbitrary momentum separating the long-distance scale $1/|a|$ and the short-distance scale m_π. Any contribution from soft particles inside a subdiagram all of whose external legs are hard can be Taylor-expanded in the momentum of the soft particles, leading to suppression factors of $1/(a\Lambda)$. The diagrams with the fewest suppression factors will be ones that can be separated into a part for which all the internal lines are hard particles and a part that involves only soft particles. This separation leads to the factorization formula.

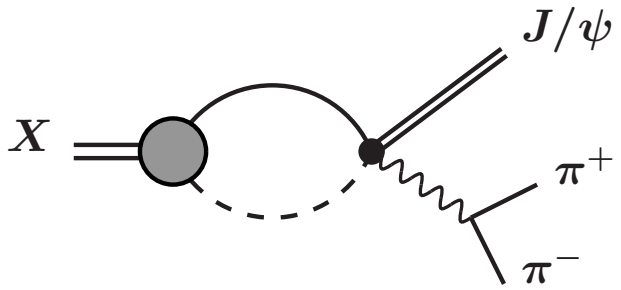

Figure 5.1: Feynman diagram for $X \to J/\psi\,\pi^+\pi^-$ that scale like $(am_\pi)^{-1/2}$. The $(DD^*)^0_+$ wavefunction of the X is the integral over the loop energy of the product of the blob and the attached propagators.

The leading terms in the T-matrix element for $X \to H$ in the limit $|a|m_\pi \gg 1$ can be represented by the Feynman diagrams in Fig. 5.1 and can be expressed as

$$\mathcal{T}[X \to H] = \sqrt{2m_X} \int \frac{d^3p}{(2\pi)^3}\, \psi(p)\, \mathcal{A}^{(\Lambda)}[(DD^*)^0_+ \to H], \tag{5.5}$$

where $\psi(p)$ is the universal wavefunction in Eq. (3.7). The factor $\mathcal{A}^{(\Lambda)}$, which is represented by a dot in Fig. 5.1, is an amplitude for the transition $(DD^*)^0_+ \to H$ in which all virtual particles are off their energy shells by more than $\Lambda^2/(2\mu)$. It is therefore insensitive to the relative momentum $\boldsymbol{p}$ of the D and D^*. If that momentum dependence is neglected and if the integral in Eq. (5.5) is regularized by a momentum cutoff $|\boldsymbol{p}| < \Lambda$, the wavefunction factor reduces in the limit $|a| \gg \Lambda^{-1}$ to

$$\int \frac{d^3p}{(2\pi)^3}\psi(p) = \sqrt{\frac{2}{\pi^3}}\Lambda a^{-1/2}. \tag{5.6}$$

The factorization formula in Eq. (5.1) is then obtained by absorbing a factor of $(\mu/\pi^2)\Lambda$ into $\mathcal{A}^{(\Lambda)}$ to obtain the short-distance factor:

$$\mathcal{A}_{\rm short}[(DD^*)^0_+ \to H] = \left(\frac{\mu}{\pi^2}\Lambda\right) \mathcal{A}^{(\Lambda)}[(DD^*)^0_+ \to H]. \tag{5.7}$$

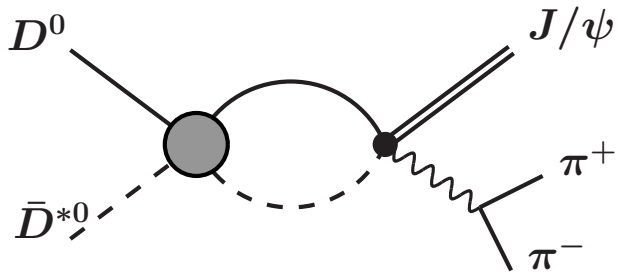

Figure 5.2: Feynman diagrams for $D^0\bar{D}^{*0} \to J/\psi\,\pi^+\pi^-$ that are enhanced near the $D^0\bar{D}^{*0}$ threshold by a factor of am_π. The blob represents the geometric series of Feynman diagrams in Fig. 4.1.

Since the T-matrix element in Eq. (5.1) is independent of the arbitrary separation scale, the dependence on Λ must cancel between the two factors on the right side of Eq. (5.7).

The leading term in the T-matrix element for $D^0\bar{D}^{*0} \to H$ in the limits $|a| \gg \Lambda^{-1}$ and $E \ll \Lambda^2/(2\mu)$ can be represented by the Feynman diagram in Fig. 5.2 and can be expressed as

$$\mathcal{T}[D^0\bar{D}^{*0} \to H] = \frac{1}{\sqrt{2}}\sqrt{4m_{D^0}m_{D^{*0}}}\,\mathcal{A}(E)\,L(\Lambda,E)\,\mathcal{A}^{(\Lambda)}[(DD^*)^0_+ \to H]. \qquad (5.8)$$

The factor $L(\Lambda, E)$ is the amplitude for the propagation of the D and D^* between successive contact interactions, which is given in Eq. (4.4). The approximation $E \ll \Lambda^2/(2\mu)$ justifies neglecting the $\sqrt{2\mu E}$ term in $L(\Lambda, E)$. The factorization formula in Eq. (5.3) is then obtained by absorbing the remaining term $(\mu/\pi^2)\Lambda$ into $\mathcal{A}^{(\Lambda)}$ to obtain the short-distance factor in Eq. (5.7).

The factorization formula for the T-matrix element in Eq. (5.1) implies a factorization formula for the decay rate for $X \to H$. The decay rate $\Gamma[X \to H]$ can be

expressed as the product of a short-distance factor and the long-distance factor

$$|\mathcal{A}_X|^2 = \frac{2\pi}{\mu^2}\sqrt{\gamma_{\rm re}^2 + \gamma_{\rm im}^2}. \tag{5.9}$$

Using the expressions for the binding energy and the total width of the X in Eqs. (3.12) and (3.11b), the long-distance factor in Eq. (5.9) can be expressed as

$$|\mathcal{A}_X|^2 = \sqrt{\frac{8\pi^2}{\mu^3}}[E_X + \Gamma_X^2/(16E_X)]^{1/2}. \tag{5.10}$$

If the partial width for a short-distance decay mode of the X has been calculated using a model with a specific binding energy, the factorization formula for the decay rate can be used to extrapolate the prediction to other values of the binding energy and to take into account the effect of the width of the X. This is useful because numerical calculations in models often become increasingly unstable as the binding energy is tuned to zero. Swanson has estimated the partial widths for various short-distance decays of X using a potential model, but only for binding energies down to about 1 MeV and without taking into account the effect of the width of the X [33, 72]. His predictions can be extrapolated to other values of the binding energy and the width of the X can be taken into account by using the long-distance factor in Eq. (5.10).

5.2 Production of X

The production of X necessarily involves the long-distance momentum scale $1/|a|$ through the $(DD^*)_+^0$ wavefunction of the X. The production also involves much larger momentum scales. Unless there are already hadrons in the initial state containing a c and $\bar{c}$, the production process involves the scale m_c associated with the creation of a $c\bar{c}$ pair. Even if the initial state includes hadrons that contain c and $\bar{c}$, such as J/ψ or D^+

and D^-, the production process involves the scale m_π associated with the formation of the D^0 and $\bar{D}^{*0}$ that bind to form the X. We will define a *short-distance production* process to be one for which the initial state either does not include any of the charm mesons D^0, $\bar{D}^{*0}$, D^{*0}, or $\bar{D}^0$, or if it does, the momentum of the charm meson in the rest frame of the X is of order m_π or larger. All practical production mechanisms for X in high energy physics are short-distance processes. Long-distance production mechanisms could arise in a hadronic medium that includes charm mesons, such as that produced by relativistic heavy-ion collisions.

In a short-distance production process, the separation between the long-distance scale $1/|a|$ and all the shorter-distance momentum scales can be exploited through a factorization formula that expresses the leading term in the production rate as the product of a long-distance factor that involves a and a short-distance factor that is insensitive to a. To be definite, we will consider the specific production process $B \to XK$. The factorization for any other short-distance production process will have the same long-distance factor but a different short-distance factor.

There are many momentum scales that play an important role in the decay $B \to XK$, ranging from the extremely short-distance scales m_W and m_b associated with the quark decay process $b \to c\bar{c}s$ to the smaller short-distance scales $\Lambda_{\rm QCD}$ and m_π involved in formation of the final-state hadrons to the long-distance scale $1/|a|$ associated with the $(DD^*)^0_+$ wavefunction of the X. We denote the arbitrary boundary between the long-distance momentum region and the short-distance momentum region by Λ.

The separation between the long-distance scale $1/|a|$ and all the short-distance momentum scales in the decay $B \to XK$ can be exploited through a factorization

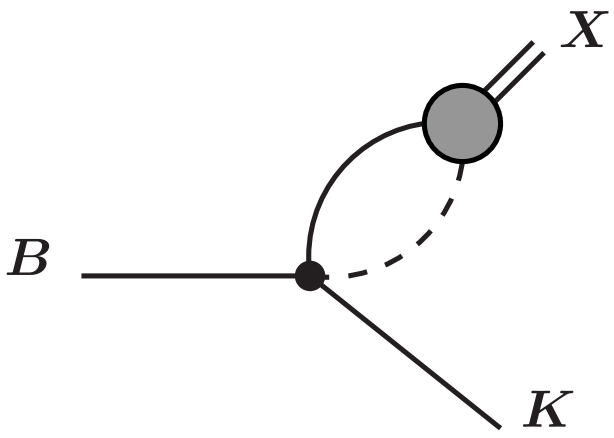

Figure 5.3: Feynman diagram for $B \to XK$ that scales like $(am_\pi)^{-1/2}$. The $(DD^*)^0_+$ wavefunction of the X is the integral over the loop energy of the product of the blob and the attached propagators.

formula for the T-matrix element:

$$\mathcal{T}[B \to XK] = \mathcal{A}_{\rm short}[B \to (DD^*)^0_+ K] \times \mathcal{A}_X \sqrt{2m_X}. \tag{5.11}$$

In the long-distance factor, $\mathcal{A}_X$ is the universal amplitude in Eq. (5.2). The short-distance factor in Eq. (5.11) is insensitive to a and one can therefore take the limit $|a| \to \infty$ in that factor. The factorization formula in (5.11) can serve as the definition of the short-distance factor. The content of the factorization statement then resides in the fact that the same short-distance factor appears in the factorization formula for the T-matrix element for the decay $B \to D^0 \bar{D}^{*0} K$ when the DD^* invariant mass is near the $D^0 \bar{D}^{*0}$ threshold. This factorization formula is discussed in Section 5.3.

The factorization formula in Eq. (5.11) can be motivated diagrammatically by separating the loop integrals in the decay amplitude according to whether the virtual particles are off their energy shells by less than or by more than $\Lambda^2/(2\mu)$. The leading terms in the decay amplitude for $B \to XK$ are suppressed only by a factor

of $(am_\pi)^{-1/2}$. These terms can be represented by the Feynman diagram in Fig. 5.3 and can be expressed in the form

$$\mathcal{T}[B \to XK] = \sqrt{2m_X} \int \frac{d^3p}{(2\pi)^3} \psi(p)\, \mathcal{A}^{(\Lambda)}[B \to (DD^*)^0_+ K], \tag{5.12}$$

where $\psi(p)$ is the universal wavefunction in Eq. (3.7). The factor $\mathcal{A}^{(\Lambda)}$, which is represented by a dot in Fig. 5.3, is an amplitude for the decay $B \to (DD^*)^0_+ K$ in which all virtual particles are off their energy shells by more than $\Lambda^2/(2\mu)$. It is therefore insensitive to the relative momentum $\boldsymbol{p}$ of the D and D^*. If that momentum dependence is neglected, the wavefunction factor in Eq. (5.12) reduces to Eq. (5.6). The factorization formula in Eq. (5.11) then requires the short-distance factor to be

$$\mathcal{A}_{\rm short}[B \to (DD^*)^0_+ K] = \mathcal{A}^{(\Lambda)}[B \to (DD^*)^0_+ K] \left(\frac{\mu}{\pi^2}\Lambda\right). \tag{5.13}$$

Since the T-matrix element in Eq. (5.11) is independent of the arbitrary separation scale, the dependence on Λ must cancel between the two factors on the right side of Eq. (5.13).

We proceed to use the factored expression in Eq. (5.11) to evaluate the decay rate for $B^+ \to XK^+$. Lorentz invariance constrains the short-distance amplitude $\mathcal{A}_{\rm short}$ at the DD^* threshold to have the form

$$\mathcal{A}_{\rm short}[B^+ \to (DD^*)^0_+ K^+] = c_+\, P \cdot \epsilon_{D^*}, \tag{5.14}$$

where P is the 4-momentum of the B^+ and ϵ_{D^*} is the polarization 4-vector of the D^*. Heavy quark spin symmetry guarantees that the polarization vector ϵ_{D^*} can be identified with the polarization vector ϵ_X of the X. The decay rate is obtained by squaring the amplitude in Eq. (5.11), summing over the spin of the X, and integrating

over phase space. The resulting expression for the decay rate is

$$\Gamma[B^+ \to XK^+] = |c_+|^2 \frac{\lambda^{3/2}(m_B, m_X, m_K)}{32\pi m_B^3 m_X} |\mathcal{A}_X|^2, \tag{5.15}$$

where $\lambda(x, y, z)$ is the triangle function:

$$\lambda(x, y, z) = x^4 + y^4 + z^4 - 2(x^2y^2 + y^2z^2 + z^2x^2). \tag{5.16}$$

The long-distance factor $|\mathcal{A}_X|^2$ is given in Eq. (5.9). The result in Eq. (5.15) was obtained in Ref. [43] for the special case $\gamma_{\rm im} = 0$ and used to estimate the order of magnitude of the decay rate for $B^+ \to XK^+$. The estimate is consistent with the measurement of the product of the branching fractions for $B^+ \to XK^+$ and $X \to J/\psi\,\pi^+\pi^-$ [5] provided $J/\psi\pi^+\,\pi^-$ is one of the major decay modes of X.

The factorization formula for the decay rate for $B^0 \to XK^0$ has the same form as in Eq. (5.15) except that the coefficient c_+ in the short-distance decay amplitude in Eq. (5.14) has a different value. In Ref. [44], it was pointed out that the decay rate for $B^0 \to XK^0$ should be suppressed compared to $B^+ \to XK^+$. That suppression can be understood by considering the short-distance amplitude for $B \to DD^*K$. The dominant contributions to most decay amplitudes of the B meson are believed to be factorizable into the product of matrix elements of currents. The factorizable contributions to the decay amplitude for $B^+ \to (DD^*)^0_+ K^+$ have three terms: the product of $B^+ \to \bar{D}^{*0}$ and $\emptyset \to D^0K^+$ matrix elements, where $\emptyset$ is the QCD vacuum, the product of $B^+ \to \bar{D}^0$ and $\emptyset \to D^{*0}K^+$ matrix elements, and the product of $B^+ \to K^+$ and $\emptyset \to (DD^*)^0_+$ matrix elements. The factorizable contributions to the decay amplitude for $B^0 \to (DD^*)^0_+ K^0$ have only one term: the product of $B^0 \to K^0$ and $\emptyset \to (DD^*)^0_+$ matrix elements. Heavy quark symmetry implies that the $\emptyset \to (DD^*)^0_+$ matrix element vanishes at the $D^0\bar{D}^{*0}$ threshold. The decay $B^0 \to (DD^*)^0_+ K^0$ near

the $D^0\bar{D}^{*0}$ threshold must therefore proceed through nonfactorizable terms in the decay amplitude. The resulting suppression of the coefficient c_+ in the short-distance factor for $B^0 \to (DD^*)^0_+ K^0$ results in a suppression of the rate for $B^0 \to XK^0$ relative to the rate for $B^+ \to XK^+$. In Ref. [44], a quantitative analysis of Babar data on the branching fractions for $B \to D^{(*)}D^{(*)}K$ [73] was used to estimate the suppression factor to be an order of magnitude or more.

5.3 Production of $D^0\bar{D}^{*0}$ near threshold

It was pointed out in Ref. [43] that the identification of X as a DD^* molecule could be confirmed by observing a peak in the invariant mass distribution for $D^0\bar{D}^{*0}$ (or $D^{*0}\bar{D}^0$) near the DD^* threshold in the decay $B \to DD^*K$. The shape of that invariant mass distribution was given for a real scattering length a. The shape would be the same for any other short-distance production process. In this section, we consider the effect of an imaginary part of the scattering length on the DD^* invariant mass distribution for a short-distance production process. To be specific, we consider the short-distance production process $B \to D^0\bar{D}^{*0}K$.

The separation between the long-distance scale $1/|a|$ and all the short-distance momentum scales in the decay $B \to D^0\bar{D}^{*0}K$ can be exploited through a factorization formula for the T-matrix element:

$$\mathcal{T}[B \to D^0\bar{D}^{*0}K] = \mathcal{A}_{\rm short}[B \to (DD^*)^0_+ K] \times \mathcal{A}(E)\,\sqrt{4m_{D^0}m_{D^{*0}}}\,\frac{1}{\sqrt{2}}. \qquad (5.17)$$

In the long-distance factor, $\mathcal{A}(E)$ is the universal amplitude in Eq. (5.4) and the factor $1/\sqrt{2}$ is the amplitude for $D^0\bar{D}^{*0}$ to be in the channel $(DD^*)^0_+$ with the large scattering length. The short-distance factor $\mathcal{A}_{\rm short}$ is the same as in the factorization formula for $B \to XK$ in Eq. (5.11).

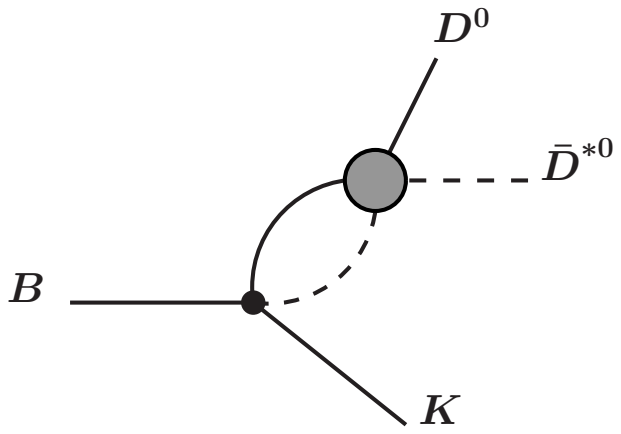

Figure 5.4: Feynman diagrams for $B \to D^0 \bar{D}^{*0} K$ that are enhanced near the $D^0 \bar{D}^{*0}$ threshold by a factor of am_π. The blob represents the geometric series of diagrams shown in Fig. 4.1.

The factorization formula in Eq. (5.17) can be motivated diagrammatically by separating the loop integrals in the decay amplitude according to whether the virtual particles are off their energy shells by less than or by more than $\Lambda^2/(2\mu)$. There are terms in the T-matrix element for the decay $B \to D^0 \bar{D}^{*0} K$ that are enhanced near the DD^* threshold by a factor of am_π. These terms can be represented by the Feynman diagrams in Fig. 5.4 and can be expressed in the form

$$\mathcal{T}[B \to D^0 \bar{D}^{*0} K] = \mathcal{A}^{(\Lambda)}[B \to (DD^*)^0_+ K]\, L(\Lambda, E)\, \mathcal{A}(E)\, \sqrt{4 m_{D^0} m_{D^{*0}}}\, \frac{1}{\sqrt{2}}. \quad (5.18)$$

The first factor $\mathcal{A}^{(\Lambda)}$, which is represented by the dot in Fig. 5.4, is an amplitude for the decay into $(DD^*)^0_+ K$ in which all virtual particles are off their energy shells by more than $\Lambda^2/(2\mu)$. It is therefore insensitive to the relative momentum $\boldsymbol{p}$. The second factor $L(\Lambda, E)$ is the amplitude for the propagation of the D and D^* between contact interactions, which is given in Eq. (4.4). The condition $|E| \ll \Lambda^2/(2\mu)$ implies that the $\sqrt{-2\mu E}$ term in $L(\Lambda, E)$ can be neglected. The resulting expression for the

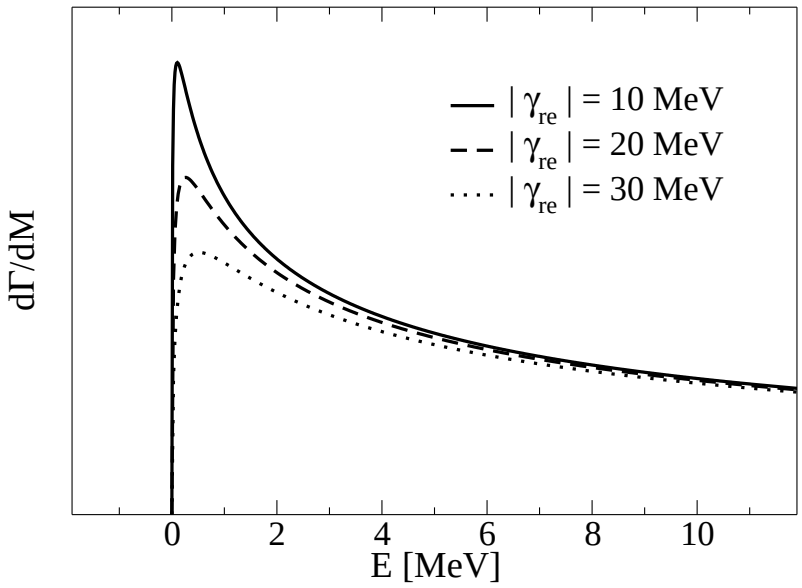

Figure 5.5: The DD^* invariant mass distribution in $B \to D^0 \bar{D}^{*0} K$ for $\gamma_{\rm im} = 10$ MeV and various values of $|\gamma_{\rm re}|/\gamma_{\rm im}$. The horizontal axis is the difference $E = M - (m_{D^0} + m_{D^{*0}})$ between the invariant mass M and the $D^0 \bar{D}^{*0}$ threshold.

T-matrix element is the factorization formula in Eq. (5.17), with the short-distance factor $\mathcal{A}_{\rm short}$ given in Eq. (5.13).

We proceed to use the factorized expression for the decay amplitude in Eq. (5.17) to calculate the DD^* invariant mass distribution near the $D^0 \bar{D}^{*0}$ threshold in the decay $B^+ \to D^0 \bar{D}^{*0} K^+$. Lorentz invariance constrains the short-distance amplitude $\mathcal{A}_{\rm short}$ at the DD^* threshold to have the form in Eq. (5.14). The decay rate is obtained by squaring the amplitude in Eq. (5.17), summing over the spins of the $\bar{D}^{*0}$, and integrating over phase space. The resulting expression for the differential decay rate with respect to the DD^* invariant mass M near the $D^0 \bar{D}^{*0}$ threshold is

$$\frac{d\Gamma}{dM}[B^+ \to D^0 \bar{D}^{*0} K^+] = |c_+|^2 \frac{\mu \lambda^{3/2}(m_B, M, m_K)}{256\pi^3 m_B^3 M^2} \, \lambda^{1/2}(M, m_{D^0}, m_{D^{*0}}) |\mathcal{A}(E)|^2, \quad (5.19)$$

where E is the energy of the $D^0\bar{D}^{*0}$ in its rest frame relative to the $D^0\bar{D}^{*0}$ threshold:

$$E = M - (m_{D^0} + m_{D^{*0}}). \tag{5.20}$$

We have used the fact that M is near the $D^0\bar{D}^{*0}$ threshold to replace a factor of $m_{D^0}m_{D^{*0}}$ in Eq. (5.19) by μM. The result in Eq. (5.19) was obtained previously in Ref. [43] for the special case $\gamma_{\rm im} = 0$. For M near the $D^0\bar{D}^{*0}$ threshold, the only significant variation with M is through the long-distance factor $|\mathcal{A}(E)|^2$ and the threshold factor

$$\lambda^{1/2}(M, m_{D^0}, m_{D^{*0}}) \approx 2M\sqrt{2\mu E}. \tag{5.21}$$

If the complex scattering length is parameterized as in Eq. (3.10), the long-distance factor is

$$|\mathcal{A}(E)|^2 = \frac{4\pi^2/\mu^2}{((2\mu E)^{1/2} + \gamma_{\rm im})^2 + \gamma_{\rm re}^2}. \tag{5.22}$$

The shape of the $D^0\bar{D}^{*0}$ invariant mass distribution in Eq. (5.19) is given by the factor $\sqrt{2\mu E}\,|\mathcal{A}(E)|^2$. Note that it depends on $\gamma_{\rm re}$ and $\gamma_{\rm im}$ but not on the sign of $\gamma_{\rm re}$. The invariant mass distribution is shown in Fig. 5.5 for $\gamma_{\rm im} = 10$ MeV and three values of $|\gamma_{\rm re}|$: 10, 20, and 30 MeV. The peak in the invariant mass distribution occurs at $E = |\gamma|^2/(2\mu)$, where $|\gamma| = \sqrt{\gamma_{\rm re}^2 + \gamma_{\rm im}^2}$. The value at the peak is proportional to $(|\gamma| + \gamma_{\rm im})^{-1}$. The full width at half maximum is $2(2|\gamma| + \gamma_{\rm im})[(|\gamma| + \gamma_{\rm im})(3|\gamma| + \gamma_{\rm im})]^{1/2}/\mu$.

The Babar collaboration has measured the branching fractions for $B \to D^0\bar{D}^{*0}K$ and $B \to D^{*0}\bar{D}^0K$ using a data sample of about 8×10^7 $B\bar{B}$ events [73]. The strongest signal was observed in the channel $B^+ \to D^{*0}\bar{D}^0K^+$: 221 ± 27 events above the background, but with a contamination of about 37 events due to crossfeed from other

decay channels. If the invariant mass distributions could be measured with resolution much better than $m_\pi^2/(2\mu) \simeq 10$ MeV and if the histograms included enough events, one could actually resolve the resonant enhancement near threshold that is illustrated in Figure 5.5 and determine both a and $|c_+|^2$ directly from the data. The resolution that would be required may not be out of the question, since Babar has presented a histogram of $d\Gamma/dM$ for the decay $B^0 \to D^{*-}\bar{D}^{*0}K^+$ with 20 MeV bins [73]. However the region $q < m_\pi$ in which the enhancement is expected to occur accounts for only about 0.2% of the available phase space for the decay $B \to D^0\bar{D}^{*0}K$. Even with an enhancement in this region by a factor of 3 from a very large scattering length, it may be difficult to accumulate enough events in this region to resolve the structure in Figure 5.5.

5.4 The X line shape

The X is observed as a peak in the invariant mass distribution of its decay products, such as $J/\psi\,\pi^+\pi^-$. Its mass and width are extracted from that invariant mass distribution. For instance, the Belle collaboration obtained their value for the mass and the upper bound on the width by fitting the $J/\psi\,\pi^+\pi^-$ invariant mass distribution in $B^+ \to J/\psi\,\pi^+\pi^-\,K^+$ near the $D^0\bar{D}^{*0}$ threshold to a resolution-broadened Breit-Wigner function on top of a polynomial background. The shape of the invariant mass distribution of the decay products of the X is called the *line shape*. The resonant interactions in the $D^0\bar{D}^{*0}/D^{*0}\bar{D}^0$ system can significantly modify the line shape, so it need not have the conventional Breit-Wigner form. In this section, we compute the line shape of the X in short-distance decays of the X. To be definite, we consider the production process $B \to HK$, where H is the hadronic system consisting

of $J/\psi\,\pi^+\pi^-$ with invariant mass near the $D^0\bar{D}^{*0}$ threshold. However our results on the line shape will apply more generally to any short-distance production process for X and any short-distance decay mode of X.

The separation between the long-distance scale $1/|a|$ and all the short-distance momentum scales in the decay $B \to HK$ can be exploited through a factorization formula for the T-matrix element:

$$\mathcal{T}[B \to HK] = \mathcal{A}_{\rm short}[B \to (DD^*)^0_+ K] \times \mathcal{A}(E) \times \mathcal{A}_{\rm short}[(DD^*)^0_+ \to H]. \quad (5.23)$$

There is an implied sum over the spin states of the D^*. The long-distance factor $\mathcal{A}(E)$ depends on the complex-valued scattering length a and is given in Eq. (5.4). Its argument E is the difference between the invariant mass M of the hadronic system H and the $D^0\bar{D}^{*0}$ threshold, as given in Eq. (5.20). The short-distance factor $\mathcal{A}_{\rm short}$ associated with the initial state is the same one that appears in the factorization formulas for $B \to XK$ in Eq. (5.11) and for $B \to D^0\bar{D}^{*0}K$ in Eq. (5.17). The short-distance factor $\mathcal{A}_{\rm short}$ associated with the final state is the same one that appears in the factorization formulas for $X \to H$ in Eq. (5.1) and for $D^0\bar{D}^{*0} \to H$ in Eq. (5.3).

The factorization formula in Eq. (5.23) can be motivated diagrammatically by separating the loop integrals in the decay amplitude according to whether the virtual particles are off their energy shells by less than or by more than $\Lambda^2/(2\mu)$. There are terms in the decay amplitude for $B \to HK$ that are enhanced by a factor of am_π when the invariant mass of H is near the $D^0\bar{D}^{*0}$ threshold. These terms can be represented by the Feynman diagrams in Fig. 5.6 and can be expressed in the form

$$\mathcal{T}[B \to HK] = \mathcal{A}^{(\Lambda)}[B \to (DD^*)^0_+ K]\, L(\Lambda, E)\, \mathcal{A}(E)\, L(\Lambda, E)\, \mathcal{A}^{(\Lambda)}[(DD^*)^0_+ \to H]. \quad (5.24)$$

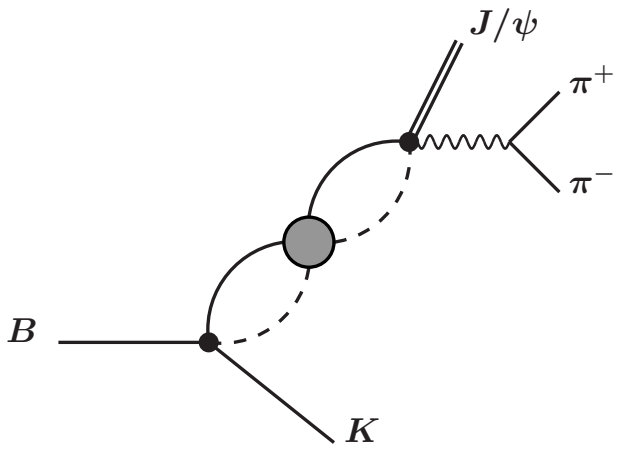

Figure 5.6: Feynman diagrams for $B \to J/\psi\,\pi^+\pi^-\,K$ that are enhanced near the $D^0\bar{D}^{*0}$ threshold by a factor of am_π. The blob represents the geometric series of diagrams given in Fig. 4.1.

The factors $\mathcal{A}^{(\Lambda)}$, which are represented by dots in Fig. 5.6, are amplitudes in which all virtual particles are off their energy shells by more than $\Lambda^2/(2\mu)$. The factors of $L(\Lambda, E)$, which is given in Eq. (4.4), are the amplitudes for the propagation of the D and D^* between contact interactions. The condition $|E| \ll \Lambda^2/(2\mu)$ implies that the $\sqrt{-2\mu E}$ term in $L(\Lambda, E)$ can be neglected. The resulting expression for the T-matrix element is the factorization formula in Eq. (5.23), with the short-distance factors $\mathcal{A}_{\rm short}$ given in Eqs. (5.13) and (5.7).

The factorization formula for the T-matrix element in (5.23) implies a factorization formula for the invariant mass distribution for the hadronic system H near the $D^0\bar{D}^{*0}$ threshold. If the hadronic system consists of particles with momenta p_i and invariant

mass M, the factorization formula is

$$\begin{aligned}
&\frac{d\Gamma}{dM}[B^+ \to K^+ H] \\
&= \frac{M}{2\pi m_B} \int \left|\mathcal{A}_{\rm short}[B \to (DD^*)^0_+ K]\right|^2 (2\pi)^4 \delta^4(P_B - P_H - P_K) \frac{d^3P_H}{(2\pi)^3 2E_H} \frac{d^3P_K}{(2\pi)^3 2E_K} \\
&\quad \times |\mathcal{A}(E)|^2 \times \int \left|\mathcal{A}_{\rm short}[(DD^*)^0_+ \to H]\right|^2 (2\pi)^4 \delta^4(P_H - \textstyle\sum_i p_i) \displaystyle\prod_i \frac{d^3p_i}{(2\pi)^3 2E_i}. \quad (5.25)
\end{aligned}$$

For M near the $D^0\bar{D}^{*0}$ threshold, the only significant variation with M is through the long-distance factor $|\mathcal{A}(E)|^2$, where E is the energy defined in Eq. (5.20). If the complex scattering length is parameterized as in Eq. (3.10), the long-distance factor is

$$\begin{aligned}
\left|\mathcal{A}(E)\right|^2 &= \frac{4\pi^2/\mu^2}{(|2\mu E|^{1/2} - \gamma_{\rm re})^2 + \gamma_{\rm im}^2} \qquad E \le 0, \quad (5.26a) \\
&= \frac{4\pi^2/\mu^2}{((2\mu E)^{1/2} + \gamma_{\rm im})^2 + \gamma_{\rm re}^2} \qquad E \ge 0. \quad (5.26b)
\end{aligned}$$

This factor gives the line shape of the X. Note that for $E > 0$, the line shape does not depend on the sign of $\gamma_{\rm re}$. However for $E < 0$, the line shape is completely different for $\gamma_{\rm re} > 0$ and $\gamma_{\rm re} < 0$.

In the case $\gamma_{\rm re} > 0$, the peak in the invariant mass distribution occurs below the $D^0\bar{D}^{*0}$ threshold by the amount $\gamma_{\rm re}^2/(2\mu)$. The X line shape is illustrated in the upper panel of Fig. 5.7 for $\gamma_{\rm im} = 10$ MeV and for three positive values of $\gamma_{\rm re}$: 10, 20, and 30 MeV. If $\gamma_{\rm im} < \gamma_{\rm re}$, the full width of the peak at half maximum is $2\gamma_{\rm re}\gamma_{\rm im}/\mu$. The line shape for $E < 0$ is symmetric about the peak as a function of $|E|^{1/2}$ but not as a function of E. If $\gamma_{\rm im} \ll \gamma_{\rm re}$, the line shape in Eq. (5.26) is sharply peaked at $E = -\gamma_{\rm re}^2/(2\mu)$ and it can be approximated by a delta function:

$$|\mathcal{A}(E)|^2 \approx \frac{4\pi^3\gamma_{\rm re}}{\mu^3\gamma_{\rm im}} \delta\big(E + \gamma_{\rm re}^2/(2\mu)\big). \quad (5.27)$$

Note that the condition $\gamma_{\rm im} \ll \gamma_{\rm re}$ is equivalent to $\Gamma_X \ll E_X/4$.

In the case $\gamma_{\rm re} < 0$, the peak in the invariant mass distribution occurs at the $D^0\bar{D}^{*0}$ threshold. The X line shape is illustrated in the lower panel of Fig. 5.7 for $\gamma_{\rm im} = 10$ MeV and for three negative values of $\gamma_{\rm re}$: -10, -20, and -30 MeV. The line shape has a cusp at $E = 0$. Bugg has proposed that the X can be identified with this cusp at the $D^0\bar{D}^{*0}$ threshold [46]. The normalization is the same in the upper and lower panels of Fig. 5.7. Note that the area under the cusp in the lower panel of Fig. 5.7 is much smaller than the area under the resonance in the upper panel for the same values of $\gamma_{\rm im}$ and $|\gamma_{\rm re}|$. Thus a cusp seems less likely as an interpretation for the $X(3872)$ than a resonance, although a quantitative analysis would be required to rule out that possibility.

The integral over all energies of the line shape of a conventional Breit-Wigner resonance is convergent. In contrast, the integral of the line shape in Eq. (5.26) diverges logarithmically as the endpoints $E_{\rm min}$ and $E_{\rm max}$ of the integral increase in magnitude. This follows from the fact that the line shape in Eq. (5.26) decreases as $1/|E|$ for $(2\mu|E|)^{1/2} \gg |\gamma_{\rm re}|, \gamma_{\rm im}$. That expression for the line shape is of course only accurate for $|E|$ lower than $\Lambda^2/(2\mu) \sim 10$ MeV, where $\Lambda \sim m_\pi$ is the natural momentum scale for low-energy DD^* scattering. Thus the logarithmic dependence on $E_{\rm min}$ and $E_{\rm max}$ holds only for $|E_{\rm min}|, E_{\rm max} < \Lambda^2/(2\mu)$. It is convenient to define $p_{\rm min}$ and $p_{\rm max}$ by $E_{\rm min} = -p_{\rm min}^2/(2\mu)$ and $E_{\rm max} = +p_{\rm max}^2/(2\mu)$. The integral of the factor in Eq. (5.26) reduces in the limit $p_{\rm min}, p_{\rm max} \gg |\gamma_{\rm re}|, \gamma_{\rm im}$ to

$$\int_{E_{\rm min}}^{E_{\rm max}} |\mathcal{A}(E)|^2 dE \approx \frac{4\pi^2}{\mu^3} \left(\log \frac{p_{\rm min} p_{\rm max}}{\gamma_{\rm re}^2 + \gamma_{\rm im}^2} + \frac{\pi\gamma_{\rm re}}{\gamma_{\rm im}}\, \theta(\gamma_{\rm re}) - f(\gamma_{\rm re}/\gamma_{\rm im}) \right), \qquad (5.28)$$

where $f(x)$ is the function

$$f(x) = x \arctan(1/x) + (1/x) \arctan(x). \qquad (5.29)$$

This function has a limited range, varying from 1 at $x = 0$ and $x = \pm\infty$ to $\pi/2$ at $x = \pm 1$.

The factorization formula for the invariant mass distribution of H in the case $\gamma_{\rm re} > 0$ has important implications for measurements of the branching fractions of X. Since the two short-distance factors in Eq. (5.25) are insensitive to E, we can set M to $m_{D^0} + m_{D^{*0}}$ or to m_X in those factors. The short-distance factor associated with the decay of the B^+ reduces to $\Gamma[B \to XK]/(2\pi|\mathcal{A}_X|^2)$. If $\gamma_{\rm re} > 0$, the short-distance factor associated with the formation of H reduces to $\Gamma[X \to H]/|\mathcal{A}_X|^2$. Thus the differential decay rate in Eq. (5.25) reduces to

$$\frac{d\Gamma}{dM}[B \to HK] = \Gamma[B \to XK]\,{\rm Br}[X \to H]\,\frac{\Gamma_X\,|\mathcal{A}(E)|^2}{2\pi\,|\mathcal{A}_X|^4}. \tag{5.30}$$

If the product of $\Gamma[B \to XK]$ and ${\rm Br}[X \to H]$ is measured by integrating $d\Gamma/dM$ over the energy interval from $E_{\rm min}$ to $E_{\rm max}$ with $|E_{\rm min}|, E_{\rm max} \gg E_X, \Gamma_X$, it will be in error by the factor

$$\begin{aligned}\frac{\Gamma_X}{2\pi|\mathcal{A}_X|^4}\int_{E_{\rm min}}^{E_{\rm max}}|\mathcal{A}(E)|^2 dE \;&\approx\; \left[1 + \frac{\Gamma_X^2}{16E_X^2}\right]^{-1} \\ &\times\left[1 + \left(\log\frac{|E_{\rm min}|^{1/2}E_{\rm max}^{1/2}}{E_X + \Gamma_X^2/(16E_X)} - f(4E_X/\Gamma_X)\right)\frac{\Gamma_X}{4\pi E_X}\right].\end{aligned} \tag{5.31}$$

The error would cancel in the ratio of the branching fractions for any two short-distance decay modes of X. The error would not cancel in the ratio of the branching fractions for a short-distance decay mode of X and one of the long-distance decay modes $D^0\bar{D}^0\pi^0$ and $D^0\bar{D}^0\gamma$. This effect should be taken into account in analyzing the decays of the $X(3872)$.

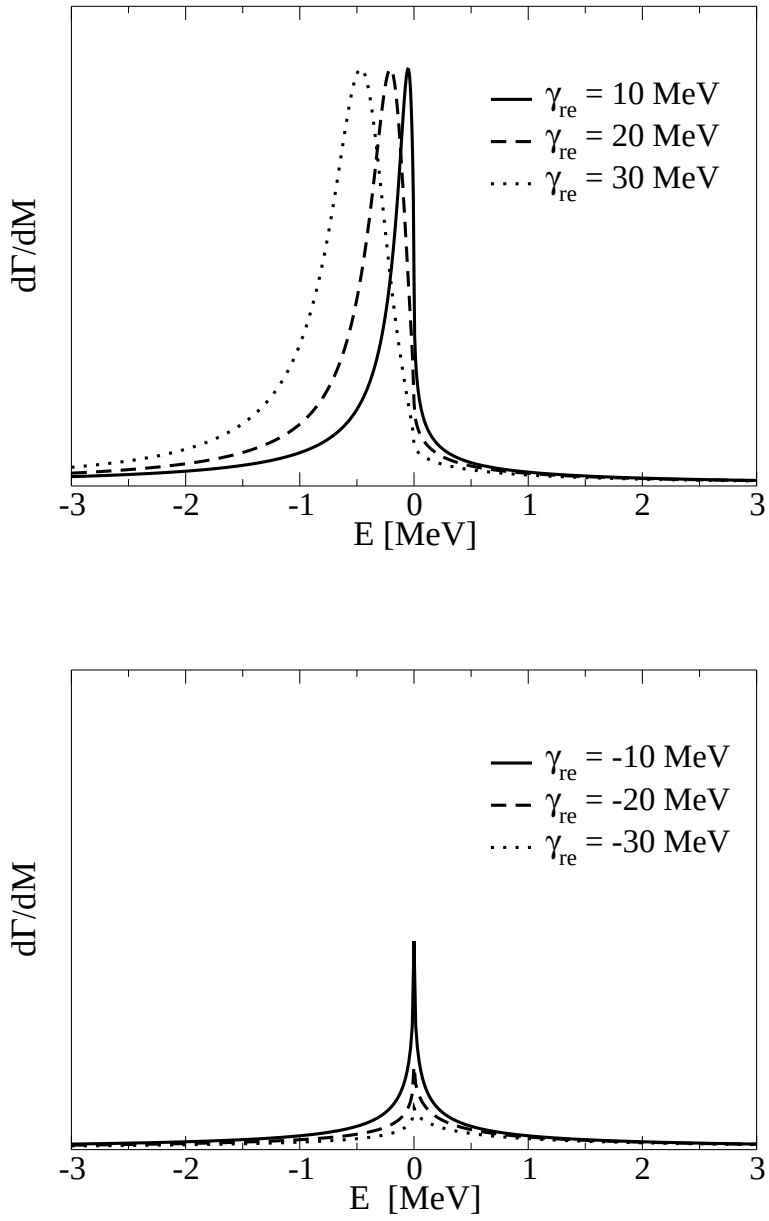

Figure 5.7: The X line shape in a short-distance decay channel, such as $J/\psi\,\pi^+\pi^-$, for $\gamma_{\rm im} = 10$ MeV and for various positive values (upper panel) and various negative values (lower panel) of $\gamma_{\rm re}/\gamma_{\rm im}$. The horizontal axis is the difference $E = M - (m_{D^0} + m_{D^{*0}})$ between the invariant mass M and the $D^0\bar{D}^{*0}$ threshold.

CHAPTER 6

PRODUCTION OF THE $X(3872)$ VIA $B \to XK$

The long-distance factors in the amplitude for the decay $B \to XK$ are determined by the binding energy and the full width of the X, while the short-distance factors are essentially determined by the amplitudes for $B \to D^0 \bar{D}^{*0} K$ and $B \to D^{*0} \bar{D}^0 K$ near the thresholds for the charm mesons. We obtain a crude determination of the short-distance amplitudes by analyzing data from the Babar collaboration on the branching fractions for $B \to \bar{D}^{(*)} D^{(*)} K$ using a factorization assumption, heavy quark symmetry, and isospin symmetry. The resulting order-of-magnitude estimate of the branching fraction for $B^+ \to XK^+$ is compatible with observations provided that $J/\psi\,\pi^+\pi^-$ is a major decay mode of the X. The branching fraction for $B^0 \to XK^0$ is predicted to be suppressed by more than an order of magnitude compared to that for $B^+ \to XK^+$.

6.1 The decay $B \to XK$

We proceed to apply the separation of the long-distance scale a from the shorter distance scales of QCD to the decay process $B \to XK$. The factorization formula in Eq. (5.11) lead to the expression for the decay rate for $B \to XK$ in Eq. (5.15), where c_+ was the unknown short-distance coefficient.

We will need the explicit expressions for the the short-distance decay amplitudes for $B \to D^0 \bar{D}^{*0} K$ and $B \to D^0 \bar{D}^{*0} K$. Lorentz invariance constrains the short-distance decay amplitudes to have the very simple forms

$$\mathcal{A}_{\rm short}[B \to D^0 \bar{D}^{*0} K] = c_1(\Lambda)\, P \cdot \epsilon^*, \tag{6.1a}$$

$$\mathcal{A}_{\rm short}[B \to D^{*0} \bar{D}^0 K] = c_2(\Lambda)\, P \cdot \epsilon^*, \tag{6.1b}$$

where P is the 4-momentum of the B and ϵ is the polarization 4-vector of the D^*. The coefficients c_1 and c_2, which depend on the separation scale Λ, have dimensions of inverse energy. They are related to c_+ defined in Eq. (5.14) by

$$c_1(\Lambda) + c_2(\Lambda) = c_+ \left(\frac{\pi^2}{\mu\Lambda}\right) \sqrt{4 m_{D^0} m_{D^{*0}}}\, \frac{1}{\sqrt{2}}, \tag{6.2}$$

where the $\pi^2/\mu\Lambda$ is the factor appearing in Eq. (5.13), the $1/\sqrt{2}$ is the amplitude for $D^0 \bar{D}^{*0}$ to be in the channel $(DD^*)^0_+$, and the factor of $\sqrt{4 m_{D^0} m_{D^{*0}}}$ takes into account the difference between the standard nonrelativistic and relativistic normalizations of states.

The expression for the differential decay rate in Eq. (5.19) applies only in the scaling region $q \ll m_\pi$. At larger values of q that are still small compared to the scale $m_b - 2m_c$, the resonant terms disappear and the decay amplitude reduces to the short-distance term $c_1(\Lambda) P \cdot \epsilon^*$ in Eqs. (6.1a). The corresponding invariant mass distribution $d\Gamma/dM$ for q just above the scaling region follows the phase space distribution, which is proportional to q in the limit $q \to 0$. The crossover from the resonant distribution proportional to $a^2 q/(1+a^2 q^2)$ to the phase space distribution proportional to q occurs at a momentum scale that we will denote by Λ_π. We expect Λ_π to be comparable to m_π. Just above the crossover region, the differential decay rate can be approximated

by

$$\frac{d\Gamma}{dM}[B \to D^0 \bar{D}^{*0} K] \approx |c_1(\Lambda_\pi)|^2 \frac{\lambda^{3/2}(m_B, m_X, m_K)}{256\pi^3 m_B^3 m_X^2}\, q. \tag{6.3}$$

A crude model of the crossover from the phase space distribution in Eq. (6.3) to the resonant distribution in Eq. (5.19) is a sudden but continuous transition at $q = \Lambda_\pi$, as illustrated in Figure 5.5. This requires

$$|c_1(\Lambda_\pi)| \approx |c_+| \, \frac{(8\pi^2 m_{D^0} m_{D^{*0}})^{1/2}}{\mu \Lambda_\pi}. \tag{6.4}$$

The integral of $d\Gamma/dM$ over the region $0 < q < \Lambda_\pi$ increases with a. In the limit $a \to \infty$, it is 3 times larger than the integral of a phase space distribution normalized to the same value at $q = \Lambda_\pi$.

The factorization formula gave the decay rate $B \to XK$ in Eq. (5.15). Using the expression for the coalescence amplitude squared in Eq. (5.10), the decay rate is

$$\Gamma[B \to XK] = |c_+|^2 \, \frac{\lambda^{3/2}(m_B, m_X, m_K)}{16 m_B^3 m_X \mu^{3/2}} \, [2E_X + \Gamma_X^2/(8E_X)]^{1/2}. \tag{6.5}$$

This formula applies equally well to the decays $B^+ \to XK^+$ and $B^0 \to XK^0$, with the only difference being the values of the coefficient c_+. The only sensitivity to long distances is through the factor E_X.

6.2 Analysis of $B \to \bar{D}^{(*)} D^{(*)} K$ branching fractions

A prediction of the branching fraction for $B \to XK$ requires the determination of the prefactor $|c_+|^2$ in the expression for the decay rate in Eq. (6.5). That same prefactor appears in the differential decay rate $d\Gamma/dM$ in Eq. (5.19) for $B \to D^0 \bar{D}^{*0} K$ in the resonant region. Thus measurements of the DD^* invariant mass distribution in the resonant region could in principle be used to predict the decay rate for $B \to XK$.

However the resonance region $q < m_\pi$ accounts for only about 0.2% of the available phase space for the decay $B \to DD^*K$. It might therefore be difficult to accumulate enough events to determine $|c_+|^2$ directly from the data. There is a crossover from the resonant distribution in Eq. (5.19) to the phase space distribution in Eq. (6.3) at an unknown momentum scale Λ_π. The fraction of the phase space in which $d\Gamma/dM$ is described by Eq. (6.3) should be much larger than the 0.2% that corresponds to the resonant region. If one could determine the prefactor $|c_1(\Lambda_\pi)|^2$ in Eq. (6.3) from measurements of the DD^* invariant mass distribution, one could then estimate the desired factor $|c_+|^2$ from the relation in Eq. (6.4), which is based on a crude model for the crossover. The estimate will involve the unknown scale Λ_π, which is expected to be comparable to m_π.

Measurements of $d\Gamma/dM$ for the decays $B \to DD^*K$ are not available. The Babar collaboration has however measured the branching fractions for decays of B^+ (and B^-) and of B^0 (and $\bar{B}^0$) into $\bar{D}^{(*)}D^{(*)}K$, where $D^{(*)}$ stands for D^0, D^+, D^{*0}, or D^{*+} [73]. The branching fractions are given in Tables 6.1 and 6.2. A substantial fraction of $b \to c\bar{c}s$ decays results in $\bar{D}^{(*)}D^{(*)}K$ final states as predicted in Ref. [74]. The sum of the branching fractions is $(3.5 \pm 0.3 \pm 0.5)\%$ for B^+ and $(4.3 \pm 0.3 \pm 0.6)\%$ for B^0. An isospin analysis of these decays has been carried out [75]. We will use this data to make a rough determination of the prefactor $|c_1(\Lambda_\pi)|^2$ in Eq. (6.3).

The most important terms in the effective weak Hamiltonian for $b \to c\bar{c}s$ decays at a renormalization scale of order m_b is

$$\mathcal{H}_W = \frac{G_F}{\sqrt{2}} V_{cb} V_{cs}^* \left(C_1 \, \mathcal{O}_1 + C_2 \, \mathcal{O}_2 \right) + \text{h.c.}, \tag{6.6}$$

B^+ decay mode	Br [%]	3-parameter fit	7-parameter fit
$\bar{D}^0 D^+ K^0$	$0.18 \pm 0.07 \pm 0.04$	0.17	0.18
$\bar{D}^{*0} D^+ K^0$	$0.41 \pm 0.15 \pm 0.08$	0.31	0.31
$\bar{D}^0 D^{*+} K^0$	$0.52 \pm 0.10 \pm 0.07$	0.44	0.45
$\bar{D}^{*0} D^{*+} K^0$	$0.78 \pm 0.23 \pm 0.14$	0.86	0.88
$\bar{D}^0 D^0 K^+$	$0.19 \pm 0.03 \pm 0.03$	0.17	0.18
$\bar{D}^{*0} D^0 K^+$	$0.18 \pm 0.07 \pm 0.04$	0.31	0.31
$\bar{D}^0 D^{*0} K^+$	$0.47 \pm 0.07 \pm 0.07$	0.44	0.50
$\bar{D}^{*0} D^{*0} K^+$	$0.53 \pm 0.11 \pm 0.12$	0.86	0.72
$D^- D^+ K^+$	$0.00 \pm 0.03 \pm 0.01$	0	0.00
$D^- D^{*+} K^+$	$0.02 \pm 0.02 \pm 0.01$	0	0.03
$D^{*-} D^+ K^+$	$0.15 \pm 0.03 \pm 0.02$	0	0.03
$D^{*-} D^{*+} K^+$	$0.09 \pm 0.04 \pm 0.02$	0	0.13

Table 6.1: Branching fractions (in %) for $B^+ \to \bar{D}^{(*)} D^{(*)} K$: measurements from Ref. [73], our 3-parameter fit, and our 7-parameter fit.

where C_1 and C_2 are Wilson coefficients and $\mathcal{O}_1$ and $\mathcal{O}_2$ are local four-fermion operators:

$$\mathcal{O}_1 = \bar{c}\gamma_L^\mu b\ \bar{s}\gamma_{L\mu} c, \tag{6.7a}$$

$$\mathcal{O}_2 = \bar{s}\gamma_L^\mu b\ \bar{c}\gamma_{L\mu} c. \tag{6.7b}$$

We have used the notation $\gamma_L^\mu = \gamma^\mu(1-\gamma_5)$. Both operators are products of color-singlet currents. We make the simplifying assumption that matrix elements of the operators $\mathcal{O}_1$ and $\mathcal{O}_2$ between the initial-state B and the final-state $\bar{D}^{(*)} D^{(*)} K$ can be factorized into products of matrix elements of currents. For example, the matrix

B^0 decay mode	Br [%]	3-parameter fit	7-parameter fit
$D^- D^0 K^+$	$0.17 \pm 0.03 \pm 0.03$	0.16	0.16
$D^- D^{*0} K^+$	$0.46 \pm 0.07 \pm 0.07$	0.41	0.42
$D^{*-} D^0 K^+$	$0.31 \pm 0.04 \pm 0.04$	0.29	0.29
$D^{*-} D^{*0} K^+$	$1.18 \pm 0.10 \pm 0.17$	0.79	0.81
$D^- D^+ K^0$	$0.08 \pm 0.06 \pm 0.03$	0.16	0.16
$D^{*-} D^+ K^0$, $D^- D^{*+} K^0$	$0.65 \pm 0.12 \pm 0.10$	$0.29 + 0.41$	$0.29 + 0.46$
$D^{*-} D^{*+} K^0$	$0.88 \pm 0.15 \pm 0.13$	0.79	0.67
$\bar{D}^0 D^0 K^0$	$0.08 \pm 0.04 \pm 0.02$	0	0.00
$\bar{D}^0 D^{*0} K^0$, $\bar{D}^{*0} D^0 K^0$	$0.17 \pm 0.14 \pm 0.07$	$0 + 0$	$0.02 + 0.02$
$\bar{D}^{*0} D^{*0} K^0$	$0.33 \pm 0.21 \pm 0.14$	0	0.12

Table 6.2: Branching fractions (in %) for $B^0 \to \bar{D}^{(*)} D^{(*)} K$: measurements from Ref. [73], our 3-parameter fit, and our 7-parameter fit.

elements for decays into $D^0 \bar{D}^{*0} \bar{K}$ and $D^{*0} \bar{D}^0 \bar{K}$ are

$$\langle D^0 \bar{D}^{*0} K^- | \mathcal{H}_W | B^- \rangle = (G_F/\sqrt{2}) V_{cb}^* V_{sc} \Big(C_1 \langle D^0 | \bar{c} \gamma_L^\mu b | B^- \rangle \langle \bar{D}^{*0} K^- | \bar{s} \gamma_{L\mu} c | \emptyset \rangle + C_2 \langle K^- | \bar{s} \gamma_L^\mu b | B^- \rangle \langle D^0 \bar{D}^{*0} | \bar{c} \gamma_{L\mu} c | \emptyset \rangle \Big), \quad (6.8a)$$

$$\langle D^{*0} \bar{D}^0 K^- | \mathcal{H}_W | B^- \rangle = (G_F/\sqrt{2}) V_{cb}^* V_{sc} \Big(C_1 \langle D^{*0} | \bar{c} \gamma_L^\mu b | B^- \rangle \langle \bar{D}^0 K^- | \bar{s} \gamma_{L\mu} c | \emptyset \rangle + C_2 \langle K^- | \bar{s} \gamma_L^\mu b | B^- \rangle \langle D^{*0} \bar{D}^0 | \bar{c} \gamma_{L\mu} c | \emptyset \rangle \Big), \quad (6.8b)$$

$$\langle D^0 \bar{D}^{*0} \bar{K}^0 | \mathcal{H}_W | \bar{B}^0 \rangle = (G_F/\sqrt{2}) V_{cb}^* V_{sc} \, C_2 \langle \bar{K}^0 | \bar{s} \gamma_L^\mu b | \bar{B}^0 \rangle \langle D^0 \bar{D}^{*0} | \bar{c} \gamma_{L\mu} c | \emptyset \rangle, \quad (6.8c)$$

$$\langle D^{*0} \bar{D}^0 \bar{K}^0 | \mathcal{H}_W | \bar{B}^0 \rangle = (G_F/\sqrt{2}) V_{cb}^* V_{sc} \, C_2 \langle \bar{K}^0 | \bar{s} \gamma_L^\mu b | \bar{B}^0 \rangle \langle D^{*0} \bar{D}^0 | \bar{c} \gamma_{L\mu} c | \emptyset \rangle. \quad (6.8d)$$

The accuracy of the factorization assumption for this process has been discussed in detail in Ref. [76].

The terms in Eqs. (6.8) with coefficient C_2 are called "color-suppressed" amplitudes, because C_2 is suppressed by $1/N_c$ relative to C_1. Only the color-suppressed amplitudes contribute to the decays $B^+ \to \bar{D}^{(*)} D^{(*)} K^+$ with $\bar{D}^{(*)}$ and $D^{(*)}$ both charged and to the decays $B^0 \to \bar{D}^{(*)} D^{(*)} K^0$ with $\bar{D}^{(*)}$ and $D^{(*)}$ both neutral. In

particular, the only contributions to the decays of B^0 into $D^0\bar{D}^{*0}K^0$ and $D^{*0}\bar{D}^0K^0$ are from the color-suppressed amplitudes. As is evident in Tables 6.1 and 6.2, the branching fractions for these color-suppressed channels are observed to be significantly smaller than those for other decay channels.

Lorentz invariance can be used to reduce each of the current matrix elements to a linear combination of independent tensor structures whose coefficients are form factors. Heavy quark symmetry provides constraints between the form factors that can be deduced using the covariant representation formalism described in Ref. [77]. Matrix elements of operators with a heavy quark field Q (or $\bar{Q}$) and a $Q\bar{q}$ meson in the initial (or final) state can be expressed in terms of a heavy meson field H_v (or $\bar{H}_v$) defined by

$$H_v = \frac{1+\not{v}}{2}\left[V_v^\mu \gamma_\mu + iP_v\gamma_5\right], \tag{6.9a}$$

$$\bar{H}_v = \left[V_v^{\mu\dagger}\gamma_\mu + iP_v^\dagger\gamma_5\right]\frac{1+\not{v}}{2}, \tag{6.9b}$$

where V_v^μ and P_v are operators that annihilate vector and pseudoscalar $Q\bar{q}$ mesons with 4-velocity v. We also require the matrix elements of operators with a heavy quark field Q and a $\bar{Q}q$ meson in the final state. They can be expressed in terms of a heavy meson field H'_v that creates a $\bar{Q}q$ meson with 4-velocity v:

$$H'_v = \frac{1-\not{v}}{2}\left[V_v^\mu \gamma_\mu - iP_v\gamma_5\right], \tag{6.10}$$

The relative phase between the V_v^μ and P_v terms has been deduced by demanding that vacuum-to-$D^{(*)}\bar{D}^{(*)}$ matrix elements of operators of the form $\bar{Q}\Gamma Q$ have the correct charge conjugation properties.

We now list the expressions for the matrix elements of the currents that follow from heavy-quark symmetry. We denote the velocity 4-vectors of the $\bar{B}$, $D^{(*)}$, and

$\bar{D}^{(*)}$ by V, v and $\bar{v}$, respectively. We denote the polarization 4-vectors of the D^* and $\bar{D}^*$ by ϵ and $\bar{\epsilon}$, respectively. They satisfy $v\cdot\epsilon = 0$ and $\bar{v}\cdot\bar{\epsilon} = 0$. The $\bar{B}$-to-$D^{(*)}$ matrix elements are

$$\langle D(v)|\bar{c}\gamma_L^\mu b|\bar{B}(V)\rangle = \xi(w)(v+V)^\mu, \tag{6.11a}$$

$$\langle D^*(v,\epsilon)|\bar{c}\gamma_L^\mu b|\bar{B}(V)\rangle = i\xi(w)\left[(1+v\cdot V)\epsilon^\mu - (V\cdot\epsilon)v^\mu - i\varepsilon^\mu(v,V,\epsilon)\right], \tag{6.11b}$$

where the form factor ξ is a function of $w = v\cdot V$. We have used the notation $\varepsilon^\mu(p,q,r) = \varepsilon^{\mu\nu\alpha\beta}p_\nu q_\alpha r_\beta$ and the sign convention $\varepsilon^{0123} = +1$. The vacuum-to-$\bar{D}^{(*)}\bar{K}$ matrix elements are

$$\langle \bar{D}(\bar{v})\bar{K}(k)|\bar{s}\gamma_L^\mu c|\emptyset\rangle = \eta_1(\kappa)\,\bar{v}^\mu + \eta_2(\kappa)\,k^\mu, \tag{6.12a}$$

$$\langle \bar{D}^*(\bar{v},\bar{\epsilon})\bar{K}(k)|\bar{s}\gamma_L^\mu c|\emptyset\rangle = -i\eta_1(\kappa)\,\bar{\epsilon}^\mu - i\eta_2(\kappa)\,\left[(\bar{v}\cdot k)\bar{\epsilon}^\mu - (k\cdot\bar{\epsilon})\bar{v}^\mu + i\varepsilon^\mu(\bar{v},k,\bar{\epsilon})\right], \tag{6.12b}$$

where the form factors η_1 and η_2 are functions of $\kappa = \bar{v}\cdot k$. The vacuum-to-$D^{(*)}\bar{D}^{(*)}$ matrix elements are

$$\langle D(v)\bar{D}(\bar{v})|\bar{c}\gamma_L^\mu c|\emptyset\rangle = \zeta(w')(v-\bar{v})^\mu, \tag{6.13a}$$

$$\langle D(v)\bar{D}^*(\bar{v},\bar{\epsilon})|\bar{c}\gamma_L^\mu c|\emptyset\rangle = i\zeta(w')\left[(1-v\cdot\bar{v})\bar{\epsilon}^\mu + (v\cdot\bar{\epsilon})\bar{v}^\mu + i\varepsilon^\mu(v,\bar{v},\bar{\epsilon})\right], \tag{6.13b}$$

$$\langle D^*(v,\epsilon)\bar{D}(\bar{v})|\bar{c}\gamma_L^\mu c|\emptyset\rangle = i\zeta(w')\left[(1-v\cdot\bar{v})\epsilon^\mu + (\bar{v}\cdot\epsilon)v^\mu + i\varepsilon^\mu(v,\bar{v},\epsilon)\right], \tag{6.13c}$$

$$\langle D^*(v,\epsilon)\bar{D}^*(\bar{v},\bar{\epsilon})|\bar{c}\gamma_L^\mu c|\emptyset\rangle = \zeta(w')\left[\epsilon\cdot\bar{\epsilon}(v-\bar{v})^\mu + (\bar{v}\cdot\epsilon)\bar{\epsilon}^\mu - (v\cdot\bar{\epsilon})\epsilon^\mu - i\varepsilon^\mu(v-\bar{v},\epsilon,\bar{\epsilon})\right], \tag{6.13d}$$

where the form factor ζ is a function of $w' = v\cdot\bar{v}$. The $\bar{B}$-to-$\bar{K}$ matrix elements are

$$\langle \bar{K}(k)|\bar{s}\gamma_L^\mu b|\bar{B}(V)\rangle = \omega_1(\kappa')\,V^\mu + \omega_2(\kappa')\,k^\mu, \tag{6.14}$$

where the form factors ω_1 and ω_2 are functions of $\kappa' = V \cdot k$. In the current matrix elements in Eqs. (6.11), (6.12), (6.13), and (6.14), the heavy meson states have the standard nonrelativistic normalizations. To obtain the standard relativistic normalizations, matrix elements involving B, D or $\bar{D}$, and D^* or $\bar{D}^*$ must be multiplied by $m_B^{1/2}$, $m_D^{1/2}$, and $m_{D^*}^{1/2}$, respectively.

The amplitudes for the decays $\bar{B} \to \bar{D}^{(*)} D^{(*)} \bar{K}$ at leading-order in $\Lambda_{\rm QCD}/m_b$ and $\Lambda_{\rm QCD}/m_c$ are obtained by inserting the current matrix elements in Eqs. (6.11), (6.12), (6.13), and (6.14) into the factorized expressions for the decay amplitudes, such as those in Eqs. (6.8). For example, the amplitudes for the decays into $D^0 \bar{D}^{*0} \bar{K}$ and $D^{*0} \bar{D}^0 \bar{K}$ are

$$\begin{aligned}
\mathcal{A}[B^- \to D^0 \bar{D}^{*0} K^-] &= -iG_1 (v+V)\cdot\epsilon \\
&\quad - i(G_2/m_B)\left[v_*\cdot k\,(v+V)\cdot\epsilon - v_*\cdot(v+V)\,k\cdot\epsilon + i\varepsilon(v+V, v_*, k, \epsilon)\right] \\
&\quad + iG_3\left[(1-v\cdot v_*)\,V\cdot\epsilon + (v_*\cdot V)\,v\cdot\epsilon + i\varepsilon(v, v_*, V, \epsilon)\right], \\
&\quad + i(G_4/m_B)\left[(1-v\cdot v_*)\,k\cdot\epsilon + (v_*\cdot k)\,v\cdot\epsilon + i\varepsilon(v, v_*, k, \epsilon)\right], \qquad (6.15a) \\
\mathcal{A}[B^- \to D^{*0} \bar{D}^0 K^-] &= iG_1\left[(1+v_*\cdot V)\,v\cdot\epsilon - (v\cdot v_*)\,V\cdot\epsilon - i\varepsilon(v, v_*, V, \epsilon)\right] \\
&\quad + i(G_2/m_B)\left[(1+v_*\cdot V)\,k\cdot\epsilon - (v_*\cdot k)\,V\cdot\epsilon - i\varepsilon(v_*, V, k, \epsilon)\right] \\
&\quad + iG_3\left[(1-v\cdot v_*)\,V\cdot\epsilon + (v_*\cdot V)\,v\cdot\epsilon - i\varepsilon(v, v_*, V, \epsilon)\right] \\
&\quad + i(G_4/m_B)\left[(1-v\cdot v_*)\,k\cdot\epsilon + (v_*\cdot k)\,v\cdot\epsilon - i\varepsilon(v, v_*, k, \epsilon)\right], \qquad (6.15b) \\
\mathcal{A}[\bar{B}^0 \to D^0 \bar{D}^{*0} \bar{K}^0] &= iG_3\left[(1-v\cdot v_*)\,V\cdot\epsilon + (v_*\cdot V)\,v\cdot\epsilon + i\varepsilon(v, v_*, V, \epsilon)\right] \\
&\quad + i(G_4/m_B)\left[(1-v\cdot v_*)\,k\cdot\epsilon + (v_*\cdot k)\,v\cdot\epsilon + i\varepsilon(v, v_*, k, \epsilon)\right], \qquad (6.15c) \\
\mathcal{A}[\bar{B}^0 \to D^{*0} \bar{D}^0 \bar{K}^0] &= iG_3\left[(1-v\cdot v_*)\,V\cdot\epsilon + (v_*\cdot V)\,v\cdot\epsilon - i\varepsilon(v, v_*, V, \epsilon)\right] \\
&\quad + i(G_4/m_B)\left[(1-v\cdot v_*)k\cdot\epsilon + (v_*\cdot k)v\cdot\epsilon - i\varepsilon(v, v_*, k, \epsilon)\right], \qquad (6.15d)
\end{aligned}$$

where V, v, and v_* are the velocity 4-vectors of the B, D, and D^* and ϵ is the polarization 4-vector of the D^* which satisfies $v_* \cdot \epsilon = 0$. We have used the notation $\varepsilon(p,q,r,s) = \varepsilon^{\mu\nu\alpha\beta} p_\mu q_\nu r_\alpha s_\beta$. The four independent dimensionless form factors are

$$G_1((P-q)^2) = (G_F/\sqrt{2}) V_{cb}^* V_{sc}\, C_1\, (m_B m_{D^0} m_{D^{*0}})^{1/2}\, \xi(v\cdot V)\, \eta_1(v_*\cdot k), \qquad (6.16a)$$

$$G_2((P-q_*)^2) = (G_F/\sqrt{2}) V_{cb}^* V_{sc}\, C_1\, (m_B^3 m_{D^0} m_{D^{*0}})^{1/2}\, \xi(v_*\cdot V)\, \eta_2(v\cdot k), \qquad (6.16b)$$

$$G_3((P-k)^2) = (G_F/\sqrt{2}) V_{cb}^* V_{sc}\, C_2\, (m_B m_{D^0} m_{D^{*0}})^{1/2}\, \zeta(v\cdot v_*)\, \omega_1(V\cdot k), \qquad (6.16c)$$

$$G_4((P-k)^2) = (G_F/\sqrt{2}) V_{cb}^* V_{sc}\, C_2\, (m_B^3 m_{D^0} m_{D^{*0}})^{1/2}\, \zeta(v\cdot v_*)\, \omega_2(V\cdot k). \qquad (6.16d)$$

The amplitudes for the other $\bar{B} \to \bar{D}^{(*)} D^{(*)} \bar{K}$ decays are obtained similarly. Isospin symmetry, in addition to the factorization assumption and heavy quark symmetry, can be used to express all 24 decay amplitudes in terms of the four form factors $G_1(q^2)$, $G_2(q^2)$, $G_3(q^2)$, and $G_4(q^2)$.

We proceed to use our expressions for the decay amplitudes to analyze the data from the Babar collaboration on the branching fractions for $B \to \bar{D}^{(*)} D^{(*)} K$ [73]. For simplicity, we approximate the form factors $G_i(q^2)$ by constants. We can choose the overall phase so that G_1 is real-valued. After integrating over the phase space, we obtain expressions for the branching fractions that are quadratic in the constants G_i and their complex conjugates. The Babar data consists of the 12 branching fractions for B^+ given in Table 6.1 and the 10 branching fractions for B^0 given in Table 6.2. For each of the data points, we add the statistical and systematic errors in quadrature. We then determine the best fits for the constants G_i by minimizing the χ^2 for the 22 data points.

The decays $B^+ \to \bar{D}^{(*)} D^{(*)} K^+$ with $\bar{D}^{(*)}$ and $D^{(*)}$ both charged and $B^0 \to \bar{D}^{(*)} D^{(*)} K^0$ with $\bar{D}^{(*)}$ and $D^{(*)}$ both neutral have branching fractions that are significantly smaller than other decay channels. The only factorizable contributions to their decay amplitudes come from the color-suppressed amplitudes with form factors G_3 and G_4. Their small branching fractions motivates a simplified analysis in which G_3 and G_4 are set to 0. The only parameters that remain are the real constant G_1 and the complex constant G_2. Thus there are 3 real parameters to fit the 22 branching fractions. The parameters that minimize the χ^2 are

$$G_1 = 1.9 \times 10^{-6}, \tag{6.17a}$$

$$G_2 = (-21.2 + 5.5i) \times 10^{-6}. \tag{6.17b}$$

The fitted value of G_2 is about an order of magnitude larger than that of G_1. The branching fractions for this 3-parameter fit are shown in Tables 6.1 and 6.2. The χ^2 per degree of freedom is $42.0/19 = 2.2$. There are 7 decay modes for which the deviations from the data are significantly larger than one standard deviation, including $B^+ \to \bar{D}^{*0} D^0 K^+$.

We have also carried out a fit that allows nonzero values of the color-suppressed form factors G_3 and G_4. If these form factors are approximated by complex-valued constants, there are 7 real parameters to fit the 22 branching fractions. The parameters that minimize the χ^2 are

$$G_1 = 1.8 \times 10^{-6}, \tag{6.18a}$$

$$G_2 = (-21.6 + 5.0i) \times 10^{-6}, \tag{6.18b}$$

$$G_3 = (2.6 + 0.01i) \times 10^{-6}, \tag{6.18c}$$

$$G_4 = (-1.5 - 0.7i) \times 10^{-6}. \tag{6.18d}$$

Note that the values of G_1 and G_2 are essentially identical to those from the 3-parameter fit in Eqs. (6.17). The branching fractions for this 7-parameter fit are shown in Tables 6.1 and 6.2. The χ^2 per degree of freedom is $29.2/15 = 1.9$. There are still 4 decay modes for which the deviations from the data are significantly larger than one standard deviation, including $B^+ \to \bar{D}^{*0} D^0 K^+$.

One could of course improve the fits to the branching fractions by allowing for dependence of each the form factors G_1, G_2, G_3, and G_4 on the appropriate momentum transfer q^2. However allowing even for linear dependence on q^2 would introduce 8 additional real parameters. Such an analysis might be worthwhile if Dalitz plots for the decays were available and could also be used in the fits.

6.3 Predictions for $B \to XK$ decays

In this section, we use the results of our analysis of the branching fractions for $B \to D^{(*)} \bar{D}^{(*)} K$ to estimate the branching fractions for the decays $B^+ \to XK^+$ and $B^0 \to XK^0$. Our strategy once again is to use that data to provide a rough determination of the prefactor $|c_1(\Lambda_\pi)|^2$ in the differential decay rate $d\Gamma/dM$ for $B \to D^0 \bar{D}^{*0} K$ in the region near the $D^0 D^{*0}$ threshold where the DD^* invariant mass distribution follows the phase space distribution in Eq. (6.3). The crossover to the resonant distribution in Eq. (5.19) occurs at an unknown momentum scale Λ_π, which is expected to be comparable to m_π. Given a value for $|c_1(\Lambda_\pi)|^2$, we can use the relation in Eq. (6.4), which follows from a crude model for the crossover, to estimate $|c_+|^2$. This value can then be inserted in Eq. (6.5) to get an estimate of the decay rate for $B \to XK$.

We first consider the decay $B^+ \to XK^+$, whose branching fraction should be the same as for $B^- \to XK^-$. The coefficient $c_1(\Lambda_\pi)$ for the decay $B^- \to D^0 \bar{D}^{*0} K^-$ and the corresponding coefficient $c_2(\Lambda_\pi)$ for the decay $B^- \to D^{*0} \bar{D}^0 K^-$ can be deduced by matching the amplitudes in Eqs. (6.15a) and (6.15b) at the DD^* threshold to the expressions in Eqs. (6.1):

$$c_1(\Lambda_\pi) = c_2(\Lambda_\pi) = -iG_1/m_B + iG_2(m_B + m_D + m_{D^*})/m_B^2. \tag{6.19}$$

Using the numerical values for G_1 and G_2 in either Eqs. (6.17) or Eqs. (6.18), the estimate from Eq. (6.4) is

$$|c_+| \approx 5.7 \times 10^{-8}\, \Lambda_\pi/m_\pi. \tag{6.20}$$

Inserting this into the expression for the decay rate in Eq. (6.5) and dividing by the measured width of the B^+, we obtain

$$\mathrm{Br}[B^+ \to XK^+] \approx 2.7 \times 10^{-5} \left(\frac{\Lambda_\pi}{m_\pi}\right)^2 \left(\frac{E_X}{0.5\ \mathrm{MeV}}\right)^{1/2} \left[1 + \frac{\Gamma_X^2}{16 E_X^2}\right]^{1/2}. \tag{6.21}$$

If we set $E_X = 0.5$ MeV and vary Γ_X from 0 to an experimental upper limit 2.3 MeV in Eq. (2.2), the last factor in Eq. (6.21) varies from 1 to 1.5. The estimate in Eq. (6.21) is sensitive to the unknown momentum scale Λ_π at which the invariant mass distribution crosses over from the phase space distribution in Eq. (6.3) to the resonant distribution in Eq. (5.19). The natural scale for Λ_π may be m_π, but we should not be surprised if it differs by a factor of 2 or 3. Thus the result in Eq. (6.21) is only an order-of-magnitude estimate of the branching fraction. It can be compared to the product of the branching fractions for $B^+ \to XK^+$ and $X \to J/\psi\, \pi^+\pi^-$ in Eq. (2.3). Our estimate is compatible with this measurement if $J/\psi\, \pi^+\pi^-$ is one of the major decay modes of X. If $E_b = 0.5$ MeV and if we allow for Λ_π to differ from

m_π by a factor of 2, the branching fraction for $X \to J/\psi\,\pi^+\pi^-$ should be greater than 10^{-1}.

We next consider the decay $B^0 \to XK^0$, whose branching fraction should be the same as for $\bar{B}^0 \to X\bar{K}^0$. The amplitudes in Eqs. (6.15c) and (6.15d) approach 0 as the DD^* approaches its threshold. Thus our assumptions of factorization and heavy quark symmetry imply that $c_1(\Lambda_\pi) = c_2(\Lambda_\pi) = 0$ for this decay. We proceed to consider the size of the coefficients that would be expected from the violation of these assumptions. The factorization assumption for the $B \to \bar{D}^{(*)}D^{(*)}K$ amplitudes can be justified by the large N_c limit. Since we have included terms up to $O(1/N_c)$ in the amplitude, we expect the deviations from the factorization assumptions to be $O(1/N_c^2)$ in the amplitude. Violation of heavy quark symmetry would give rise to terms of $O(\Lambda_{\rm QCD}/m_c)$ in the amplitudes. We expect the largest nonzero contributions to the coefficients $c_1(\Lambda_\pi)$ and $c_2(\Lambda_\pi)$ to come from violations of heavy quark symmetry.

To obtain an estimate of the decay rate for $B^0 \to XK^0$, we relax the assumption of heavy quark symmetry. Lorentz invariance allows three independent tensor structures in the matrix elements $\langle D\bar{D}^*|\bar{c}\gamma^\mu_L c|\emptyset\rangle$ and $\langle D^*\bar{D}|\bar{c}\gamma^\mu_L c|\emptyset\rangle$, but heavy quark symmetry requires those terms to enter in the particular linear combinations given in Eqs. (6.13b) and (6.13c). Lorentz invariance implies that only one of the three independent terms can be nonzero at the DD^* threshold: the $\bar{\epsilon}^\mu$ term in Eq. (6.13b) and the ϵ^μ term in Eq. (6.13c). Heavy quark symmetry constrains the coefficients of $\bar{\epsilon}^\mu$ and ϵ^μ to be $i\zeta(w')(1-v\cdot\bar{v})$, which vanishes at the threshold. The constraint of heavy quark symmetry can be relaxed by adding to the coefficients of $\bar{\epsilon}^\mu$ in Eq. (6.13b) and ϵ^μ in Eq. (6.13c) the term $i\chi\zeta(1)$, which is nonzero at the threshold. This corresponds to adding the terms $i\chi[G_3(V\cdot\epsilon) + G_4/m_B(k\cdot\epsilon)]$ to the amplitudes in Eqs. (6.15c) and

(6.15d). In Table 6.2, the 7-parameter fit gives 0.04 for the sum of the two branching fractions for B^0 to decay into $D^0\bar{D}^{*0}K^0$ and $\bar{D}^0D^{*0}K^0$, which is about one standard deviation below the measured value. The complex parameter χ can be adjusted so that the sum of the two branching fractions is equal to the central value 0.17 given in Table 6.2. Using the values of G_3 and G_4 in Eq. (6.18), the required values of χ form a curve that passes through the real values $\chi = -1.9$ and $\chi = 5.8$ and the imaginary values $\chi = \pm 3.3\, i$. If χ is allowed to vary over the region in which the sum of the two branching fractions is within one standard deviation of the central value, its absolute value has the range $0 < |\chi| < 7.3$.

We proceed to make a quantitative estimate of the decay rate for $B^0 \to XK^0$. The coefficient $c_1(\Lambda_\pi)$ for the decay $\bar{B}^0 \to D^0\bar{D}^{*0}\bar{K}^0$ and the corresponding coefficient $c_2(\Lambda_\pi)$ for the decay $\bar{B}^0 \to D^{*0}\bar{D}^0\bar{K}^0$ can be deduced by matching the amplitudes $i\chi[G_3(V\cdot\epsilon) + G_4/m_B(k\cdot\epsilon)]$ to the expressions in Eqs. (6.1):

$$c_1(\Lambda_\pi) = c_2(\Lambda_\pi) = i\chi(G_3 + G_4)/m_B. \tag{6.22}$$

If we use the estimate in Eq. (6.4) to deduce the values of $|c_+|^2$ for both $B^0 \to XK^0$ and $B^+ \to XK^+$, the ratio of their branching fractions is

$$\frac{\mathrm{Br}[B^0 \to XK^0]}{\mathrm{Br}[B^+ \to XK^+]} \approx \frac{|\chi|^2|G_3 + G_4|^2}{|G_1 - G_2(m_B + m_D + m_{D^*})/m_B|^2}\,\frac{\tau[B^0]}{\tau[B^+]}. \tag{6.23}$$

The ratio of the lifetimes of the B^0 and B^+ is 0.921 ± 0.014. If χ is allowed to vary over the region $0 < |\chi| < 7.3$, the ratio in Eq. (6.23) ranges from 0 to 8×10^{-2}. We conclude that the branching fraction for $B^0 \to XK^0$ is likely to be suppressed by at least an order of magnitude compared to that for $B^+ \to XK^+$.

This prediction stands in sharp contrast to the observed pattern of exclusive decays of B^0 and B^+ into a charmonium H plus K. The ratios of the branching fractions for

$B^0 \to HK^0$ and $B^+ \to HK^+$ for the charmonium states η_c, J/ψ, $\psi(2S)$, and $\chi_{c1}(1P)$ are 1.33 ± 0.60, 0.85 ± 0.06, 0.91 ± 0.12, and 0.59 ± 0.20, respectively. Because charmonium is an isospin singlet and the weak decay operators in Eqs. (6.7) are also isospin singlets, isospin symmetry implies that the ratio of the branching fractions for $B^0 \to HK^0$ and $B^+ \to HK^+$ should be equal to the ratio of the lifetimes $\tau[B^0]$ and $\tau[B^+]$, which is 0.921 ± 0.014. The observed deviations from this lifetime ratio are all less than 2 standard deviations. If X were an isosinglet, isospin symmetry would imply that the ratio of the branching fractions for $B^0 \to XK^0$ and $B^+ \to XK^+$ should also be equal to $\tau[B^0]/\tau[B^+]$. Thus the observation of suppression of $B^0 \to XK^0$ relative to this prediction would disfavor any charmonium interpretation and support the interpretation of X as a DD^* molecule.

CHAPTER 7

DECAYS OF THE $X(3872)$ INTO J/ψ AND LIGHT HADRONS

If the $X(3872)$ is a loosely-bound molecule of the charm mesons $D^0\bar{D}^{*0}$ and $D^{*0}\bar{D}^0$, it can decay through the decay of a constituent in a hadronic channel with a nearby threshold, such as $J/\psi\,\omega$ or $J/\psi\,\rho$. The differential decay rates of the X into $J/\psi\,\pi^+\pi^-$, $J/\psi\,\pi^+\pi^-\pi^0$, $J/\psi\,\pi^0\gamma$, and $J/\psi\,\gamma$ are calculated in terms of $XJ/\psi\,\rho$ and $XJ/\psi\,\omega$ coupling constants using an effective lagrangian that reproduces the decay rates of the ω and the ρ. The dependence of the coupling constants on the binding energy and the total width of the X is determined by a factorization formula. Results from a model by Swanson are used to predict the partial width of X into $J/\psi\,\pi^+\pi^-\pi^0$ as a function of the binding energy and the total width of the X.

7.1 Swanson's model

Swanson has constructed a model of the X and the hadronic states with nearby thresholds and used it to predict some of the properties of the X [33, 72]. In particular, he predicted correctly that the branching fraction for $X \to J/\psi\,\pi^+\pi^-\pi^0$ is comparable to that for $X \to J/\psi\,\pi^+\pi^-$. In addition to the channel $D^0\bar{D}^{*0} + D^{*0}\bar{D}^0$, Swanson's

model includes $D^+D^{*-} + D^{*+}D^-$, $J/\psi\,\rho$, and $J/\psi\,\omega$. It includes the S-wave and D-wave channels for DD^*, but only the S-wave channel for $J/\psi\,V$, where V is the vector meson ρ or ω. Thus the model has 6 coupled channels. The interactions between the hadrons are modeled by potentials: one-pion-exchange potentials for the S-wave and D-wave DD^* channels and for transitions between those channels and Gaussian potentials for the transitions between the S-wave DD^* channels and the S-wave $J/\psi\,V$ channels to simulate the effects of quark exchange. The one-pion-exchange potential is singular at short distances and it was regularized by an ultraviolet momentum cutoff Λ. The nonrelativistic Schrödinger equation for the 6 coupled channels was solved numerically. A bound state with the quantum numbers $J^{PC} = 1^{++}$ of X appeared when the ultraviolet cutoff exceeded the critical value $\Lambda_c = 1.45$ GeV. The binding energy of the X could be adjusted by varying the ultraviolet cutoff.

Swanson solved the coupled channel problem under the assumption that the ρ and ω are stable hadrons with equal masses $m_\rho = m_\omega = 782.6$ MeV. The reason for using an unphysical value for m_ρ is that the central PDG value from 2002 and earlier, $m_\rho = 771.1$ MeV, is below the $D^0\bar{D}^{*0}$ threshold. If such a value had been used, it would have been necessary to treat $J/\psi\,\rho$ states as scattering states. This complication was avoided by using a value of m_ρ above the $D^0\bar{D}^{*0}$ threshold. Note that in Eq. (3.16b), we have taken the updated 2004 PDG value $m_\rho = 775.8 \pm 0.5$ MeV [56], which gives a $J/\psi\,\rho$ threshold that is a few MeV above the mass of the X.

Swanson calculated the probabilities for each component of the wavefunction of X for values of the ultraviolet cutoff that correspond to varying the binding energy E_X from 0.7 MeV to 23.2 MeV [33]. His results for the probabilities $Z_{\psi\omega}$ and $Z_{\psi\rho}$ are shown as dots in Fig. 7.1. Since the binding energy of the X is known to be less

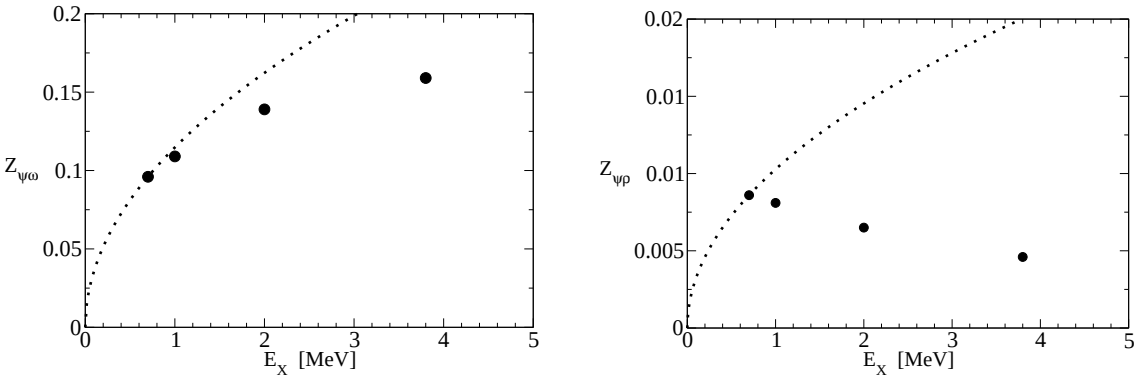

Figure 7.1: The probabilities $Z_{\psi\omega}$ and $Z_{\psi\rho}$ for the $J/\psi\,\omega$ and $J/\psi\,\rho$ components of the $X(3872)$ as a function of its binding energy E_X. The dots are the results from Swanson's model [33]. The dotted curves have the scaling behavior $E_X^{1/2}$ and pass through the model result for $E_X = 0.7$ MeV.

than 1 MeV, only the lowest two values of E_X could be physically relevant. For the lowest value $E_X = 0.7$ MeV, the probabilities were $Z_{\psi\omega} = 9.6\%$, $Z_{D^\pm D^{*\mp}} = 7.9\%$, and $Z_{\psi\rho} = 0.86\%$. The total probability for the $D^0\bar{D}^{*0}$ and $D^{*0}\bar{D}^0$ components of the wavefunction is 81.6%.

In Fig. 7.1, the dotted lines have the scaling behavior $E_X^{1/2}$ predicted by universality and are normalized so that they pass through the dot at $E_X = 0.7$ MeV. The probability $Z_{\psi\omega}$ clearly exhibits the universal behavior. The probability $Z_{\psi\rho}$ does not. This may be related to the fact that $Z_{\psi\rho}$ is more than an order of magnitude smaller than $Z_{\psi\omega}$. Because of the weaker coupling of the X to isospin-1 states, the scaling region for isospin-1 states may not set in until a much smaller value of E_X.

Swanson estimated the partial widths for the decays of X into $J/\psi\,h$, where h is the light hadronic state $\pi^+\pi^-$, $\pi^+\pi^-\pi^0$, $\pi^0\gamma$, or $\pi^+\pi^-\gamma$, using a simple ad hoc recipe. The partial width into $J/\psi\,h$ was taken to be the sum over the vector mesons $V = \rho, \omega$

of the product of the probability $Z_{\psi V}$ for the $J/\psi\, V$ component of the wavefunction and the partial width $\Gamma[V \to h]$ for the decay of the vector meson:

$$\Gamma[X \to J/\psi\, h] \approx \sum_V Z_{\psi V} \Gamma[V \to h]. \tag{7.1}$$

For the smallest value of the binding energy that was considered, $E_X = 0.7$ MeV, the resulting estimates of the partial widths for decay into $J/\psi\, h$ were 1290 keV, 720 keV, 70 keV, and 13 keV for $h = \pi^+\pi^-$, $\pi^+\pi^-\pi^0$, $\pi^0\gamma$, and $\pi^+\pi^-\gamma$, respectively. The ratio of the partial widths into $J/\psi\,\pi^+\pi^-\pi^0$ and $J/\psi\,\pi^+\pi^-$ was predicted to be 0.56 for $E_X = 0.7$ MeV. Remarkably, this prediction agrees with the subsequent measurement by the Belle collaboration given in Eq. (2.5) to within the experimental errors [57]. The approximately equal branching fractions are a fortuitous result of an amplitude for $X \to J/\psi\,\omega$ that is much larger than the amplitude for $X \to J/\psi\,\rho$ and an amplitude for $\omega \to \pi^+\pi^-\pi^0$ that is much smaller than that for $\rho \to \pi^+\pi^-$. The suppression of the amplitude for $X \to J/\psi\,\rho$ is related to the fact that in the isospin symmetric limit in which the mass difference between neutral and charged D's is neglected, there is binding in the isospin-0 channel but not in the isospin-1 channel [38].

Swanson has also used his model to calculate the rates for several other decay modes of the X [72]. The decay rate into $J/\psi\,\gamma$ has contributions from transitions to $J/\psi\,\rho$ and $J/\psi\,\omega$ that can be calculated using vector meson dominance. It also has contributions from the annihilation of the u and $\bar{u}$ from the charm mesons that are the constituents of the X. Swanson's prediction for the partial width into $J/\psi\,\gamma$ for an X with a binding energy of 1 MeV is 8 keV. Decay modes that receive contributions only from $u\bar{u}$ annihilation, such as $\psi(2S)\,\gamma$, KK^*, and $\pi\rho$, have much smaller partial widths.

7.2 Decays of X into $J/\psi\, h$

In this section, we calculate the differential decay rates of the X into $J/\psi\, h$, where the hadronic system h is $\pi^+\pi^-\pi^0$, $\pi^+\pi^-$, $\pi^0\gamma$, or γ. We assume that these decays proceed through transitions of X to $J/\psi\,\rho$ and $J/\psi\,\omega$. We calculate the differential decay rates in terms of two unknown complex coupling constants using an effective lagrangian that reproduces the decays of the light vector mesons.

7.2.1 Vector meson decay amplitudes

We assume that the decay of X into $J/\psi\, h$, where h is a system of light hadrons, proceeds through transitions to $J/\psi\, V$, where V is one of the vector mesons ρ or ω, followed by the decay of the vector meson into h. Because the mass of the X is so close to the threshold for $J/\psi\, V$, the vector meson is almost on its mass shell. Any model that reproduces the decays of the vector mesons should also accurately describe the decay of the virtual vector meson in the $J/\psi\, V$ component of X. In Ref. [78], the semileptonic branching fractions for the τ lepton were calculated using an effective lagrangian for light pseudoscalar and vector mesons with $U(3) \times U(3)$ chiral symmetry. All the parameters in the effective lagrangian, aside from the pion decay constant, were determined directly from decays of the vector mesons ρ and ω. That same effective lagrangian can be used to calculate the partial widths of X into $J/\psi\, h$. An updated determination of the parameters in that effective lagrangian is given in the Appendix.

The T-matrix element for the decay of a vector meson V into the light hadronic state h can be expressed in the form

$$\mathcal{T}[V \to h] = \epsilon_V^\mu \mathcal{A}_\mu[V \to h], \tag{7.2}$$

where ϵ_V is the polarization vector of the vector meson. The amplitude $\mathcal{A}_\mu$ for the decay $\rho \to \pi^+\pi^-$ is

$$\mathcal{A}_\mu[\rho \to \pi^+\pi^-] = \tfrac{1}{2}\, G_{v\pi\pi}\, (p_+ - p_-)_\mu \,. \tag{7.3}$$

The value of the coupling constant $G_{v\pi\pi}$ is given in Eq. (B.1a). The amplitude $\mathcal{A}_\mu$ for the decay $\omega \to \pi^+\pi^-\pi^0$ is

$$\begin{aligned}\mathcal{A}_\mu[\omega \to \pi^+\pi^-\pi^0] &= \frac{4\sqrt{3}(\cos\theta_v + \sqrt{2}\sin\theta_v)}{F_\pi^3}\, \varepsilon_{\mu\nu\alpha\beta}\, p_+^\nu\, p_-^\alpha\, p_0^\beta \\ &\times \left(C_{v3\pi} + \frac{G_{v\pi\pi} C_{vv\pi} F_\pi^2}{m_v^2} \left(1 - \tfrac{1}{3}\, [f_\rho(s_{12}) + f_\rho(s_{23}) + f_\rho(s_{31})]\right)\right), \end{aligned} \tag{7.4}$$

where s_{12}, s_{23}, and s_{31} are the invariant masses of the three different pion pairs and

$$f_V(s) \equiv \frac{s}{s - M_V^2 + i m_V \Gamma_V} \tag{7.5}$$

is a vector meson resonance factor that vanishes at $s = 0$. We have denoted the 4-momenta of π^+, π^-, and π^0 by p_+, p_-, and p_0, respectively. The pion decay constant is $F_\pi = 93$ MeV, the values of the parameters $C_{v3\pi}$ and $G_{v\pi\pi} C_{vv\pi} F_\pi^2/m_v^2$ are given by Eqs. (B.1b) and (B.1c), and the value of the light vector meson mixing angle θ_v is given by Eq. (B.3). The amplitudes $\mathcal{A}_\mu$ for the radiative decays of the vector mesons are

$$\mathcal{A}_\mu[\rho^+ \to \pi^+\gamma] = \frac{4e}{3F_\pi} \left(C_{v\pi\gamma} + \frac{G_{v\gamma}\, C_{vv\pi}\, F_\pi^2}{m_v^2} \right) \varepsilon_{\mu\nu\alpha\beta} Q^\nu p^\alpha \epsilon_\gamma^\beta, \tag{7.6a}$$

$$\mathcal{A}_\mu[\omega \to \pi^0\gamma] = \frac{4(\cos\theta_v + \sqrt{2}\sin\theta_v)e}{\sqrt{3}F_\pi} \left(C_{v\pi\gamma} + \frac{G_{v\gamma}\, C_{vv\pi}\, F_\pi^2}{m_v^2} \right) \varepsilon_{\mu\nu\alpha\beta} Q^\nu p^\alpha \epsilon_\gamma^\beta, \tag{7.6b}$$

where Q and p are the 4-momenta of the vector meson and the pion and ϵ_γ is the polarization vector of the photon. The values of the parameters $C_{v\pi\gamma}$ and $G_{v\gamma} C_{vv\pi} F_\pi^2/m_v^2$ are given by Eqs. (B.2b) and (B.2c).

The amplitudes $\mathcal{A}_\nu$ in Eqs. (7.3), (7.4), and (7.6) all satisfy $Q^\nu \mathcal{A}_\nu = 0$, where Q is the 4-momentum of the vector meson. This condition is satisfied in any model consistent with vector meson dominance. The assumption of vector meson dominance is that the amplitude for the production of a real photon in a hadronic process can be expressed as the sum of over vector mesons V of the amplitude for producing V multiplied by a coupling constant for the transition $V \to \gamma$. The condition $Q^\nu \mathcal{A}_\nu = 0$ is required for the gauge invariance of the resulting amplitude for real photon production.

The T-matrix element for X to decay into J/ψ and a light hadronic system h through a virtual vector meson resonance V can be expressed as

$$\mathcal{T}[X \to J/\psi\, h] = \mathcal{A}_\mu[X \to J/\psi\, V] \frac{-g^{\mu\nu}}{Q^2 - m_V^2 + i m_V \Gamma_V} \mathcal{A}_\nu[V \to h], \tag{7.7}$$

where Q is the total 4-momentum of the hadronic system h or, equivalently, of the virtual vector meson. We have used the condition $Q^\nu \mathcal{A}_\nu = 0$ to simplify the numerator of the vector meson propagator. The quantum numbers of the particles, together with Lorentz invariance, constrains the amplitude for $X \to J/\psi\, V$ to be the sum of two terms. One of them is

$$\mathcal{A}_\mu[X \to J/\psi\, V] = G_{X\psi V}\, \varepsilon_{\mu\nu\alpha\beta} Q^\nu \epsilon_X^\alpha \epsilon_\psi^{*\beta}, \tag{7.8}$$

where ϵ_X and ϵ_ψ are the polarization 4-vectors of the X and the J/ψ and $G_{X\psi V}$ is a dimensionless constant. The contraction of this amplitude with the polarization vector ϵ_V^* of the vector meson reduces in the rest frame of the vector meson to $G_{X\psi V} m_V \boldsymbol{\epsilon_X} \cdot (\boldsymbol{\epsilon}_\psi \times \boldsymbol{\epsilon}_V)^*$. The other independent amplitude $\mathcal{A}_\mu$ has the Lorentz structure $\varepsilon_{\mu\nu\alpha\beta} P^\nu \epsilon_X^\alpha \epsilon_\psi^{*\beta}$. In the rest frame of the X, its contraction with ϵ_V^* is $m_X \boldsymbol{\epsilon_X} \cdot (\boldsymbol{\epsilon}_\psi \times \boldsymbol{\epsilon}_V)^*$. Since the mass of the X is so close to the threshold for $J/\psi\, V$,

the rest frames of the X and V are essentially identical. Thus the two independent Lorentz structures are essentially equivalent for decays that are dominated by the vector meson resonance. They give similar predictions for the partial widths for X into $J/\psi\, h$ for $h = \pi^+\pi^-\pi^0$, $\pi^+\pi^-$, or $\pi^0\gamma$. The amplitude in Eq. (7.8) has the advantage that it is also consistent with the constraint $Q^\mu \mathcal{A}_\mu = 0$ required by vector meson dominance. Thus this amplitude can be used to calculate the decay of X into $J/\psi\,\gamma$. We therefore take the transition amplitude for X into $J/\psi\, V$ to be the expression in Eq. (7.8).

7.2.2 Decay into $J/\psi\,\pi^+\pi^-$

We assume that the decay of X into $J/\psi\,\pi^+\pi^-$ proceeds through a transition of X to $J/\psi\,\rho$. The T-matrix element is then given in terms of the unknown coupling constant $G_{X\psi\rho}$ by Eqs. (7.7) and (7.8) with $V = \rho$. The expression for the amplitude $\mathcal{A}_\nu$ for $\rho \to \pi^+\pi^-$ is given in Eq. (7.3). We obtain the decay rate by squaring the amplitude, summing over spins, and integrating over phase space. The differential decay rate into $J/\psi\,\pi^+\pi^-$ as a function of the invariant mass Q of the two pions is

$$\begin{aligned}\frac{d\Gamma}{dQ}[X \to J/\psi\,\pi^+\pi^-] &= \frac{|G_{X\psi\rho}|^2 G_{v\pi\pi}^2}{9216\pi^3 m_X^5 m_\psi^2} \frac{(Q^2-4m_\pi^2)^{3/2}\lambda^{1/2}(m_X,m_\psi,Q)}{(Q^2-m_\rho^2)^2+m_\rho^2\Gamma_\rho^2} \\ &\quad\times\left[(m_X^2+m_\psi^2)(m_X^2-m_\psi^2)^2 - 2(m_X^4-4m_X^2m_\psi^2+m_\psi^4)Q^2 + (m_X^2+m_\psi^2)Q^4\right],\end{aligned} \tag{7.9}$$

where $\lambda(x,y,z)$ is the triangle function:

$$\lambda(x,y,z) = x^4+y^4+z^4-2(x^2y^2+y^2z^2+z^2x^2). \tag{7.10}$$

After integrating over the pion invariant mass, the decay rate is

$$\Gamma[X \to J/\psi\,\pi^+\pi^-] \;=\; |G_{X\psi\rho}|^2\,(223\,\mathrm{keV}). \tag{7.11}$$

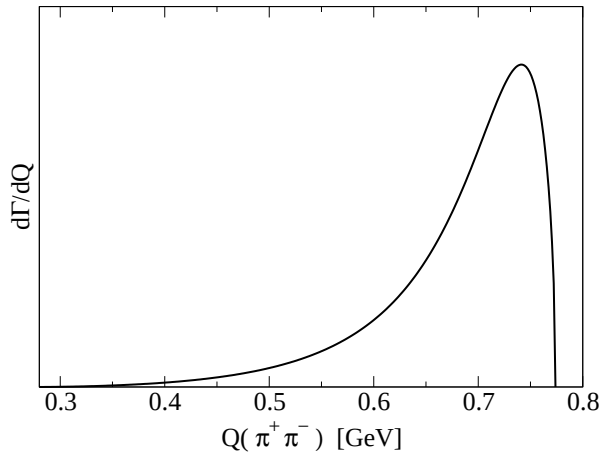

Figure 7.2: Invariant mass distributions for the pions in the decay $X \to J/\psi\,\pi^+\pi^-$.

The shape of the pion invariant mass distribution for the decay of X into $J/\psi\,\pi^+\pi^-$ is shown in Fig. 7.2. Its qualitative features are dominated by the phase space factor $\lambda^{1/2}(m_X, m_\psi, Q)$, which cuts the distribution off at the endpoint $Q = m_X - m_\psi$, and the vector meson resonance factor, which has its maximum at $Q = m_\rho$ just outside the kinematic region. Most of the support for $d\Gamma/dQ$ comes from within Γ_ρ of the upper endpoint.

7.2.3 Decay into $J/\psi\,\pi^+\pi^-\pi^0$

We assume that the decay of X into $J/\psi\,\pi^+\pi^-\pi^0$ proceeds through a transition of X to $J/\psi\,\omega$. The T-matrix element is then given in terms of the unknown coupling constant $G_{X\psi\omega}$ by Eqs. (7.7) and (7.8) with $V = \omega$. The expression for the amplitude for $\omega \to 3\pi$ is given in Eq. (7.4). We obtain the decay rate by squaring the amplitude, summing over spins, and integrating over phase space. The differential decay rate into $J/\psi\,\pi^+\pi^-\pi^0$ as a function of the invariant mass Q of the 3 pions can be reduced to a

2-dimensional integral:

$$\begin{aligned}\frac{d\Gamma}{dQ}[X \to J/\psi\,\pi^+\pi^-\pi^0] &= \frac{|G_{X\psi\omega}|^2(\cos\theta_v + \sqrt{2}\sin\theta_v)^2}{3072\pi^5 m_X^5 m_\psi^2 F_\pi^6}\frac{\lambda^{1/2}(m_X, m_\psi, Q)}{Q[(Q^2-m_\omega^2)^2 + m_\omega^2\Gamma_\omega^2]} \\ &\times \left[(m_X^2+m_\psi^2)(m_X^2-m_\psi^2)^2 - 2(m_X^4 - 4m_X^2 m_\psi^2 + m_\psi^4)Q^2 + (m_X^2+m_\psi^2)Q^4\right] \\ &\times \int ds_{12}\int ds_{23}\left[s_{12}\,s_{23}\,s_{31} - m_\pi^2(Q^2-m_\pi^2)^2\right] \\ &\times \left|C_{v3\pi} + \frac{G_{v\pi\pi}C_{vv\pi}F_\pi^2}{m_v^2}\left(1 - \tfrac{1}{3}\,[f_\rho(s_{12}) + f_\rho(s_{23}) + f_\rho(s_{31})]\right)\right|^2, \quad (7.12)\end{aligned}$$

where s_{12}, s_{23}, and s_{31} are the squares of the invariant masses of the three pairs of pions. We have suppressed the limits of integration in the integrals over s_{12} and s_{23}. After integrating over the pion invariant masses, the decay rate is

$$\Gamma[X \to J/\psi\,\pi^+\pi^-\pi^0] = |G_{X\psi\omega}|^2(19.4\,\mathrm{keV}). \quad (7.13)$$

In Fig. 7.3, the shape of the pion invariant mass distributions for the decay of X into $J/\psi\,\pi^+\pi^-\pi^0$ is shown. Its qualitative features are dominated by the phase space factor $\lambda^{1/2}(m_X, m_\psi, Q)$, which cuts the distribution off at the endpoint $Q = m_X - m_\psi$, and the vector meson resonance factor, which has its maximum at $Q = m_\omega$ just outside the kinematic region. Most of the support for $d\Gamma/dQ$ comes from within a few widths Γ_ω of the upper endpoint.

The ratio of the decay rates in Eqs. (7.11) and (7.13) is

$$\frac{\Gamma[X \to J/\psi\,\pi^+\pi^-\pi^0]}{\Gamma[X \to J/\psi\,\pi^+\pi^-]} = 0.0870\,\frac{|G_{X\psi\omega}|^2}{|G_{X\psi\rho}|^2}. \quad (7.14)$$

By comparing this to Belle's result in Eq. (2.5) for the ratio of the branching fractions, we can obtain an estimate of the ratio of the coupling constants:

$$\frac{|G_{X\psi\omega}|^2}{|G_{X\psi\rho}|^2} \approx 11.5 \pm 5.7. \quad (7.15)$$

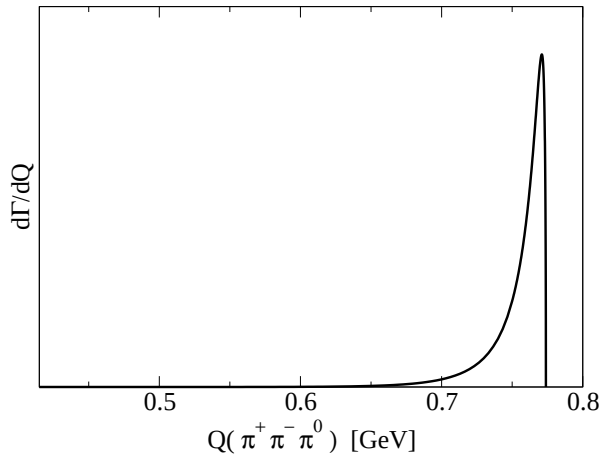

Figure 7.3: Invariant mass distributions for the three pions in the decays $X \to J/\psi\,\pi^+\pi^-\pi^0$.

7.2.4 Decay into $J/\psi\,\pi^0\gamma$

We assume that the decay of X into $J/\psi\,\pi^0\gamma$ proceeds through transitions of X to $J/\psi\,\rho$ and $J/\psi\,\omega$. The T-matrix element is then given by Eq. (7.7) summed over $V = \rho, \omega$. The amplitudes for $V \to \pi^0\gamma$ are given in Eqs. (7.6). The differential decay rate with respect to the invariant mass Q of the $\pi^0\gamma$ is

$$\begin{aligned}\frac{d\Gamma}{dQ}[X \to J/\psi\,\pi^0\gamma] &= \frac{\alpha_{\rm em}\left(C_{v\pi\gamma} + G_{v\gamma}C_{vv\pi}F_\pi^2/m_v^2\right)^2}{648\pi^2 m_X^5 m_\psi^2 F_\pi^2}\,\frac{(Q^2-m_\pi^2)^3\lambda^{1/2}(m_X,m_\psi,Q)}{Q} \\ &\times\left[(m_X^2+m_\psi^2)(m_X^2-m_\psi^2)^2 - 2(m_X^4 - 4m_X^2m_\psi^2 + m_\psi^4)Q^2 + (m_X^2+m_\psi^2)Q^4\right] \\ &\times\left|\frac{G_{X\psi\rho}}{Q^2-m_\rho^2+im_\rho\Gamma_\rho} + \frac{G_{X\psi\omega}\sqrt{3}(\cos\theta_v+\sqrt{2}\sin\theta_v)}{Q^2-m_\omega^2+im_\omega\Gamma_\omega}\right|^2 . \qquad (7.16)\end{aligned}$$

After integrating over the $\pi^0\gamma$ invariant mass, the decay rate is

$$\begin{aligned}\Gamma[X \to J/\psi\,\pi^0\gamma] =& \big[|G_{X\psi\omega}|^2 + 0.026\,|G_{X\psi\rho}|^2 \\ &+ (0.163\cos\phi + 0.215\sin\phi)|G_{X\psi\omega}||G_{X\psi\rho}|\big](3.24\,\text{keV}), \qquad (7.17)\end{aligned}$$

where $\exp(i\phi)$ is the relative phase between $G_{X\psi\omega}$ and $G_{X\psi\rho}$. The estimate of the ratio $|G_{X\psi\omega}|^2/|G_{X\psi\rho}|^2$ in Eq. (7.15) suggests that the $|G_{X\psi\omega}|^2$ term in Eq. (7.17) dominates. If this is the case, the branching fraction for the decay of X into $J/\psi\,\pi^0\gamma$ should be smaller than that for $J/\psi\,\pi^+\pi^-\pi^0$ by a factor of about 0.17.

7.2.5 Decay into $J/\psi\,\gamma$

Having chosen the transition amplitude in Eq. (7.8) so that it satisfies $Q^\mu \mathcal{A}_\mu = 0$, we can use vector meson dominance to calculate the partial width for the decay of X into $J/\psi\,\gamma$. The T-matrix element is

$$\mathcal{T}[X \to J/\psi\,\gamma] = G_{v\gamma} F_\pi^2 e \left(\frac{G_{X\psi\rho}}{m_\rho^2 - i m_\rho \Gamma_\rho} + \frac{G_{X\psi\omega}\cos\theta_v/\sqrt{3}}{m_\omega^2 - i m_\omega \Gamma_\omega} \right) \varepsilon_{\mu\nu\alpha\beta} Q^\mu \epsilon_X^\nu \epsilon_\psi^{\alpha *} \epsilon_\gamma^{\beta *}, \tag{7.18}$$

where Q is the 4-momentum of the photon. The value of the coupling constant $G_{v\gamma}$ is given in Eq. (B.2a). The result for the decay rate is

$$\begin{aligned} \Gamma[X \to J/\psi\,\gamma] &= \frac{\alpha_{\rm em} G_{v\gamma}^2 F_\pi^4 (m_X^2 + m_\psi^2)(m_X^2 - m_\psi^2)^3}{24 m_X^5 m_\psi^2} \\ &\quad \times \left| \frac{G_{X\psi\rho}}{m_\rho^2 - i m_\rho \Gamma_\rho} + \frac{G_{X\psi\omega}\cos\theta_v/\sqrt{3}}{m_\omega^2 - i m_\omega \Gamma_\omega} \right|^2 . \end{aligned} \tag{7.19}$$

If the widths in the vector meson propagators are neglected and if we use $m_\rho \approx m_\omega$, the decay rate in Eq. (7.19) reduces to

$$\Gamma[X \to J/\psi\,\gamma] = |G_{X\psi\rho} + 0.30\, G_{X\psi\omega}|^2 (5.51\,\text{keV}). \tag{7.20}$$

Our estimate in Eq. (7.15) implies that $|G_{X\psi\omega}|$ is much larger than $|G_{X\psi\rho}|$. However, the larger magnitude of $G_{X\psi\omega}$ is compensated by the vector meson mixing factor $\cos\theta_v/\sqrt{3} = 0.30$, so the $G_{X\psi\rho}$ and $G_{X\psi\omega}$ terms may be equally important. Using the partial widths in Eqs. (7.11) and (7.13), we can relate the branching fractions for

$J/\psi\,\gamma$ to those for $J/\psi\,\pi^+\pi^-$ and $J/\psi\,\pi^+\pi^-\pi^0$:

$$\begin{aligned}\mathrm{Br}[X \to J/\psi\,\gamma] &= 0.025\,\mathrm{Br}[X \to J/\psi\,\pi^+\pi^-] + 0.026\,\mathrm{Br}[X \to J/\psi\,\pi^+\pi^-\pi^0] \\ &\quad + 0.050\cos\phi\,\left(\mathrm{Br}[X \to J/\psi\,\pi^+\pi^-]\,\mathrm{Br}[X \to J/\psi\,\pi^+\pi^-\pi^0]\right)^{1/2}, \quad (7.21)\end{aligned}$$

where $\exp(i\phi)$ is the relative phase between $G_{X\psi\omega}$ and $G_{X\psi\rho}$. This prediction is compatible with the measurements of the branching ratios in Eqs. (2.5) and (2.7) if the angle ϕ is small.

7.3 Factorization of short-distance decay rates

Short-distance decays of the X into a hadronic final state H involve well-separated momentum scales. The DD^* wavefunction of the X involves the momentum scale $1/|a|$ set by the large scattering length. The transition of the DD^* to H involves momentum scales m_π and larger. The separation of scales $|a| \gg 1/m_\pi$ can be exploited by using a factorization formula for the decay rate [45]. In limit $|a| \gg 1/m_\pi$, the leading term in the T-matrix element for the decay $X \to H$ can be separated into a short-distance factor and a long-distance factor as shown in Eq. (5.1). The short-distance factor $\mathcal{A}_{\rm short}$ in Eq. (5.1) has a well-behaved limit as $|a| \to \infty$. The long-distance factor $\mathcal{A}_X$ is the universal amplitude given in Eq. (3.8). If the complex scattering length is parameterized as in Eq. (3.10), this factor is given by Eq. (5.2). When applied to decays of X into J/ψ and light hadrons, the factorization formula in Eq. (5.1) implies that the coupling constants $G_{X\psi\rho}$ and $G_{X\psi\omega}$ have a long-distance factor $\mathcal{A}_X$.

The factorization formula for the T-matrix element in Eq. (5.1) implies a factorization formula for the decay rate:

$$\Gamma[X \to H] = \Gamma_{\rm short}[X \to H] \times |\mathcal{A}_X|^2. \quad (7.22)$$

The short-distance factor $\Gamma_{\rm short}$ in Eq. (7.22) has a well-behaved limit as $|a| \to \infty$.

Predictions for the rates for short-distance decays of the X can be obtained from models for low-energy hadrons in which the parameters have been tuned to obtain a small binding energy E_X, such as Swanson's model [33]. In such models, calculations using the most straightforward numerical methods tend to become increasingly unstable as the binding energy is tuned toward 0, because the small binding energy results from a delicate cancellation. The factorization formula in Eqs. (7.22) and (5.9) can be useful for extrapolating the predictions of a model to other values of the binding energy E_X. In many models, it is difficult to take into account effects of the width Γ_X of the molecule. Given the prediction of a model in which the width has been neglected, the factorization formula in Eqs. (7.22) and (5.9) can be used to take into account the nonzero width Γ_X consistently.

In order to use the factorization formula in Eqs. (7.22) and (5.9) to extrapolate a partial width calculated using a model to other values of the binding energy and the width, the calculation must be carried out for small enough binding energy that the model is in the universal scaling regime where observables scale as powers of the binding energy. For example, the probabilities for components of the wavefunction other than $D^0\bar{D}^{*0}$ and $D^{*0}\bar{D}^0$ should scale as $E_X^{1/2}$. In Swanson's model with $E_X = 0.7$ MeV, this universal scaling behavior is satisfied by the probability $Z_{\psi\omega}$ but not by $Z_{\psi\rho}$, as is evident in Fig. 7.1. The delayed onset of the universal behavior for the probability $Z_{\psi\rho}$ can perhaps be attributed to the weaker coupling of X to isospin-1 states. In the next section, we will use Swanson's result for $Z_{\psi\omega}$ to estimate the coupling constant $G_{X\psi\omega}$.

7.4 Partial width for $X \to J/\psi\,\pi^+\pi^-\pi^0$

The partial widths of the X calculated in Section 7.2 are expressed in terms of unknown coupling constants $G_{X\psi\rho}$ and $G_{X\psi\omega}$. In this section, we use a simple 2-channel scattering model described in Section 4.3 to show that $|G_{X\psi\omega}|$ can be deduced from the probability $Z_{\psi\omega}$ for the $J/\psi\,\omega$ component of the X. We then use the probability $Z_{\psi\omega}$ in Swanson's model to give a quantitative prediction for the partial width for the X to decay into $J/\psi\,\pi^+\pi^-\pi^0$.

We can use results from Swanson's model to estimate $|G_{X\psi\omega}|$, thereby determining the unknown constant in the expression in Eq. (7.13) for the partial width for $X \to J/\psi\,\pi^+\pi^-\pi^0$. The relativistic amplitude for the transition from X to $J/\psi\,\omega$ is given by the contraction of the amplitude $\mathcal{A}_\mu$ in Eq. (7.8) with a polarization vector for the ω. The corresponding nonrelativistic amplitude $\mathcal{A}_{X\psi\omega}$ is the analog of the transition amplitude $\mathcal{A}_{X2}$ in Eq. (4.37) for the 2-channel model. In the rest frame of the X, the relativistic amplitude differs from the nonrelativistic amplitude by a factor of $\sqrt{2m_i}$ for every external particle:

$$\epsilon_\omega^{\mu *} \mathcal{A}_\mu[X \to J/\psi\,\omega] = (8 m_X m_\psi m_\omega)^{1/2} \mathcal{A}_{X\psi\omega}. \tag{7.23}$$

Using the expression for the amplitude $\mathcal{A}_\mu$ in Eq. (7.8) and the fact that the rest frame of the X is almost identical to that of the ω, the left side of Eq. (7.23) is

$$\epsilon_\omega^{\mu *} \mathcal{A}_\mu[X \to J/\psi\,\omega] = G_{X\psi\omega} m_\omega \boldsymbol{\epsilon}_X \cdot (\boldsymbol{\epsilon}_\psi \times \boldsymbol{\epsilon}_\omega)^*. \tag{7.24}$$

The transition amplitude $\mathcal{A}_{X\psi\omega}$ on the right side of Eq. (7.23) must have the same dependence on the polarization vectors of the J/ψ and ω. There are two independent pairs of spin states for J/ψ and ω that couple to any given spin state of X. If the

analog of the factorization formula in Eq. (4.39) is summed over the spin states of the J/ψ and ω, it gives

$$\sum_{\text{spins}} |\mathcal{A}_{X\psi\omega}|^2 = \sqrt{8\pi^2 \Delta_{\psi\omega}/\mu_{\psi\omega}^3}\, Z_{\psi\omega}, \tag{7.25}$$

where $\Delta_{\psi\omega}$ is the energy gap in Eq. (3.16c), $\mu_{\psi\omega}$ is the reduced mass of the J/ψ and ω, and $Z_{\psi\omega}$ is the probability for the $J/\psi\,\omega$ component of X. Squaring both sides of Eq. (7.23) and summing over the spin states of J/ψ and ω, we get

$$2m_\omega^2 |G_{X\psi\omega}|^2 = 16\pi m_X (m_\psi + m_\omega) \sqrt{2\Delta_{\psi\omega}/\mu_{\psi\omega}}\, Z_{\psi\omega}. \tag{7.26}$$

Inserting Swanson's result $Z_{\psi\omega} = 9.6\%$ for $E_X = 0.7$ MeV and using the factorization formula in Eqs. (7.22) and (5.9), this reduces to

$$|G_{X\psi\omega}|^2 = 9.59 \left(\frac{E_X + \Gamma_X^2/(16E_X)}{0.7\,\text{MeV}} \right)^{1/2}. \tag{7.27}$$

Inserting the result into the expression in Eq. (7.13), we get a quantitative result for the partial width:

$$\Gamma[X \to J/\psi\,\pi^+\pi^-\pi^0] \;=\; (222\,\text{keV}) \left(\frac{E_X + \Gamma_X^2/(16E_X)}{1\,\text{MeV}} \right)^{1/2}. \tag{7.28}$$

We can use the result in Eq. (7.28) to set a lower bound on the partial width into $J/\psi\,\pi^+\pi^-\pi^0$. As a function of the binding energy E_X, the right side of Eq. (7.28) is minimized at $E_X = \Gamma_X/4$. The lower bound on the width is $\Gamma_X > 2\Gamma[D^{*0}] = 136 \pm 32$ keV. Thus the lower bound on the partial width into $J/\psi\,\pi^+\pi^-\pi^0$ in Swanson's model is about 58 keV.

As is evident in Fig. 7.1, Swanson did not calculate the probability $Z_{\psi\rho}$ for the $J/\psi\,\rho$ component of X for a binding energy small enough to be in the scaling region where $Z_{\psi\rho}$ scales like $E_X^{1/2}$. If he had, we could use an equation analogous to Eq. (7.26)

to determine $|G_{X\psi\rho}|$. If we assume that the smallest binding energy considered by Swanson is close to the scaling region, we can use his value $Z_{\psi\rho} = 0.86\%$ for $E_X = 0.7$ MeV to estimate $|G_{X\psi\rho}|$. In the analog of Eq. (7.26), we should set $\Delta_{\psi\rho} = \Delta_{\psi\omega}$ rather than using the value $\Delta_{\psi\rho}$ in Eq. (3.16b), because Swanson set $m_\rho = m_\omega$ in his calculation. The resulting estimate is

$$|G_{X\psi\rho}|^2 \approx 0.86 \left(\frac{E_X + \Gamma_X^2/(16E_X)}{0.7\,\mathrm{MeV}} \right)^{1/2} . \tag{7.29}$$

We can insert this estimate into Eq. (7.11) to get an estimate of the partial width for decay into $J/\psi\,\pi^+\pi^-$. We can also insert this estimate of $|G_{X\psi\rho}|^2$ and the value of $|G_{X\psi\omega}|^2$ from Eq. (7.27) into Eqs. (7.17) and (7.20) to get ranges of estimates of the partial widths for the decays into $J/\psi\,\pi^0\gamma$ and $J/\psi\,\gamma$. The ranges arise from the unknown relative phase between $G_{X\psi\omega}$ and $G_{X\psi\rho}$.

CHAPTER 8

CONCLUSION

If the $X(3872)$ is a loosely-bound S-wave molecule corresponding to a $C = +$ superposition of $D^0\bar{D}^{*0}$ and $D^{*0}\bar{D}^0$, the scattering length a in the $(DD^*)^0_+$ channel is large compared to all other relevant length scales of QCD. Nonrelativistic few-body systems with short-range interactions and a large scattering length a have universal properties that depend on the scattering length but are otherwise insensitive to details at distances small compared to a. Many of these universal properties are encoded in the universal transition amplitude $\mathcal{A}(E)$ in Eq. (3.9), which depends only on the scattering length a and the energy E of the pair of particles in their center-of-momentum frame. Various universal properties of the DD^* molecule can be extracted from $\mathcal{A}(E)$. The decays of the X implies that the large scattering length has an imaginary part. It can be conveniently parameterized in terms of the real and imaginary parts of $1/a$ as in Eq. (3.10). The binding energy E_X and the width Γ_X of the DD^* molecule are expressed in terms of those parameters in Eqs. (3.12) and (3.11b).

Fine-tuning mechanisms that can generate a large scattering length for the $(DD^*)^0_+$ channel were discussed using three scattering models. It was explicitly shown that these models have the same universal properties that are compactly encoded in the universal amplitude $\mathcal{A}(E)$ in Eq. (3.9). The three models differ in their predictions for

the approach to the universal limit. The zero-range model may describe the approach to the universal limit more accurately if the large scattering length arises from a fine-tuning of the depth of the interaction potential between D^0 and $\bar{D}^{*0}$ and between D^{*0} and $\bar{D}^0$. The resonance model may describe the approach more accurately if the large scattering length is given by a fine-tuning of the mass of the $\chi_{c1}(2P)$ to the $D^0\bar{D}^{*0}$ threshold. The two-channel model may describe the approach more accurately if the large scattering length is given by a fine-tuning of the S-wave scattering parameters associated with channels with nearby thresholds such as D^+D^{*-}, $D^{*+}D^-$, $J/\psi\,\rho$, and $J/\psi\,\omega$. The two-channel model is also useful for understanding the decays of X that proceed through decays of constituents in channels with nearby thresholds.

The large scattering length can be exploited through factorization formulas for decay rates of X. For short-distance decay modes that do not proceed through the decay of a constituent D^* of the X, the long-distance factor in the factorization formula is proportional to $1/|a|$ and is given in Eq. (5.10). If a partial width of the X is calculated using some model with a specific binding energy for the X, the factorization formulas can be used to extrapolate the prediction to other values of the binding energy and to take into account the width of the X.

The large scattering length can also be exploited through factorization formulas for production rates of X, of $D^0\bar{D}^{*0}$ near threshold, of $D^{*0}\bar{D}^0$ near threshold, and of decay products of X with invariant mass near the $D^0\bar{D}^{*0}$ threshold. The long-distance factor in the factorization formula for production rates of X is proportional to $1/|a|$. For production of $D^0\bar{D}^{*0}$ and $D^{*0}\bar{D}^0$ near threshold, the factorization formula implies that the dependence on the invariant mass is through the factor $\sqrt{2\mu E}|\mathcal{A}(E)|^2$, where E is the invariant mass relative to the $D^0\bar{D}^{*0}$ threshold and $|\mathcal{A}(E)|^2$ is given in

Eq. (5.22). The peak in the invariant mass distribution is above the threshold by the amount $E_X + \Gamma_X^2/(16E_X)$. The factorization formulas also relate the rates for production of X to those for production of $D^0\bar{D}^{*0}$ and $D^{*0}\bar{D}^0$ near threshold. The line shape of the X can be measured through the invariant mass distribution of its decay products. In the case of short-distance decay modes, the factorization formulas imply that near the $D^0\bar{D}^{*0}$ threshold, the shape of the invariant mass distribution is given by the factor $|\mathcal{A}(E)|^2$ in Eq. (5.26). If $\mathrm{Re}(a) < 0$, the distribution has a cusp at $E = 0$, as shown in the lower panel of Fig. 5.7. If $\mathrm{Re}(a) > 0$, the distribution has a peak at $E = -E_X$, as shown in the upper panel of Fig. 5.7. In contrast to a Breit-Wigner resonance, the integral over the line shape is logarithmically sensitive to the endpoints of the integration region. This effect should be taken into account in analyzing the production and decay of the X.

We analyzed the production of X via $B \to XK$ by exploiting the factorization formula that relates the decay rate to the rates for $B \to D^0\bar{D}^{*0}K$ and $B \to D^*\bar{D}^0K$ near the charm meson threshold. Those rates were estimated by an analysis of Babar data on the branching fractions for the decays $B \to D^{(*)}\bar{D}^{(*)}K$. Our estimate for the branching fraction for $B^+ \to XK^+$ is given in Eq. (6.21). It scales with the binding energy E_X of X as $E_X^{1/2}$ as required by the factorization formulas. It also scales as Λ_π^2, where Λ_π is an unknown crossover momentum scale that is expected to be comparable to m_π. If we take $E_X = 0.5$ MeV, neglect Γ_X, and allow Λ_π to vary between $m_\pi/2$ and $2m_\pi$, our estimate of the branching fraction varies from about 7×10^{-6} to about 1×10^{-4}. This range is compatible with the measured product of the branching fractions for $B^+ \to XK^+$ and $X \to J/\psi\,\pi^+\pi^-$ if $\mathrm{Br}[X \to J/\psi\,\pi^+\pi^-]$ is greater than about 10^{-1}.

Our result for the ratio of the branching fractions for $B^0 \to XK^0$ and $B^+ \to XK^+$ is given in Eq. (6.23). It is expressed in terms of parameters G_1, G_2, G_3, G_4, and χ that appear in the amplitudes for $B \to \bar{D}^{(*)} D^{(*)} K$. The result is independent of the binding energy E_X of the X and also independent of the crossover scale Λ_π. Based on the determination of the parameters G_i and χ from our analysis of Babar data on the branching fractions for the decays $B \to D^{(*)} \bar{D}^{(*)} K$, we concluded that the ratio of the branching fractions in Eq. (6.23) should be less than about 8×10^{-2}. The suppression of $B^0 \to XK^0$ can be explained partly by the decays of B^0 into $D^0 \bar{D}^{*0} K^0$ and $D^{*0} \bar{D}^0 K^0$ being dominated by color-suppressed amplitudes and partly by heavy quark symmetry forcing these amplitudes to vanish at the DD^* threshold. The suppression of the decay $B^0 \to XK^0$ compared to $B^+ \to XK^+$ is a nontrivial prediction of the interpretation of $X(3872)$ as a DD^* molecule. This prediction stands in sharp contrast to the observed pattern of exclusive decays of B into a charmonium H plus K, where the ratio for $B^0 \to HK^0$ and $B^+ \to HK^+$ are equal to within errors.

In our analysis of the Babar data on the decays $B \to D^{(*)} \bar{D}^{(*)} K$, we made the crude assumption that the form factors $G_1(q^2)$, $G_2(q^2)$, $G_3(q^2)$, and $G_4(q^2)$ are constants. The primary reason for this assumption was that the available experimental information was limited to branching fractions for the decays $B \to D^{(*)} \bar{D}^{(*)} K$. Measurements of Dalitz plot distributions and invariant mass distributions for those decays would allow a more rigorous analysis that takes into account the q^2-dependence of the form factors. This could be used to make a more precise prediction of the ratio of the branching fractions for $B^0 \to XK^0$ and $B^+ \to XK^+$. Measurements of the invariant mass distributions for the decays $B \to D^0 \bar{D}^{*0} K$ and $B \to D^{*0} \bar{D}^0 K$

would be particularly valuable. They might reveal the enhancement near the $D^0\bar{D}^{*0}$ threshold that would confirm the interpretation of the X as a DD^* molecule.

We have analyzed the decays of X into J/ψ plus light hadrons under the assumption that X is a DD^* molecule and that these decays proceed through transitions to $J/\psi\,\rho$ and $J/\psi\,\omega$. The differential decay rates were calculated in terms of unknown coupling constants $G_{X\psi\rho}$ and $G_{X\psi\omega}$ by using an effective lagrangian that reproduces the decays of the light vector mesons. The dependence on the unknown coupling constants enters only through multiplicative factors, so the angular distributions are completely determined. Quantitative predictions of the partial widths for the decays of X into J/ψ plus light hadrons require numerical values for the coupling constants $G_{X\psi\rho}$ and $G_{X\psi\omega}$. We pointed out that the dependence of these coupling constants on the binding energy E_X and the total width Γ_X are determined by factorization formulas. We showed how $|G_{X\psi\omega}|^2$ could be determined from the probability $Z_{\psi\omega}$ for the $J/\psi\,\omega$ component of X in Swanson's model. We used this result to give a quantitative prediction for the partial width for $X \to J/\psi\,\pi^+\pi^-\pi^0$ as a function of E_X and Γ_X.

In summary, we have analyzed the $X(3872)$ under the assumption that it is an S-wave DD^* molecule. This system provides a beautiful example of the predictive power of universality in systems with a large scattering length. It gives nontrivial predictions for the dependence of the production and decay rates of the X on its binding energy and width. It also implies nontrivial relations between the production rates of X and production rates of $D^0\bar{D}^{*0}$ and $D^{*0}\bar{D}^0$ near the charm meson threshold. The factorization formulas we have derived for the production and decay rates of X

can also be applied to other systems with large scattering, not only in particle physics but also in nuclear and atomic physics.

If our interpretation of X as a DD^* molecule is confirmed by experiment, it will have deep implications for QCD and hadronic physics. The $X(3872)$, with quark content $cu\bar{c}\bar{u}$, will be the first exotic hadron to be unambiguously identified. Tornqvist's analysis of the one-pion-exchange potential model [38] suggests that there may also be charm meson molecules with constituents $D^*\bar{D}^*$. It implies that there must be bottom meson molecules with constituents $B\bar{B}^*$, $B^*\bar{B}$, and $B^*\bar{B}^*$. These molecules are predicted to have binding energies that are much larger than the natural energy scale 3 MeV associated with pion exchange, so the constituents will not have a large scattering length. This methods based on universality that we have applied to the $X(3872)$ will not be applicable. However the insights into the $X(3872)$ provided by universality can be used to fine-tune other models for mesonic molecules and therefore lead indirectly to a deeper understanding of these exotic hadrons.

APPENDIX A

ABSENCE OF EFIMOV STATES

The most remarkable predictions of low-energy universality, which were discovered by Efimov [79], occur in the 3-body sector. At sufficiently low energies, the effective interaction between three nonrelativistic particles with short-range forces can be described by an effective potential $V_{\text{eff}}(R)$ that depends only on the *hyperspherical radius* R, which is a weighted average of the separations of the three particles [80]. If the scattering length is large compared to the range ℓ of the force, the effective potential in the region $\ell \ll R \ll |a|$ is scale-invariant. In the case of identical particles of mass m, the hyperspherical radius is just the root-mean-square separation of the three pairs of particles and the scale-invariant potential is

$$V_{\text{eff}}(R) \approx -\frac{4-\lambda_0}{2mR^2}, \tag{A.1}$$

where λ_0 is the minimum of the nontrivial solutions to

$$\sqrt{3}\lambda^{1/2}\cos(\pi\lambda^{1/2}/2) = 8\sin(\pi\lambda^{1/2}/6). \tag{A.2}$$

The minimum solution is $\lambda_0 = -s_0^2$, where $s_0 \approx 1.00624$. In the *resonant limit* $a \to \infty$ in which the scattering length is tuned to be infinitely large, the 2-body bound state has zero binding energy and there are infinitely many arbitrarily-shallow 3-body

bound states called *Efimov states*. If the particles are identical bosons, the ratio of the binding energies of adjacent states approaches a universal constant $e^{2\pi/s_0} \approx 515.03$. The 3-body spectrum in the resonant limit has an asymptotic discrete scaling symmetry with discrete scaling factor $e^{\pi/s_0} \approx 22.7$. This symmetry is related to an infrared *renormalization group limit cycle* [81]. A limit that is more relevant to a physical problem with a large but finite scattering length is the *scaling limit* defined by $\Lambda \to \infty$ with a fixed, where Λ is the natural momentum scale set by the inverse of the range of the interaction. In the scaling limit, the binding energies B_3 and B_3' of the shallowest and next-to-shallowest Efimov states for identical bosons are in the intervals $B_2 < B_3 < 6.75B_2$ and $6.75B_2 < B_3' < 1406B_2$, where $B_2 = 1/(ma^2)$ is the 2-body binding energy [82]. If these binding energies are smaller than the natural energy scale Λ^2/m, these Efimov states should appear as real states in the spectrum. Thus, there should be at least one Efimov state if $\Lambda^2/m > 6.75B_2$ and at least two if $\Lambda^2/m > 1406B_2$. As an illustration, we consider helium atoms, which have a large scattering length [82]. The helium dimer is very shallow: its binding energy $B_2 \approx 1.3$ mK is smaller than the natural low-energy scale $\Lambda^2/m \approx 400$ mK by about a factor of 300. Thus we would expect either one or two Efimov states. There are in fact two helium trimers: a ground state and an excited state with binding energies $B_3' \approx 130$ mK and $B_3 \approx 2$ mK. Both can be interpreted as Efimov states [82].

The large $D^0\bar{D}^{*0}$ scattering length raises the exciting possibility of shallow $D^0D^0\bar{D}^{*0}$ molecules within 10 MeV of the $D^0D^0\bar{D}^{*0}$ threshold generated by the Efimov effect. Unfortunately, this possibility can be excluded. The $D^0D^0\bar{D}^{*0}$ sector involves only two identical bosons and only two of the three pairs of particles have a resonant interaction with a large scattering length. Furthermore a $D^0\bar{D}^{*0}$ pair can fluctuate into a

$\bar{D}^0 D^{*0}$ pair, and the other D^0 has no resonant interaction with this component of the wavefunction. Low-energy interactions in the 3-body sector can again be described by an effective potential which in the region $m_\pi^{-1} \ll R \ll |a|$ has the scale-invariant form (A.1). The form of the potential can be derived from results given in Ref. [80]. If we ignore the 8% mass difference between the D^0 and $\bar{D}^{*0}$, the only difference is that the equation for λ_0 is

$$\sqrt{3}\lambda^{1/2}\cos(\pi\lambda^{1/2}/2) = 2\sin(\pi\lambda^{1/2}/6). \tag{A.3}$$

Of the factor of 4 difference with (A.2), one factor of 2 comes from there being only two identical bosons instead of three and the other factor of 2 comes from the 3-body system being a superposition of a $D^0 D^0 \bar{D}^{*0}$ molecule and a $D^0 \bar{D}^0 D^{*0}$ molecule. The minimum nontrivial solution to (A.3) is $\lambda_0 \approx 0.3533$. Since this is positive, the Efimov effect does not arise and there are no shallow 3-body bound states.

APPENDIX B

VECTOR MESON DECAYS

In this appendix, we present an updated determination of the coupling constants in the effective lagrangian for the light pseudoscalar and vector mesons that was used in Ref. [78] to calculate the semileptonic branching fractions for the τ lepton. The same effective lagrangian is used in Section 7.2 to calculate the decay rates of the X into J/ψ and light hadrons.

The pion decay constant $F_\pi = 93$ MeV and the hadron masses have all been determined accurately [56]. The other parameters in the effective lagrangian can be determined from the partial widths for decays of ρ^0, $\rho^\pm$, and ω given in Table B.1. The most useful combinations of the parameters in the amplitudes for the decays of the vector mesons into pions in Eqs. (7.3) and (7.4) are

$$G_{v\pi\pi} = 11.99 \pm 0.06, \tag{B.1a}$$

$$C_{v3\pi} + G_{v\pi\pi} C_{vv\pi} F_\pi^2/m_v^2 = (8.03 \pm 0.48)/(16\pi^2), \tag{B.1b}$$

$$G_{v\pi\pi} C_{vv\pi} F_\pi^2/m_v^2 = (10.2 \pm 1.3)/(16\pi^2). \tag{B.1c}$$

The coupling constant $G_{v\gamma}$ associated with vector meson dominance and the most useful combinations of parameters in the amplitudes for the radiative decays of the

Decay mode	Partial width
$\rho^0 \to \pi^+\pi^-$	150.3 ± 1.6 MeV
$\rho^0 \to e^+e^-$	7.02 ± 0.11 keV
$\rho^- \to \pi^-\gamma$	67.6 ± 7.5 keV
$\omega \to e^+e^-$	0.60 ± 0.02 keV
$\omega \to \pi^0\gamma$	0.76 ± 0.05 MeV
$\omega \to \pi^0\mu^+\mu^-$	0.82 ± 0.20 keV
$\omega \to \pi^+\pi^-\pi^0$	7.56 ± 0.093 MeV

Table B.1: Inputs that are used to determine the coupling constants in the vector meson decay amplitudes. The partial widths are taken from Ref. [56].

vector mesons in Eqs. (7.6) are

$$G_{v\gamma} = 14.01 \pm 0.11, \tag{B.2a}$$

$$C_{v\pi\gamma} + G_{v\gamma}\, C_{vv\pi}\, F_\pi^2/m_v^2 = (7.99 \pm 0.45)/(16\pi^2), \tag{B.2b}$$

$$G_{v\gamma} C_{vv\pi}\, F_\pi^2/m_v^2 = (11.9 \pm 1.5)/(16\pi^2). \tag{B.2c}$$

The vector meson mixing angle is given by[2]

$$\cos\theta_v = 0.51 \pm 0.01. \tag{B.3}$$

Another function of θ_v that is often encountered is $\cos\theta_v + \sqrt{2}\sin\theta_v \approx 1.73 \pm 0.01$. The errors in the parameters in Eqs. (B.1), (B.2), and (B.3) are determined using the uncertainties in the measurements of the vector meson decay widths only. The uncertainties in the hadron masses and the pion decay constant are negligible in comparison. Variations in the parameters associated with $U(3) \times U(3)$ symmetry breaking are neglected in this analysis.

[2]The cosine of the angle θ_v here is the sine of the vector meson mixing angle used in Ref. [78].

The inputs that were used to determine the parameters in Eqs. (B.1), (B.2), and (B.3) are listed in Table B.1. Following Ref. [78], we determine the parameters by the following steps:

1. The coupling constant $G_{v\pi\pi}$ in Eq. (B.1a) is determined from the partial width for $\rho \to \pi^+\pi^-$:

$$\Gamma[\rho \to \pi^+\pi^-] = \frac{G_{v\pi\pi}^2 m_\rho}{192\pi} \left(1 - 4m_\pi^2/m_\rho^2\right)^{3/2}. \tag{B.4}$$

2. The coupling constant $G_{v\gamma}$ in Eq. (B.2a) is determined from the partial width for $\rho \to e^+e^-$:

$$\Gamma[\rho \to e^+e^-] = \frac{4\pi\alpha_{\rm em}^2\, G_{v\gamma}^2\, F_\pi^4}{3\, m_\rho^3}. \tag{B.5}$$

3. The combination of parameters in Eq. (B.2b) is determined from the partial width for $\rho^- \to \pi^-\gamma$:

$$\Gamma[\rho^- \to \pi^-\gamma] = \frac{2\alpha_{\rm em} m_\rho^3}{27F_\pi^2} \left(C_{v\pi\gamma} + \frac{G_{v\gamma}\, C_{vv\pi}\, F_\pi^2}{m_v^2}\right)^2 (1 - m_\pi^2/m_\rho^2)^3. \tag{B.6}$$

4. The combination of parameters $G_{v\gamma}\, C_{vv\pi}\, F_\pi^2/m_v^2$ in Eq. (B.2c) is determined from the ratio of the partial widths for $\omega \to \pi^0\mu^+\mu^-$ and $\omega \to \pi^0\gamma$. The possibility of a relative phase between $C_{v\pi\gamma}$ and $G_{v\gamma}\, C_{vv\pi}\, F_\pi^2/m_v^2$ is ignored. The partial width for $\omega \to \pi^0\mu^+\mu^-$ is

$$\Gamma[\omega \to \pi^0\mu^+\mu^-] = \frac{1}{256\pi^3 m_\omega^3} \int ds_{12} \int ds_{23} \overline{\sum} |\mathcal{A}[\omega \to \pi^0\mu^+\mu^-]|^2. \tag{B.7}$$

The squared amplitude, averaged over initial spin states and summed over final spin states, is

$$\begin{aligned}\overline{\sum}|\mathcal{A}[\omega\to\pi^0\mu^+\mu^-]|^2 &= \frac{128\pi^2\alpha_{\rm em}^2}{9F_\pi^2}\,(\cos\theta_v+\sqrt{2}\sin\theta_v)^2 \\ &\times\left[(s_{23}^2+4m_\mu^2)\left((m_\omega^2-s_{23}-m_\pi^2)^2-4m_\pi^2 s_{23}\right)+s_{23}(s_{12}-s_{31})^2\right] \\ &\times\frac{1}{s_{23}^2}\left|C_{v\pi\gamma}+\frac{G_{v\gamma}\,C_{vv\pi}\,F_\pi^2}{m_v^2}(1-f_\rho(s_{23}))\right|^2, \qquad \text{(B.8)}\end{aligned}$$

where s_{12}, s_{23}, and s_{31} are the squares of the invariant masses of the $\pi^0\mu^+$, $\mu^+\mu^-$, and $\mu^-\pi^0$, respectively. The partial width for $\omega\to\pi^0\gamma$ is

$$\Gamma[\omega\to\pi^0\gamma]=3(\cos\theta_v+\sqrt{2}\sin\theta_v)^2\frac{m_\omega^3(1-m_\pi^2/m_\omega^2)^3}{m_\rho^3(1-m_\pi^2/m_\rho^2)^3}\,\Gamma[\rho^-\to\pi^-\gamma], \qquad \text{(B.9)}$$

where $\Gamma[\rho^-\to\pi^-\gamma]$ is given in Eq. (B.6). Note that the factor $(\cos\theta_v+\sqrt{2}\sin\theta_v)^2$ cancels in the ratio of Eqs. (B.7) and (B.9).

5. The combination of parameters $G_{v\pi\pi}C_{vv\pi}F_\pi^2/m_v^2$ appearing in Eq. (B.1c) is determined by multiplying the combination of parameters in Eq. (B.2c) by the ratio $G_{v\pi\pi}/G_{v\gamma}$ obtained from Eqs. (B.1a) and (B.2a).

6. The combination of parameters in Eq. (B.1b) is determined from the ratio of the partial widths for ω to decay into $\pi^+\pi^-\pi^0$ and $\pi^0\gamma$ and from the value of the combination of parameters in Eq. (B.1c). The possibility of a relative phase between $C_{v3\pi}$ and $G_{v\pi\pi}C_{vv\pi}F_\pi^2/m_v^2$ is ignored. The partial width for $\omega\to\pi^0\gamma$ is given in Eq. (B.9). The partial width for $\omega\to\pi^+\pi^-\pi^0$ is

$$\Gamma[\omega\to\pi^0\pi^+\pi^-]=\frac{1}{256\pi^3 m_\omega^3}\int ds_{12}\int ds_{23}\overline{\sum}|\mathcal{A}[\omega\to\pi^+\pi^-\pi^0]|^2. \qquad \text{(B.10)}$$

The squared amplitude, averaged over the spin states of ω, is

$$\overline{\sum}|\mathcal{A}[\omega \to \pi^+\pi^-\pi^0]|^2 = \frac{4(\cos\theta_v + \sqrt{2}\sin\theta_v)^2}{F_\pi^6}\left(s_{12}s_{23}s_{31} - m_\pi^2(m_\omega^2 - m_\pi^2)^2\right) \times \left|C_{v3\pi} + \frac{G_{v\pi\pi}C_{vv\pi}F_\pi^2}{m_v^2}\left(1 - \tfrac{1}{3}\left[f_\rho(s_{12}) + f_\rho(s_{23}) + f_\rho(s_{31})\right]\right)\right|^2 . \quad \text{(B.11)}$$

Note that the factor $(\cos\theta_v + \sqrt{2}\sin\theta_v)^2$ cancels in the ratio of Eqs. (B.10) and (B.9).

7. Finally, the cosine of the vector meson mixing angle in Eq. (B.3) is determined from the ratio of the partial widths for $\omega \to e^+e^-$ and $\rho^0 \to e^+e^-$:

$$\Gamma[\omega \to e^+e^-] = \frac{\cos^2\theta_v\, m_\rho^3}{3m_\omega^3}\,\Gamma[\rho^0 \to e^+e^-]. \quad \text{(B.12)}$$

BIBLIOGRAPHY

[1] K. G. Wilson, Phys. Rev. **D10**, 2445 (1974).

[2] HPQCD, C. T. H. Davies *et al.*, Phys. Rev. Lett. **92**, 022001 (2004), hep-lat/0304004.

[3] T. Barnes, Phys. Lett. **B165**, 434 (1985).

[4] T. Barnes, F. E. Close, and H. J. Lipkin, Phys. Rev. **D68**, 054006 (2003), hep-ph/0305025.

[5] Belle, S. K. Choi *et al.*, Phys. Rev. Lett. **91**, 262001 (2003), hep-ex/0309032.

[6] CDF II, D. Acosta *et al.*, Phys. Rev. Lett. **93**, 072001 (2004), hep-ex/0312021.

[7] D0, V. M. Abazov *et al.*, Phys. Rev. Lett. **93**, 162002 (2004), hep-ex/0405004.

[8] BABAR, B. Aubert *et al.*, Phys. Rev. **D71**, 071103 (2005), hep-ex/0406022.

[9] Belle, S. K. Choi, (2004), hep-ex/0405014.

[10] K. Abe, (2005), hep-ex/0505037.

[11] F. E. Close and P. R. Page, Phys. Lett. **B578**, 119 (2004), hep-ph/0309253.

[12] S. Pakvasa and M. Suzuki, Phys. Lett. **B579**, 67 (2004), hep-ph/0309294.

[13] J. L. Rosner, Phys. Rev. **D70**, 094023 (2004), hep-ph/0408334.

[14] T. Kim and P. Ko, Phys. Rev. **D71**, 034025 (2005), hep-ph/0405265.

[15] K. Abe, (2005), hep-ex/0505038.

[16] Belle, S. L. Olsen, Int. J. Mod. Phys. **A20**, 240 (2005), hep-ex/0407033.

[17] T. Barnes and S. Godfrey, Phys. Rev. **D69**, 054008 (2004), hep-ph/0311162.

[18] E. J. Eichten, K. Lane, and C. Quigg, Phys. Rev. **D69**, 094019 (2004), hep-ph/0401210.

[19] C. Quigg, (2004), hep-ph/0403187.

[20] C. Quigg, Nucl. Phys. Proc. Suppl. **142**, 87 (2005), hep-ph/0407124.

[21] A. Tomaradze, (2004), hep-ex/0410090.

[22] FNAL-E835, C. Patrignani, (2004), hep-ex/0410085.

[23] BELLE, S. K. Choi *et al.*, Phys. Rev. Lett. **89**, 102001 (2002), hep-ex/0206002.

[24] BABAR, B. Aubert *et al.*, Phys. Rev. Lett. **92**, 142002 (2004), hep-ex/0311038.

[25] CLEO, D. M. Asner *et al.*, Phys. Rev. Lett. **92**, 142001 (2004), hep-ex/0312058.

[26] CP-PACS, M. Okamoto *et al.*, Phys. Rev. **D65**, 094508 (2002), hep-lat/0112020.

[27] X. Liao and T. Manke, (2002), hep-lat/0210030.

[28] S. Godfrey and N. Isgur, Phys. Rev. **D32**, 189 (1985).

[29] N. A. Tornqvist, (2003), hep-ph/0308277.

[30] M. B. Voloshin, Phys. Lett. **B604**, 69 (2004), hep-ph/0408321.

[31] C.-Y. Wong, Phys. Rev. **C69**, 055202 (2004), hep-ph/0311088.

[32] E. Braaten and M. Kusunoki, Phys. Rev. **D69**, 074005 (2004), hep-ph/0311147.

[33] E. S. Swanson, Phys. Lett. **B588**, 189 (2004), hep-ph/0311229.

[34] M. Bander, G. L. Shaw, P. Thomas, and S. Meshkov, Phys. Rev. Lett. **36**, 695 (1976).

[35] A. De Rujula, H. Georgi, and S. L. Glashow, Phys. Rev. Lett. **38**, 317 (1977).

[36] M. B. Voloshin and L. B. Okun, JETP Lett. **23**, 333 (1976).

[37] S. Nussinov and D. P. Sidhu, Nuovo Cim. **A44**, 230 (1978).

[38] N. A. Tornqvist, Z. Phys. **C61**, 525 (1994), hep-ph/9310247.

[39] N. A. Tornqvist, Phys. Lett. **B590**, 209 (2004), hep-ph/0402237.

[40] E. Braaten and H. W. Hammer, (2004), cond-mat/0410417.

[41] M. B. Voloshin, Phys. Lett. **B579**, 316 (2004), hep-ph/0309307.

[42] E. Braaten and M. Kusunoki, Phys. Rev. **D69**, 114012 (2004), hep-ph/0402177.

[43] E. Braaten, M. Kusunoki, and S. Nussinov, Phys. Rev. Lett. **93**, 162001 (2004), hep-ph/0404161.

[44] E. Braaten and M. Kusunoki, Phys. Rev. **D71**, 074005 (2005), hep-ph/0412268.

[45] E. Braaten and M. Kusunoki, Phys. Rev. **D72**, 014012 (2005), hep-ph/0506087.

[46] D. V. Bugg, Phys. Lett. **B598**, 8 (2004), hep-ph/0406293.

[47] D. V. Bugg, Phys. Rev. **D71**, 016006 (2005), hep-ph/0410168.

[48] F. E. Close and S. Godfrey, Phys. Lett. **B574**, 210 (2003), hep-ph/0305285.

[49] B. A. Li, Phys. Lett. **B605**, 306 (2005), hep-ph/0410264.

[50] MILC, C. W. Bernard *et al.*, Phys. Rev. **D56**, 7039 (1997), hep-lat/9707008.

[51] K. K. Seth, Phys. Lett. **B612**, 1 (2005), hep-ph/0411122.

[52] C. J. Morningstar and M. J. Peardon, Phys. Rev. **D60**, 034509 (1999), hep-lat/9901004.

[53] J. Vijande, F. Fernandez, and A. Valcarce, Int. J. Mod. Phys. **A20**, 702 (2005), hep-ph/0407136.

[54] L. Maiani, F. Piccinini, A. D. Polosa, and V. Riquer, Phys. Rev. **D71**, 014028 (2005), hep-ph/0412098.

[55] BABAR, B. Aubert *et al.*, (2004), hep-ex/0408083.

[56] Particle Data Group, S. Eidelman *et al.*, Phys. Lett. **B592**, 1 (2004).

[57] Belle, K. Abe *et al.*, (2004), hep-ex/0408116.

[58] S. L. Olsen, (2004), hep-ex/0412068.

[59] Belle, K. Abe and other, Phys. Rev. Lett. **93**, 051803 (2004), hep-ex/0307061.

[60] BABAR, B. Aubert *et al.*, Phys. Rev. Lett. **93**, 041801 (2004), hep-ex/0402025.

[61] C. Z. Yuan, X. H. Mo, and P. Wang, Phys. Lett. **B579**, 74 (2004), hep-ph/0310261.

[62] CLEO, Z. Metreveli *et al.*, (2004), hep-ex/0408057.

[63] BES, J. Z. Bai *et al.*, Phys. Rev. **D57**, 3854 (1998).

[64] CDF II, G. Bauer, (2004), hep-ex/0409052.

[65] E. Tiesinga, B. Verhaar, and H. Stoof, Phys. Rev. **A47**, 4114 (1993).

[66] S. Inouye *et al.*, Nature **392**, 151 (1998).

[67] P. Courteille, R. Freeland, D. Heinzen, and F. van Abeelen, Phys. Rev. Lett. **81**, 69 (1998).

[68] J. Roberts *et al.*, Phys. Rev. Lett. **81**, 5109 (1998).

[69] S. Kokkelmans, J. Milstein, M. Chiofalo, R. Walser, and M. Holland, Phys. Rev. **A65**, 05361 (2002).

[70] T. D. Cohen, B. A. Gelman, and U. van Kolck, Phys. Lett. **B588**, 57 (2004), nucl-th/0402054.

[71] M. J. Savage, Phys. Rev. **C55**, 2185 (1997), nucl-th/9611022.

[72] E. S. Swanson, Phys. Lett. **B598**, 197 (2004), hep-ph/0406080.

[73] BABAR, B. Aubert *et al.*, Phys. Rev. **D68**, 092001 (2003), hep-ex/0305003.

[74] G. Buchalla, I. Dunietz, and H. Yamamoto, Phys. Lett. **B364**, 188 (1995), hep-ph/9507437.

[75] M. Zito, Phys. Lett. **B586**, 314 (2004), hep-ph/0401014.

[76] C. W. Bauer, B. Grinstein, D. Pirjol, and I. W. Stewart, Phys. Rev. **D67**, 014010 (2003), hep-ph/0208034.

[77] A. Manohar and M. Wise, **Heavy Quark Physics** (Cambridge University Press, New York, 2000) .

[78] E. Braaten, R. J. Oakes, and S.-M. Tse, Int. J. Mod. Phys. **A5**, 2737 (1990).

[79] V. Efimov, Phys. Lett. **33B**, 563 (1970).

[80] E. Nielsen, D. Fedorov, A. Jensen, and E. Garrido, Phys. Rep. **347**, 373 (2001).

[81] E. Braaten and H. W. Hammer, Phys. Rev. Lett. **91**, 102002 (2003), nucl-th/0303038.

[82] E. Braaten and H. W. Hammer, Phys. Rev. **A67**, 042706 (2003), cond-mat/0203421.